

UNIVERSITÉ DE GENÈVE

Groupe de Physique Appliquée

Département de Radiologie

FACULTÉ DES SCIENCES

Professeur P. Descouts

FACULTÉ DE MÉDECINE

Dr. F. Lazeyras

**Epileptic Focus Localization Using
EEG-triggered Functional MRI**

THÈSE

présentée à la Faculté des Sciences de l'Université de Genève
pour obtenir le grade de Docteur ès Sciences, mention physique

par

Ivan ZIMINE

de
Genève (GE)

Thèse N° 3441

GENÈVE

Atelier de reproduction de la Section de physique
2003

Contents

Acknowledgments	9
List of abbreviations	11
Abstract	13
Résumé français	15
Introduction	25
1 Magnetic Resonance Imaging	27
1.1 Nuclear magnetization	27
1.1.1 Macroscopic magnetization	29
1.1.2 Resonance phenomenon	30
1.1.3 Relaxation and Signal detection	31
1.1.4 Spin echo	33
1.2 Imaging principles	35
1.2.1 k-space sampling	37
1.2.2 Image contrast	40
1.2.3 Echo planar imaging (EPI)	42
2 Functional MRI	47
2.1 Human brain	48
2.1.1 Anatomy	49
2.1.2 Functional organization	51
2.2 BOLD effect	52
2.3 BOLD fMRI	53
2.3.1 Scanning protocol	53
2.3.2 Stimulus paradigm	54
2.3.3 Data analysis	56
2.3.4 Visualization	58
2.4 fMRI applications in Epilepsy	59

3 Motion Correction in fMRI	61
3.1 Image registration	61
3.1.1 Transformations	62
3.1.2 Image resampling	63
3.1.3 Optimization	65
3.2 Effect on fMRI activation areas	66
3.2.1 Methods	66
3.2.2 Results	67
3.2.3 Discussion	69
4 Feasibility of simultaneous EEG-fMRI recording	71
4.1 EEG recording inside an MRI scanner	71
4.2 Patient safety	73
4.2.1 Temperature measurements	74
4.3 EEG quality	76
4.4 Image quality	77
4.4.1 fMRI feasibility	79
4.5 Conclusion	81
5 Epileptic focus localization using EEG-triggered fMRI	83
5.1 Epilepsy	83
5.1.1 Epileptic seizures	84
5.1.2 Treatment	85
5.1.3 Presurgical evaluation	86
5.1.4 New techniques for presurgical evaluation	86
5.2 EEG-triggered fMRI	88
5.2.1 fMRI acquisition protocols	90
5.2.2 Patient results	93
5.2.3 Discussion	98
6 Triggered Event-Related fMRI	101
6.1 Introduction	101
6.1.1 EPI sequence modification	103
6.2 Validation study	103
6.2.1 Methods	104
6.2.2 Results	107
6.2.3 Discussion	110
Conclusion	113
Bibliography	125

List of Figures

1.1	Energy level diagram of proton (spin $\frac{1}{2}$) states in a uniform magnetic field	28
1.2	Effect of the RF field on magnetization in fixed (A) and rotating (B) frames.	30
1.3	(a) Longitudinal magnetization regrowth and (b) transverse magnetization decay	32
1.4	Formation of a spin echo	34
1.5	Spin echo signal	34
1.6	Frequency encoding using linear field gradient.	35
1.7	Slice selective excitation.	37
1.8	2D k -space and Image space.	38
1.9	a) Spin echo sequence timing diagrams. b) k -space trajectory after first excitation.	39
1.10	Relaxation in tissues with different T_1 and T_2	40
1.11	Same image with proton-density, T_1 and T_2 weighting	41
1.12	Multiple gradient echoes	42
1.13	Blipped EPI pulse sequence and corresponding trajectory in the k -space.	43
1.14	Gradient echo image (a) and corresponding EPI image (b) showing susceptibility (white arrows) and distortion (red arrows) artifacts	45
1.15	Nyquist artifact a) uncorrected b) corrected EPI.	46
2.1	Schematic representation of a neuron	49
2.2	A. External view of the brain B. Cross-section cut through the brain	50
2.3	Section planes of the brain	50
2.4	A. Brain lobes B. Primary functional areas	51
2.5	Physiological basis of fMRI (adapted from Raichle et al. [19])	53
2.6	Typical EPI volume consisting of fifteen 5 mm slices.	54
2.7	Block paradigm	55

2.8	a) Example of reference functions for correlation analysis b) Hemodynamic response model	58
2.9	Z-score activation map (right-hand finger tapping) and an ac- tivation pixel time-course	59
3.1	Bilinear image interpolation	64
3.2	Degree of motion in fMRI image series.	67
3.3	Activation maps (a) head-fixed (b) head-free before motion correction (c) head-free after motion correction	68
4.1	Schematic representation of patient EEG recording inside an MR scanner (adapted from Ives et al. [69]).	72
4.2	Temperature increase vs SAR in five volunteers. The open symbols correspond to measurements without the electrodes attached to the head.	75
4.3	Ballistocardiogram (arrows) and an EPI image acquisition ar- tifacts on the EEG recording inside the MR scanner.	76
4.4	EEG recording outside and inside the MR scanner showing the α -rhythm (box).	77
4.5	a) Susceptibility artifacts due to EEG paste on an EPI image of water phantom b) Slice position of the EPI image on the phantom	78
4.6	Local susceptibility artifacts (arrows) and non-uniform SNR drop on a GRE image	79
4.7	Cross-correlation maps a) without b) with EEG	80
5.1	Example of spike-wave event used to trigger an EPI acquisition 4 s after detection of the event.	89
5.2	Stimulus correlated motion artifact (injection at frame 60). . .	91
5.3	Image acquisition protocols a) single volume per spike b) mul- tiple volumes per spike.	92
5.4	Focal activation by EEG-triggered fMRI.	94
5.5	Multi-focal activation found by EEG-fMRI (top) and 3D-localization using linear inverse solution showing propagation of electrical activity from the left to the right hemisphere (bottom).	95
5.6	^1H spectroscopy based on EEG-fMRI findings.	97
6.1	Longitudinal magnetization decay to the steady-state condi- tion (TR=1s, flip angle = 50,70,90°)	102
6.2	Raw MR signal from a single pixel from triggered ER-fMRI experiment showing signal saturation effects at the beginning of each image series (arrows indicate task series).	105

6.3	Mean task and control series (a) obtained from signal in fig. 6.2 and their difference (b).	106
6.4	Activation maps showing 3 consecutive slices of one subject obtained from (a) continuous and (b) triggered experiments. .	107
6.5	Spatially averaged time-course from left motor cortex of one subject with fitted gamma function from continuous (a) and triggered (b) experiments. Data corresponds to subject 3 in table 6.1.	109

Acknowledgments

I would like to thank Prof. Pierre Descouts for accepting to supervise this thesis and for his continual support over the last four and a half years.

I express here all my gratitude to my direct supervisor, Dr. François Lazeyras from the Radiology Department of Geneva University Hospitals, who has introduced me into the field of Magnetic Resonance Imaging. He provided me with assistance, guidance and support during the time it has taken me to complete this PhD. I also wish to thank Dr. Margitta Seeck from the Neurology Department for proposing such an interesting research project and for providing financial support.

I am very honored that Prof. Peter Boesiger, Head of Magnetic Resonance Division from the Institute of Biomedical Engineering in Zürich, and Prof. René Flükiger from the Department of Solid State Physics in the University of Geneva, have agreed to be part of the jury of this thesis and I would like to express them my gratitude.

Many people have contributed to this work. In particular, I want to thank Dr. Stephan Perrig, Dr. Olaf Blanke and Dr. Olga Prilipko, who read the EEG during lengthy EEG-triggered fMRI sessions, and who kindly answered to my naive questions about epilepsy and the EEG recording. Dr. C. M. Michel and people working in his Brain Cartography Lab are the experts in the EEG “inverse problem”. I’d like to acknowledge Dr. Laurent Spinelli and Goran Lantz for the fusion of EEG and fMRI results. Of course, I want to thank all my MR research colleagues: Dr. Jean-Paul Vallée, Dr. Mohamed Seghier, Marko Ivancevic, Dr. Emile Hiltbrand and Dr. Tiziano Binzoni, for interesting discussions about MRI, computers and everything else. Special thanks to Dominique Joliat for his interest in our research work and his incredible ability to fix any hardware and software problem on the scanner. Dr. David Foxall from Philips Medical Systems has tremendously helped us with the sequence programming on a Marconi MRI scanner.

It was a great pleasure for me to work in the Radiology Department of Geneva University Hospitals, and I wish to thank all the medical and technical personnel working here for the excellent atmosphere. I would also like to thank the Radiology Department and, in particular, Prof. François Terrier, Head of the Department, for their funding.

Finally, I would like to thank my family and friends for their encouragements and interest in my work.

List of abbreviations

AED	Antiepileptic Drug
AIR	Automated Image Registration
B ₀	static magnetic field
BOLD	Blood Oxygenation Level Dependent
CBF	Cerebral Blood Flow
CBV	Cerebral Blood Volume
CT	Computed Tomography
EEG	Electroencephalography
EPI	Echo Planar Imaging
ER-fMRI	Event Related functional MRI
FID	Free Induction Decay
FOV	Field of View
fMRI	Functional Magnetic Resonance Imaging
G	magnetic field gradient
GRE	Gradient Echo
Hb	Hemoglobin
MEG	Magnetoencephalography
MRI	Magnetic Resonance Imaging
NMR	Nuclear Magnetic Resonance
PET	Positron Emission Tomography
RF	Radio Frequency (magnetic field)
ROI	Region of Interest
SAR	Specific Absorption Rate
SNR	Signal to Noise Ratio
SPECT	Single Photon Emission Computed Tomography
SE	Spin Echo
T ₁	longitudinal relaxation time
T ₂ ^(*)	transverse relaxation time
TE	Echo Time
TR	Repetition Time
TLE	Temporal Lobe Epilepsy

Abstract

The main subject of this thesis is the combination of electroencephalography (EEG) and functional magnetic resonance imaging (fMRI) in the context of pre-surgical evaluation of epileptic patients. Many patients (20–30%) suffer from pharmaco-resistant epilepsy – the type of epilepsy when seizures can not be controlled by medications. These patients can be considered for surgical intervention consisting of elimination of epileptogenic tissue in order to achieve total or at least partial seizure control. For successful epilepsy surgery, accurate localization of the epileptic focus is necessary. This is the principle goal of pre-surgical evaluation during which several techniques are used to identify and characterize the epileptic focus as precisely as possible. EEG-triggered fMRI is a new non-invasive tool for precise focus localization, which may be particularly useful for patients with non-lesional/cryptogenic epilepsy who are still considered to be difficult surgical candidates.

As a new tool, concurrent EEG/fMRI acquisition raises some technical questions that need to be answered before it can be applied on patients. In this work, we have concentrated on the MRI side of the EEG/MRI combination. In particular we have addressed the questions of patient safety and overall fMRI feasibility with the EEG system in the MR scanner. In total, 35 patients with intractable epilepsy have been studied using EEG-triggered fMRI, and the results were compared with other localization techniques used in presurgical evaluation. As the project progressed, several improvements of the imaging protocol were made in order to overcome the problem of motion artifacts that were observed with several patients. In order to improve the localization and characterization of epileptic foci, EEG-fMRI results have been combined with two other new techniques: 3D EEG source localization and ¹H-MR spectroscopy. Another aspect we have worked on, was the development of a new image acquisition strategy that would allow better characterization of hemodynamic responses following an epileptic event. As a result we have developed and validated triggered event-related fMRI technique which may find useful applications in areas other than epileptic activation studies.

Résumé français

Le sujet principal de cette thèse est la combinaison de l'électroencéphalographie (EEG) avec l'imagerie fonctionnelle par résonance magnétique (IRMf) dans le cadre de l'évaluation préchirurgicale des patients épileptiques. De nombreux patients épileptiques (20–30%) souffrent d'une épilepsie pharmacorésistante, c'est-à-dire résistante à toute forme de traitement médicamenteux. Chez ces patients, une chirurgie peut apporter un contrôle total ou une nette diminution des crises épileptiques, mais à condition que le foyer primaire puisse être bien localisé. Ceci est le but principal de l'évaluation préchirurgicale qui vise à déterminer le foyer épileptique avec la meilleure précision possible. Les développements des techniques d'investigation cérébrale, comme l'imagerie par résonance magnétique (IRM), la tomographie par émission de positons (TEP) et l'EEG ont permis des progrès considérables dans le domaine de la localisation du foyer épileptique. Cependant, il existe encore de nombreux patients avec une épilepsie cryptogénique/non-lésionnelle chez qui la localisation reste problématique, ce qui demande le développement de nouveaux outils. Parmi les nouvelles techniques pour l'évaluation préchirurgicale, on peut citer l'IRM fonctionnelle couplée à l'EEG, les nouvelles méthodes d'analyse spatiale de l'EEG multicanaux et la spectroscopie par résonance magnétique, ainsi que la fusion des données provenants de ces différentes techniques.

Ce projet de recherche est le fruit d'une collaboration entre le Département de Radiologie et le service de Neurologie (l'Unité d'évaluation pré-chirurgicale de l'épilepsie et le Laboratoire de cartographie cérébrale). Les expériences effectuées au cours de ce travail ont été faites sur un scanner IRM clinique de 1.5 Tesla (Eclipse, Marconi/Philips Medical Systems).

Avant de rentrer dans les détails de la combinaison EEG/IRMf et de l'application de la méthode aux patients épileptiques, il est nécessaire de décrire brièvement les principes de base de l'imagerie par résonance magnétique et de l'IRM fonctionnelle. L'IRM, décrite dans le chapitre 1, est une technique d'imagerie médicale permettant d'obtenir, de façon non-invasive, des images du corps humain de très haute qualité. L'IRM est basée sur le

phénomène de la résonance magnétique nucléaire (RMN) des noyaux d'hydrogène présents en abondance dans les tissus biologiques. Lorsqu'un patient ou un sujet sain est placé dans un champ magnétique statique \mathbf{B}_0 , les spins des protons s'alignent préférentiellement dans la direction du champ appliqué, tout en précessant autour de lui à la fréquence de Larmor. Ceci crée une aimantation nucléaire macroscopique \mathbf{M} qui peut être perturbée par un champ électromagnétique tournant à la fréquence de Larmor dans un plan perpendiculaire à \mathbf{B}_0 (impulsion d'onde de radiofréquence). Après l'excitation, l'aimantation \mathbf{M} peut être mesurée par induction pendant son retour à l'état d'équilibre. Le retour à l'équilibre est caractérisé par deux paramètres: le temps de relaxation longitudinale T_1 et le temps de relaxation transverse T_2 . Ces deux grandeurs sont caractéristiques des différents tissus biologiques et avec la densité des protons, forment les 3 paramètres fondamentaux de la RMN.

La création d'une image nécessite que le signal RMN contienne l'information spatiale de l'objet d'où il provient. A l'origine de l'encodage spatial se trouve la relation de Larmor qui lie la fréquence du signal RMN au champ magnétique statique. Ainsi, en utilisant un champ magnétique qui varie d'un point à l'autre de l'échantillon d'une façon prédéterminée, on crée une dépendance entre la fréquence (ou la phase) du signal RMN d'une part et la position dans cet échantillon d'autre part. Le décodage spatial peut ensuite être obtenu en utilisant l'analyse de Fourier du signal RMN. En pratique, on utilise des combinaisons de gradients linéaires du champ magnétique dans les trois directions de l'espace, ce qui permet d'acquérir des images dans n'importe quel plan. Pour reconstruire une image bi- ou tri-dimensionnelle, le signal RMN doit être mesuré de manière répétée en présence des gradients qui varient selon un ordre précis. Il existe un grand nombre de techniques d'acquisitions ou séquences IRM qui permettent d'obtenir des images avec des contrastes différents. Initialement, les séquences IRM du type écho de spin, demandaient des temps d'acquisitions relativement longs, entre 2 et 10 minutes par coupe. Avec l'avènement des séquences rapides en écho de gradient, les temps d'acquisitions ont été réduits à quelques secondes et avec l'imagerie écho-planar (EPI), il est devenu possible d'obtenir une image en moins de 100 millisecondes. Ces méthodes rapides ont permis des études dynamiques qui ont menés à la découverte et au développement des techniques d'imagerie fonctionnelle par l'IRM.

Le chapitre 2 est consacré à l'IRM fonctionnelle. Par "fonctionnelle" on entend la localisation des fonctions cérébrales comme la motricité, la vision, le langage ou la mémoire. D'autres techniques IRM, comme la spectroscopie, l'imagerie de perfusion ou de diffusion, peuvent aussi être appelées fonctionnelles, car elles permettent d'approcher les processus physiologiques au niveau cellulaire.

L'IRMf, découverte en 1991, est une technique totalement non-invasive qui permet de mettre en évidence des zones d'activation dans le cerveau d'un sujet lors de l'exécution des tâches sensorielles, motrices ou cognitives. Comme la tomographie par émission de positons, l'IRM fonctionnelle est une méthode indirecte, basée sur la détection des changements métaboliques qui accompagnent l'activité électrique des neurones. La technique la plus utilisée repose sur les changements du signal RMN liés aux variations d'oxygénéation sanguine (technique BOLD, Blood Oxygenation Level Dependant). L'activation neuronale est accompagnée d'une augmentation locale du flux et du volume sanguin pour satisfaire l'augmentation de la demande métabolique (glucose et oxygène). En fait, l'augmentation du flux et du volume sanguin surcompensent l'augmentation modérée de la consommation d'oxygène, ce qui se traduit par une hyperoxygénation dans les capillaires veineux autour de la région activée. Les propriétés magnétiques du sang dépendent principalement de l'état d'oxygénéation de l'hémoglobine. La deoxyhémoglobine est paramagnétique, alors que l'oxyhémoglobine est diamagnétique. L'augmentation du niveau d'oxygène dans le sang, pendant l'activation, entraîne une meilleure homogénéité du champ magnétique local qui se traduit par une légère augmentation du signal RMN (1-5% à 1.5 Tesla). Ces changements du signal peuvent être observés avec des séquences rapides en écho de gradient ou EPI qui sont très sensibles aux variations de l'homogénéité du champ local. La séquence EPI est utilisée dans la majorité des études IRMf pour avoir une large couverture du cerveau, tout en gardant la résolution temporelle de l'ordre de la seconde. Le déroulement d'un examen IRMf typique correspond à l'alternance de périodes de repos et de périodes d'activation pendant lesquelles le sujet réalise une tâche. Pendant ce temps, les images couvrant une partie ou la totalité du cerveau sont acquises de façon répétée toutes les 1 à 3 secondes. Les données d'un examen IRMf sont donc des séries temporales des volumes du cerveau avec 100 à 200 volumes par série. Les images "fonctionnelles" sont obtenues par l'analyse statistique des images acquises durant les phases de repos et d'activation. Beaucoup de méthodes d'analyse ont été proposées, mais les plus fréquemment utilisées sont basées sur des modèles paramétriques de l'évolution temporelle du signal. Les résultats de cet analyse sont ensuite superposés sur les images anatomiques de haute résolution pour obtenir ce qu'on appelle les cartes

d'activation.

L'IRM fonctionnelle est en train de devenir une technique de choix pour l'exploration du cerveau normal et pathologique. Dans le contexte de l'évaluation préchirurgicale de l'épilepsie, l'utilité de l'IRM fonctionnelle est double. D'une part on peut localiser les aires épileptogènes (voire chapitre 5) et d'autre part on peut localiser des aires fonctionnelles importantes, par exemple les aires du langage, qui doivent être préservées pendant l'opération.

Le chapitre 3 est dédié au problème de la correction des mouvements du sujet pendant l'examen. En effet, les mouvements sont une source majeure d'artefacts en IRMf et il est impératif de les corriger afin d'obtenir des cartes d'activation interprétables. Une des approches pour corriger les effets de mouvement consiste à appliquer des techniques de recalage d'image sur les données IRMf. La procédure standard consiste à sélectionner une image (volume) de référence et une image test, trouver une transformation spatiale (3 angles de rotation et 3 translations) à partir d'une fonction de similarité entre les deux images et ensuite reéchantillonner l'image test pour obtenir l'image corrigée. Cette procédure est répétée sur toutes les images de la série IRMf en gardant la même image de référence.

Plusieurs algorithmes de recalage d'images ont été proposés pour des données IRMf. Comme les signaux observés en IRMf sont très faibles, les procédures de corrections des mouvements doivent satisfaire deux conditions: une détection précise de petits mouvements et une préservation des intensités de pixels pendant le reéchantillonnage. En général, l'efficacité d'un algorithme de correction est évaluée à l'aide de données simulées. L'évaluation de ces algorithmes avec des données IRMf réelles est également importante, mais c'est une tâche plus difficile car on n'a pas de données de référence pour faire une comparaison.

Pour étudier les effets des mouvements sur des aires d'activation, nous avons utilisé l'algorithme AIR (automated image registration). Quatre volontaires ont effectué une simple tâche motrice une fois avec la tête immobilisée et une deuxième fois avec la tête libre. Ainsi, les données où la tête était fixée nous ont servis de condition de contrôle. L'analyse des données avant la correction des mouvements a montré que les aires d'activation sont fortement réduites. En corrigeant les mouvements (généralement plus petits que la taille d'un pixel) avec AIR, on arrive à récupérer, en moyenne, 80% des "pixels activés". Il arrive que quelques images dans la série fonctionnelle ne sont pas corrigées correctement, mais globalement, AIR est assez efficace pour corriger les effets dus aux mouvements.

Dans le chapitre 4 nous abordons quelques aspects techniques de la combinaison EEG/IRMf. Il s'agit de tester la faisabilité de l'IRMf en présence de l'EEG et d'évaluer les risques pour les patients. A part l'épilepsie, l'acquisition simultanée de l'EEG et de l'IRM fonctionnelle pourrait devenir un outil très puissant pour des applications en neurosciences, surtout pour les études du couplage entre l'activité électrique du cerveau et les changements métaboliques qui les accompagnent.

Les problèmes de l'utilisations de l'EEG dans une IRM sont dus à une forte interférence entre les deux techniques. D'un côté la présence de l'équipement électronique dans un scanner peut affecter la qualité des images, et de l'autre côté les champs magnétiques utilisés pour l'imagerie perturbent fortement l'enregistrement EEG. De plus, il y a un certain risque de brûlures dû à un échauffement possible des électrodes et des câbles EEG où les courants sont induits par les champs magnétiques variables.

Le système EEG installé à Genève a été spécialement conçu pour l'enregistrement dans un scanner IRM par des chercheurs du Beth Israel Hospital à Boston. Dans un premier temps, nous avons évalué les risques de brûlures par des mesures de température sous les électrodes et en utilisant plusieurs séquences IRM. Le risque d'échauffement dépend principalement de l'énergie RF émise par une séquence IRM. Cette énergie dépend de l'amplitude et du nombre d'impulsions RF de la séquence. Pour les séquences EPI et en écho de gradient, qui sont nécessaires pour un examen IRMf, l'énergie RF déposée est faible due au petit nombre d'impulsions dans le cas de l'EPI et à la faible amplitude des impulsions RF dans le deuxième cas. Avec nos mesures de température, aucun échauffement d'électrodes n'a pu être détecté après une acquisition EPI de 3 minutes en continu, et pour l'écho de gradient, on a observé une augmentation de température de 1 à 2°C seulement. Deux autres séquences, l'écho de spin et l'écho de spin rapide, qui utilisent beaucoup d'impulsions de 180 degrés, étaient aussi testées. L'échauffement des électrodes était compris entre 1.5 et 3.5°C , ce qui reste en dessous de la limite de sécurité pour les objets en contact avec le patient.

Une autre série de tests portait sur la faisabilité de l'IRM fonctionnelle en présence de l'EEG. Le système EEG produit deux types d'artefacts sur les images IRM. Les artefacts de susceptibilité dus aux électrodes et la pâte conductrice sont visibles sur le cuir chevelu, mais ne pénètrent pas dans l'image du cerveau. Plus grave est la diminution globale du rapport signal-sur-bruit des images à cause de la présence des câbles EEG tout autour de la tête du sujet. Avec notre système EEG de 18 canaux, cette diminution est de l'ordre de 25% en moyenne. En effectuant des examens IRMf avec et sans l'EEG, nous avons constaté que la détection du signal BOLD, en présence de l'EEG, restait possible, mais la taille de régions d'activation était diminuée

de près de 50%. Cette réduction de la qualité des images IRMf pourrait être un facteur limitant pour les études EEG/IRMf qui nécessiteraient un plus grand nombre de canaux EEG.

En ce qui concerne la qualité de l'enregistrement EEG, elle est assez bonne pour l'observation des événements comme les décharges épileptiques, mais seulement en absence d'une acquisition IRM. Pendant l'acquisition, surtout avec la séquence EPI qui utilise un fort gradient de lecture qui commute rapidement, l'interprétation de l'EEG est impossible à cause des courants induits dans les câbles. Plusieurs méthodes ont été proposées pour enlever cet artefact, mais notre système EEG actuel ne permet pas de les appliquer à cause du problème de saturation des préamplificateurs. Toutefois, même avec cet artefact, la combinaison EEG/IRMf reste possible si on utilise un délai entre les acquisitions d'images successives pendant lequel l'EEG serait lisible.

Le chapitre 5 est consacré à la localisation du foyer épileptique par l'IRMf couplée à l'EEG. Chez un grand nombre des patients épileptiques, un discret foyer peut être la source d'activité électrique anormale qui peut se propager à travers le cerveau provoquant des crises très handicapantes. Dans environ 70% des cas, les crises peuvent être contrôlées par un traitement médicamenteux approprié. Si un tel traitement ne peut pas être trouvé, les patients, dits pharmaco-résistants, peuvent bénéficier d'un traitement par chirurgie. La chirurgie de l'épilepsie est uniquement possible dans le cas où le foyer est parfaitement localisé et séparé des parties saines du cortex. Avant l'opération, le patient doit donc subir une série d'examens qui servent à dresser un bilan pré-chirurgical. Les outils cliniques qui servent à localiser l'activité épileptique incluent: l'EEG, l'IRM anatomique, la spectroscopie RMN, la TEP et la TEMP (tomographie à émission mono-photonique). Malheureusement, il arrive que ces examens ne fournissent pas de réponses précises concernant la localisation du foyer. Cela concerne surtout les patients avec une épilepsie d'origine extra-temporale sans lésions anatomiques apparentes. Après la découverte et le développement de l'IRM fonctionnelle, on a naturellement cherché à l'exploiter pour la localisation du foyer épileptique.

Les premières démonstrations de localisation de l'activité épileptique par l'IRMf ont été réalisées avec des patients présentant des crises accompagnées de discrets signes cliniques. Cependant, seulement les patients avec des crises fréquentes qui ne provoquent pas des mouvements désordonnés peuvent bénéficier d'un tel examen IRMf. Par contre, chez pratiquement tous les patients on peut observer sur l'EEG des signes d'activité épileptique entre les vraies crises. Ces brefs événements, appelés décharges inter-ictales, ne provo-

quent pas des mouvements incontrôlables, et peuvent donc être utilisés pour déclencher l'acquisition d'images IRMf. Généralement on fait l'hypothèse que ces décharges provoquent un changement local du flux sanguin assez important pour être détecté par l'IRMf. Cette technique de localisation du foyer a pris le nom de l'IRMf déclenchée par l'EEG (EEG-triggered fMRI).

Comme en IRMf standard, nous avons besoin des images pendant les conditions d'activation et de contrôle. Ces deux conditions peuvent être obtenues de la façon suivante: d'abord on obtient des images d'activation déclenchées par des décharges, le patient reçoit une injection d'un médicament anti-épileptique, et lorsque les décharges disparaissent, on obtient les images de contrôle. Cette stratégie est utile lorsque le patient a beaucoup de décharges. Cependant cette technique est très sensible aux artefacts de mouvements qui sont difficiles à corriger . Une approche alternative consiste à entrelacer les conditions d'activation et de contrôle en déclenchant les acquisitions de contrôle pendant les périodes sans décharge.

En tout, nous avons étudié 35 patients avec l'IRMf déclenchée par l'EEG. Chez 20 patients, nous avons pu observer des régions de rehaussement local du signal BOLD, dont la localisation était en accord avec les résultats obtenus par d'autres techniques (solutions inverses de l'EEG, TEP ou spectroscopie). Chez 11 de ces 20 patients, un enregistrement EEG avec des électrodes profondes ou des grilles sous-durales a confirmé la localisation du foyer épileptique. Les données de 8 patients n'ont pas pu être analysées pour diverse causes (artefacts des mouvements, artefacts de susceptibilité ou absence quasi-totale d'activité inter-ictale). Chez les autres patients, l'absence des régions d'activation pourrait être une indication d'une forme diffuse de l'épilepsie (confirmé dans 1 cas).

Bien que nos résultats sur les patients soient très prometteurs, la localisation du foyer doit être faite en combinant plusieurs techniques. Par exemple, si les images d'activation d'IRMf déclenchée par l'EEG montrent plusieurs régions distinctes, il est fort probable que cela soit dû à une propagation rapide de l'activité épileptique du foyer primaire aux zones secondaires. Pour déterminer la localisation du foyer primaire on peut combiner les résultats de l'IRMf avec des techniques de reconstruction des sources électriques (solutions inverses de l'EEG) qui ont une très haute résolution temporelle. Une autre combinaison intéressante est entre l'IRMf et la spectroscopie RMN. La spectroscopie est très sensible aux altérations métaboliques dans un foyer épileptique. Elle est déjà utilisée chez des patients avec une épilepsie du lobe temporal. En se basant sur les résultats de l'EEG/IRMf pour définir les régions d'acquisition des spectres, on peut étendre l'utilité de la spectroscopie à l'épilepsie du lobe extra-temporal.

La technique d'IRMf déclenchée par l'EEG présente toutefois quelques inconvénients qui nous ont poussé au développement d'une approche événementielle d'acquisition d'images. Cette nouvelle méthode est décrite dans le chapitre 6.

La première limitation de l'IRMf déclenchée par l'EEG est la durée de l'examen, qui peut aller jusqu'à 2 heures chez des patients ayant très peu de décharges. Cela est dû au fait que pour l'analyse fonctionnelle, on a besoin entre 40 et 60 images acquises après les décharges dont la fréquence d'apparition peut être de l'ordre une par période de cinq minutes. Les examens de longue durée sont très fatigants pour les patients et les données qui en résultent sont souvent corrompues par d'importants mouvements du patient. La deuxième limitation est due au fait que l'on ne connaît pas la vraie forme de réponse vasculaire liée à un événement inter-ictal qui pourrait varier fortement d'un patient à l'autre et en fonction du type de décharges.

Pour surmonter ces deux problèmes, une approche d'IRMf événementielle déclenchée (triggered event-related fMRI) a été développée. L'idée est de déclencher l'acquisition d'une petite série d'images au lieu d'une seule image. Cela permettrait d'échantillonner la réponse vasculaire liée à une décharge. De plus cela permettrait de réduire la durée de l'examen, car avec seulement 10 à 15 séries (et donc des décharges), on a suffisamment de données pour une analyse fonctionnelle. Il y a toutefois une difficulté avec cette approche. Au début de la série, l'intensité des images est fortement pondérée par une fonction exponentielle à cause des effets T_1 . Pour l'analyse fonctionnelle, il est nécessaire de corriger cette pondération. La solution que nous avons choisie consiste à acquérir deux types de séries: une déclenchée par un événement (tâche) et une autre (contrôle) aussi déclenchée mais sans un événement qui la précède. Les deux séries auront exactement la même pondération, et donc la différence entre les séries tâches et les séries contrôles devrait permettre l'analyse fonctionnelle. C'est effectivement ce qu'a montré notre étude de validation de cette méthode soustractive où nous avons comparé les activations du cortex moteur obtenues avec l'IRMf événementielle standard et l'IRMf événementielle déclenchée.

Pour l'instant, l'IRMf événementielle déclenchée ne peut pas être utilisée pour les études d'activation épileptique, à cause des artefacts d'acquisition IRM sur l'EEG. L'acquisition d'une série prend environs 20 secondes pendant lesquelles l'EEG n'est pas lisible. Il se peut que des décharges épileptiques surviennent pendant ces laps de temps, ce qui invaliderait la méthode soustractive. Ce qui est possible par contre, est d'utiliser des courtes séries de 3 à 5 secondes déclenchées par des décharges ce qui permet au moins un échantillonnage partiel de la réponse "BOLD épileptique".

Le but principal de cette thèse était le développement des techniques d'IRMf couplées à l'EEG dans le cadre clinique de l'évaluation pré-chirurgicale des patients épileptiques. Les études de faisabilité ont montré que la combinaison EEG/IRMf était appliquable aux patients de point de vue de la sécurité et que la qualité des images IRM était suffisante pour mener les études d'IRM fonctionnelle. Les résultats de localisation du foyer épileptique chez les 35 patients, qui incluaient des patients pédiatriques, ont montré que l'IRMf déclenchée par EEG est un outil très prometteur pour le bilan pré-chirurgicale des patients pharmaco-résistants. La combinaison des résultats EEG/IRMf avec des techniques de reconstruction des sources électriques par l'EEG pourrait apporter une fine analyse spatio-temporelle de l'activité épileptique. D'autre part, la combinaison avec la spectroscopie permettrait une confirmation directe du foyer épileptique. Cependant, ces résultats doivent encore être validés par les résultats cliniques post-opératoires sur un plus grand nombre de patients.

Introduction

Epilepsy is one of the most common neurological disorders that affects 0.5–1% of world's general population. It is characterized by recurrent seizures, caused by bursts of abnormal electrical activity in part or the whole of the brain. The clinical manifestations of epilepsy depend on the brain areas involved and on seizures types and duration. They include transient loss of awareness or consciousness and disturbances of movement, sensation, mood or mental functions. Poor understanding and fear associated with epileptic seizures and the fact that about 65% of people suffering from epilepsy have their seizure onset before the age of 20 explain the heavy physical, psychological as well as socio-economical consequences of this disease.

Epilepsy can be successfully treated (i.e. total or markedly improved seizure control) with anti-epileptic drugs (AED) in about 70% of newly diagnosed cases. Surgical intervention constitutes another approach to the treatment of epilepsy, especially for patients with pharmaco-resistant epilepsy. As a necessary condition for successful surgical outcome, brain areas involved in seizure generation (epileptic foci) have to be identified and localized as precisely as possible. The development of neuroimaging techniques, in particular magnetic resonance imaging (MRI), positron emission tomography and high-resolution electroencephalography have greatly improved the localization and characterization of epileptic foci. However, there are still numerous cases with non-lesional epilepsy where localization remains problematic which justifies the development of new diagnostic techniques.

In the beginning of the 1990's the possibility of localizing specific brain functions using magnetic resonance imaging has been demonstrated. Due to its inherent non-invasiveness and relatively high spatial and temporal resolution, practical utility of the new imaging technique has been quickly recognized. Functional MRI is still a rapidly developing field and despite some limitations and the lack of complete theoretical model, it has already many promising applications in cognitive neuroscience and clinical research.

Naturally, functional MRI raised a lot of interest in epilepsy research as a new possible tool for epileptic focus localization. The specificity of this application is that it requires recording of electroencephalography (EEG) in parallel with functional imaging in order to obtain “activation maps” associated with epileptic activity of the brain. However, such a combination of EEG and functional MRI is not straightforward because of the strong interference between the two techniques.

In this work several technical aspects of the feasibility of EEG/fMRI combination are addressed as well as application of this new technique for epileptic focus localization.

Scope of the thesis

The simultaneous use of two interfering techniques imposes some restrictions and may require some modifications in both of them in order to increase the benefits and reduce the penalties of the combination. This is the case with simultaneous EEG/fMRI, where the EEG system has to be made MR compatible and the fMRI acquisition and analysis has to be synchronized with the EEG recording. In this work we concentrated on the MRI side of this combination. This thesis is organized as follows:

- Chapter 1:** An introduction to nuclear magnetic resonance, conventional magnetic resonance imaging and fast echo planar imaging.
- Chapter 2:** Short description of the human brain and its functional organization. General description of functional MRI including physiological bases behind the measured signal, experimental designs and data analysis.
- Chapter 3:** An emphasis on the problem of subject’s motion in functional MRI.
- Chapter 4:** Description of concurrent EEG/fMRI recording, technical aspects and the results of fMRI feasibility studies.
- Chapter 5:** Introduction to epilepsy and presurgical evaluation. Epileptic focus localization using EEG-triggered fMRI and patient’s results.
- Chapter 6:** Description and validation of triggered event-related fMRI method which was developed to overcome some limitations of image acquisition strategies depicted in Chapter 5.

Chapter 1

Magnetic Resonance Imaging

Magnetic Resonance Imaging (MRI) is a technique used to produce high quality images of biological tissues. Its physical principles are based on the phenomenon of Nuclear Magnetic Resonance (NMR) described by Bloch [1] and Purcell [2] in 1946. Until the early 1970s, NMR was used as a spectroscopic technique in solid-state physics, chemistry and biology to study structure and properties of molecules. In 1971, Damadian showed that NMR could be used to discriminate malignant tumors from normal tissues [3]. Two years later, Lauterbur proposed a method for spatial encoding of the NMR signal [4] which effectively started rapid development of a new imaging modality - MRI.

The usefulness of MRI in biomedical applications comes from the possibility to image soft tissues in the human body and some metabolic processes therein. MRI is a very rich imaging modality in terms of possible contrasts between different tissues. Another very important aspect is the “non-invasive” nature of the technique which makes possible repetitive exams without health risks associated with ionizing radiation as it is the case with X-ray based imaging modalities.

This chapter is a short overview of MRI principles. Detailed description of the NMR phenomenon and different MR imaging techniques can be found in [5] and [6].

1.1 Nuclear magnetization

NMR is based on the interaction of nuclear magnetic moment (spin) placed in an external magnetic field with applied electro-magnetic field oscillating at particular frequency. Only the nuclei with an odd number of protons and/or neutrons (e.g. ^1H , ^2H , ^{13}C) possess non zero spin and can therefore ex-

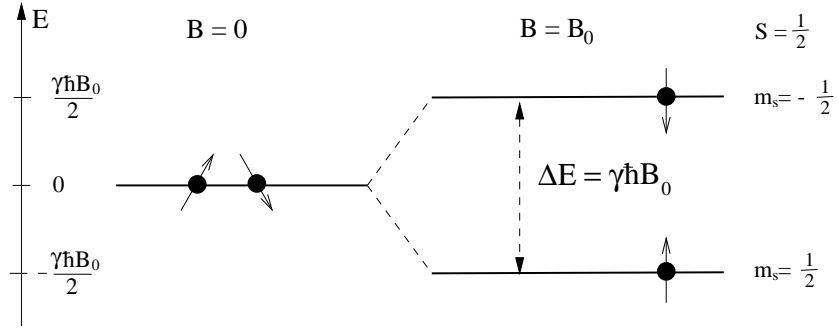


Figure 1.1: Energy level diagram of proton (spin $\frac{1}{2}$) states in a uniform magnetic field

perience NMR. In the human body there is a large amount of hydrogen atoms contained in fat and water molecules. Consequently, MR images are primarily created from the NMR signal of hydrogen nucleus - proton. Much of the NMR phenomenon can be described using classical electrodynamics because the measured signal comes from the macroscopic magnetization of an ensemble of nuclei, however rigorous NMR theory requires quantum mechanical framework [7].

Atomic nuclei possess a magnetic dipole moment $\boldsymbol{\mu}$ proportional to their spin angular momentum \boldsymbol{S}

$$\boldsymbol{\mu} = \gamma \boldsymbol{S} \quad (1.1)$$

where γ is the gyromagnetic ratio unique to each nucleus¹. In the presence of a static magnetic field $\mathbf{B} = B_0 \hat{z}$, magnetic dipoles line up with the field. Dipoles can have either parallel or anti-parallel orientation to the field pertaining to the lower or higher energy states. Due to the discrete nature of spin angular momentum, energy states of a nucleus in a constant magnetic field are also discrete:

$$E_m = -\boldsymbol{\mu} \cdot \mathbf{B} = -\gamma S_z B_0 = -\gamma \hbar m_s B_0 \quad (1.2)$$

where $m_s = -s, -s+1, \dots, s$ are possible values of spin angular momentum along the z axis and s is particle's spin quantum number. For the proton, which has spin $s = 1/2$, there are two possible energy levels, corresponding to spin-up and spin-down states (fig. 1.1), with the energy difference given by

$$\Delta E = E_{\downarrow} - E_{\uparrow} = \gamma \hbar B_0 \quad (1.3)$$

¹for protons $\gamma = 2.675 \cdot 10^8 \text{ rad s}^{-1} \text{T}^{-1}$

Actually, magnetic dipoles vectors are not completely aligned with the applied field. The orientation angle is given by $\theta = \arccos(m_s/\sqrt{s(s+1)})$. Magnetic moments experience therefore a torque which leads to the following equation of motion:

$$\frac{d\mu}{dt} = \gamma\mu \times \mathbf{B} \quad (1.4)$$

The solution of eq. (1.4) when $\mathbf{B} = B_0\hat{z}$ corresponds to a precession of the magnetic moment about the field with the angular frequency $\omega_0 = \gamma B_0$ known as the *Larmor frequency*. Considering protons in the 1.5 Tesla field, the cyclic frequency of precession is 63.86 MHz.

1.1.1 Macroscopic magnetization

In a sample containing N protons, the macroscopic magnetization \mathbf{M} is given by a vector sum of individual magnetic dipole moments. In the absence of external magnetic field, the net magnetization is zero because of random orientation of dipole moments. When the sample is placed in a static field, there is a net magnetization, determined by the difference of the number of protons in spin-up and spin-down states. The magnetization is aligned along the direction of the applied field. The transverse component is canceled out because of random precessional phases of individual magnetic dipole moments. At thermal equilibrium, the probability to find a proton in either spin-up or spin-down state is given by Boltzmann distribution:

$$P(E_\uparrow) = \frac{e^{-E_\uparrow/kT}}{e^{-E_\uparrow/kT} + e^{-E_\downarrow/kT}}, \quad P(E_\downarrow) = \frac{e^{-E_\downarrow/kT}}{e^{-E_\uparrow/kT} + e^{-E_\downarrow/kT}} \quad (1.5)$$

where k is Boltzmann's constant. So, in the applied field $B_0\hat{z}$, the equilibrium magnetization is given by:

$$\begin{aligned} M_z &= \frac{1}{V} N(P(E_\uparrow)\mu_\uparrow - P(E_\downarrow)\mu_\downarrow) \\ &= \frac{1}{V} N \frac{\gamma\hbar}{2} \frac{e^x - e^{-x}}{e^x + e^{-x}} \\ &= \frac{1}{V} N \frac{\gamma\hbar}{2} \tanh(x), \quad x = \frac{\gamma\hbar B_0}{2kT} \end{aligned} \quad (1.6)$$

where V is the volume of the sample. At room temperature, the condition $\gamma\hbar B_0 \ll kT$ is always verified, so that the expression for M_0 can be simplified to take the form of the Curie's law:

$$M_z = M_0 \simeq \rho_0 \frac{\gamma^2 \hbar^2}{4kT} B_0 \quad (1.7)$$

1.1.2 Resonance phenomenon

Nuclear magnetic resonance is the induction of transitions between the spin-up and spin-down states of the protons. The energy required to produce this transition is given by eq. (1.3), and can be provided by applying an electro-magnetic field at the Larmor frequency $\omega_0 = \gamma B_0$. This excitation field is commonly called radio-frequency (RF) field. Absorption of RF energy corresponds to transition of protons from lower (spin-up) to higher (spin-down) energy state; a process which affects the equilibrium macroscopic magnetization.

When the RF field is applied in the direction perpendicular to the main B_0 field, the effect is to rotate the magnetization away from its rest state. This effect is easily understood by considering a circularly polarized field

$$\mathbf{B}_1(t) = B_1(\cos(\omega_0 t)\hat{x} - \sin(\omega_0 t)\hat{y}) \quad (1.8)$$

For individual dipole moments precessing around B_0 field at the Larmor frequency, B_1 appears as another static field (fig. 1.2A), and a new torque $(\mu \times B_1)$ causes them, and consequently the macroscopic magnetization to rotate about it. Figure 1.2B shows the motion of M during the action of B_1 in a rotating coordinate frame, which is frequently used in NMR to describe the motion of the magnetization vector.

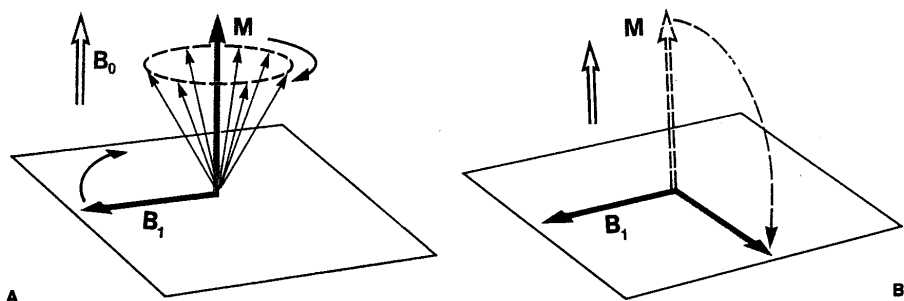


Figure 1.2: Effect of the RF field on magnetization in fixed (**A**) and rotating (**B**) frames.

The most common way to carry out an NMR experiment is to apply a short pulse of resonant RF field. If the duration of the pulse is τ , then the magnetization will rotate by an angle $\alpha = \gamma B_1 \tau$, creating a transverse component of magnitude $M_0 \sin(\alpha)$. The equilibrium magnetization is rotated completely into the transverse plane with a 90° pulse. The transverse magnetization precess about the B_0 field and thus can be measured through induction using a receive coil.

1.1.3 Relaxation and Signal detection

After the application of a resonant RF pulse, the magnetization returns back to the equilibrium state under the effect of the \mathbf{B}_0 field only. Regrowth of the longitudinal magnetization requires transitions from spin-down to spin-up states, a process which involves energy exchange between the excited protons and its surroundings. It is termed *spin-lattice* relaxation and the rate at which equilibrium is restored is characterized by the longitudinal relaxation time T_1 . The rate of the loss of the transverse magnetization, which is due to a loss of precessional phase coherence of individual dipole moments, is characterized by the transverse relaxation time T_2 .

Rapid spin-lattice relaxation is associated with high probability of transition from higher to lower energy state, which is greatest if the local electromagnetic field oscillates with frequencies close to ω_0 . The local field results from the presence of neighboring magnetic nuclei and the thermal motion of molecules containing them. Medium-size molecules (e.g. lipids) are more effective in causing T_1 relaxation than small (e.g. H₂O) or large-size molecules (e.g. proteins) because their motion (translational and rotational) produces local field variation at frequencies close to the Larmor frequency. Relaxation times of various human body tissues are listed in table 1.1. Since the Larmor frequency is proportional to B_0 , T_1 parameter is field dependent.

Transverse T_2 relaxation results from direct *spin-spin* interaction without any energy release to the lattice. The local field cause the nuclei to precess at slightly different rates which results in a loss of phase coherence. In contrast to T_1 process, any change in the local field contribute to the loss of coherence, which means that T_2 parameter is always smaller than T_1 .

Tissue	T_1 (ms)	T_2 (ms)
Fat	250	60
White matter	600	80
Gray matter	950	100
Muscle	900	50
CSF	4500	2200

Table 1.1: Approximate values of relaxation parameters T_1 and T_2 for hydrogen content of some human body tissues at 1.5 T and 37°C

The NMR signal corresponds to the voltage induced in a receive coil from the time-varying magnetic flux produced by a rotating transverse magnetization. To understand the form of the signal, we must consider the motion of the magnetization vector after the application of the RF pulse. The motion of \mathbf{M} is determined by the torque ($\mathbf{M} \times \mathbf{B}_0$) and the relaxation phenomena.

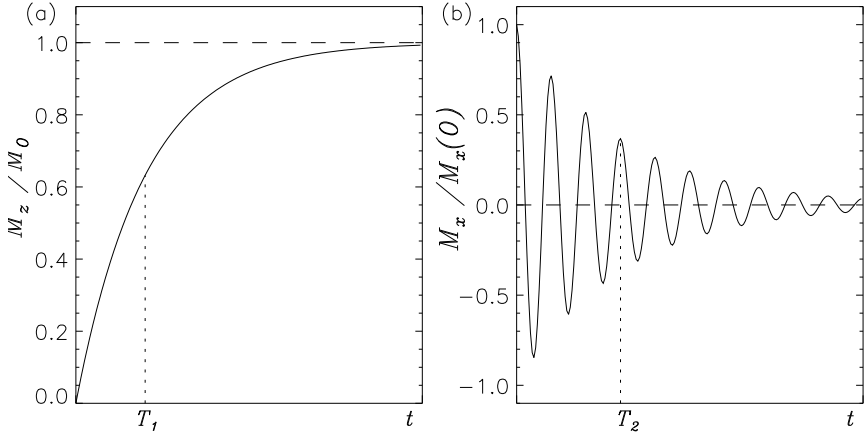


Figure 1.3: (a) Longitudinal magnetization regrowth and (b) transverse magnetization decay

For a static field $B_0\hat{z}$, the equations of motion for longitudinal and transverse components are given by the *Bloch equations*:

$$\frac{dM_z}{dt} = \frac{M_0 - M_z}{T_1} \quad (1.9a)$$

$$\frac{dM_x}{dt} = \gamma M_y B_0 - \frac{M_x}{T_2} \quad (1.9b)$$

$$\frac{dM_y}{dt} = -\gamma M_x B_0 - \frac{M_y}{T_2} \quad (1.9c)$$

Solution for the longitudinal component is straightforward, while for the transverse components, solution is easily obtained by simple variables substitution $M_{x,y} = m_{x,y}e^{-t/T_2}$

$$M_z(t) = M_z(0)e^{-t/T_1} + M_0(1 - e^{-t/T_1}) \quad (1.10a)$$

$$M_x(t) = e^{-t/T_2}(M_x(0) \cos \omega_0 t + M_y(0) \sin \omega_0 t) \quad (1.10b)$$

$$M_y(t) = e^{-t/T_2}(M_y(0) \cos \omega_0 t - M_x(0) \sin \omega_0 t) \quad (1.10c)$$

In the fixed laboratory frame, the motion of \mathbf{M} corresponds to an upward spiraling at the Larmor frequency controlled by the two relaxation times. Figure 1.3 shows the solutions of eq. (1.9) for a particular case when at time zero $\mathbf{M} = M_0\hat{x}$.

The equations (1.9) can also be solved by defining complex transverse magnetization $M_+ = M_x + iM_y$, which gives the following equation of motion

$$\frac{dM_+}{dt} = -i\omega_0 M_+ - \frac{M_+}{T_2} \quad (1.11)$$

The general solution is given by:

$$M_+(t) = |M_+(0)|e^{-t/T_2}e^{-i\phi(t)} \quad \text{with} \quad \phi(t) = \omega_0 t + \phi(0) \quad (1.12)$$

This representation is often used to express the measured NMR signal as a complex function:

$$V \propto M_0 e^{-i\phi(t)} e^{-t/T_2} \quad (1.13)$$

with the real and imaginary components given by:

$$V_{re} \propto M_0 \cos(\omega t) e^{-t/T_2} \quad (1.14a)$$

$$V_{im} \propto M_0 \sin(\omega t) e^{-t/T_2} \quad (1.14b)$$

The induced voltage has the characteristic of a damped cosine, which is called a *free induction decay* (FID). The real and imaginary components (or channels) can be measured either by two independent receive coils or by a single circularly polarized (quadrature) coil.

1.1.4 Spin echo

In reality, the transverse magnetization and, hence, the measured signal decays faster than predicted by T_2 . The reason for this shortening is the spatial inhomogeneity of the main magnetic field, which produces an additional dephasing of spins. The effective transverse relaxation time T_2^* is given by

$$\frac{1}{T_2^*} = \frac{1}{T_2} + \frac{1}{T'_2} \quad (1.15)$$

where the last term represents the contribution from field inhomogeneities.

The signal loss due to field inhomogeneities can be recovered using the *spin echo* method [8]. It is illustrated in figure 1.4. A 90°_x RF pulse rotates the magnetization in the transverse plane ($t=0$). After some time ($t=\tau$) the magnetization has precessed several revolutions and some spin dephasing occurred. At this instant, a 180°_y pulse is applied, which mirrors the magnetization in a way that the fast (F) spins are behind the slow (S) ones. At $t=2\tau$ the spins rephase creating what is called a spin-echo. The time between the initial 90° pulse and the echo is called *echo time* (TE). The intrinsic signal losses due to T_2 dephasing are not recoverable, as they are related to local, random field variations (fig. 1.5).

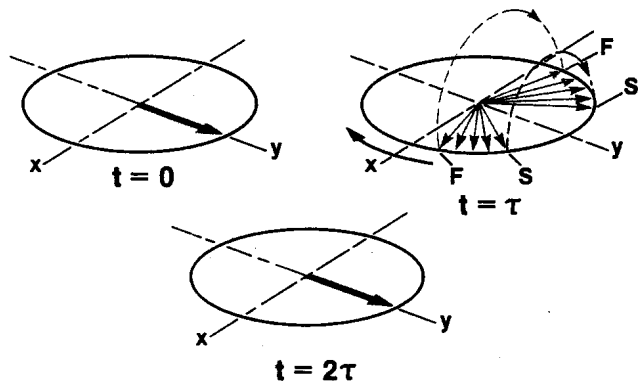


Figure 1.4: Formation of a spin echo

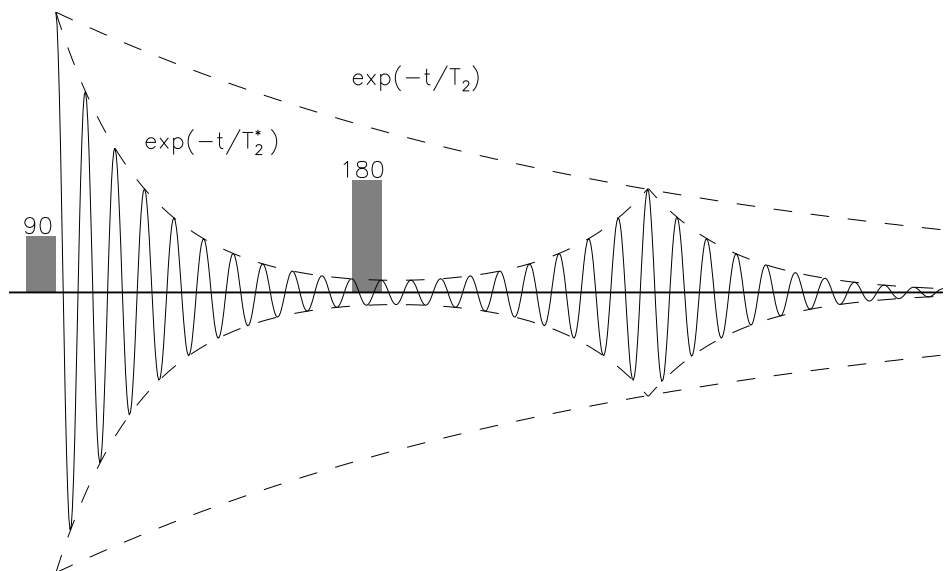


Figure 1.5: Spin echo signal

1.2 Imaging principles

The goal of MR imaging is to determine the spatial distribution of protons density within the sample. This can be achieved by exploiting the Larmor relationship ($\omega = \gamma B$) between the spins precessional frequency and the applied magnetic field. If a well-defined spatial field variation is superimposed on the homogeneous static field, spatial information can be obtained from the frequency content of the measured signal.

Spatial field variation is usually obtained by superimposing linear field gradients on the main B_0 field. A gradient along a given direction produces a linear relationship between the resonance frequency and the position of spins along that direction:

$$\omega(\mathbf{r}) = \gamma(B_0 + \gamma \frac{\partial \mathbf{B}}{\partial \mathbf{r}} \cdot \mathbf{r}) = \omega_0 + \gamma \mathbf{G} \cdot \mathbf{r} \quad (1.16)$$

The principle is illustrated in figure 1.6 with a sample consisting of two water-filled cylinders positioned at different locations along the x axis in a block of nonmagnetic material. In the absence of field gradient, protons in both cylinders resonate at exactly the same frequency because they experience the same field, and the measured FID contains only one frequency. When the gradient is turned on, the protons in the two cylinders experience two different fields, and the resulting FID is the superposition of two different frequency components. A Fourier transform of the FID will contain two peaks at frequencies determined by eq. (1.16) and amplitudes corresponding to protons density in the two cylinders.

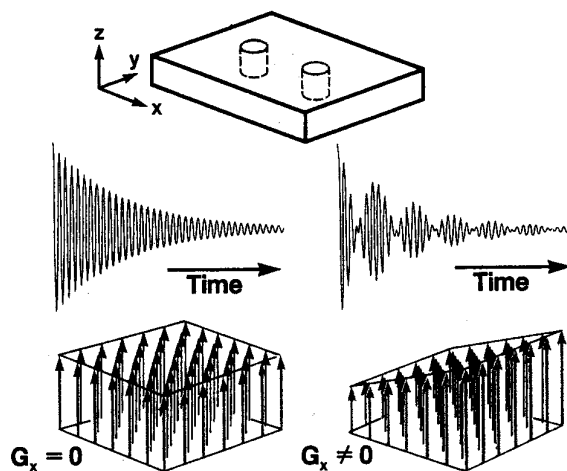


Figure 1.6: Frequency encoding using linear field gradient.

To create a complete image of protons distribution in a sample, a volume of interest must be excited by applying resonant RF field. Then, the spatial locations in the volume must be unambiguously encoded to allow image reconstruction from the Fourier analysis. However, the generalization of 1D frequency encoding into 2D or 3D is not straightforward. A linear combination of orthogonal field gradients will result in encoding of spins locations along only one direction determined by the vector sum of the gradients. All spins orthogonal to this direction will sense the same field and thus yield identical frequencies. The solution to the problem of encoding in two or three dimensions is achieved by using time-varying magnetic field gradients. If the magnetic field at each point is varied in time in a specific manner, the location of precessing spins can be established as long as the temporal variation is unambiguous for each position.

Consider a group of protons contained in a small volume element ΔV (voxel), found at position \mathbf{r} in a sample. From eqs. (1.7) and (1.13), the contribution from this volume to the total MR signal coming from the entire excited sample may be written as

$$dS(\mathbf{G}, t) \propto \rho(\mathbf{r}) \Delta V e^{(-t/T_2)} e^{-i(\omega_0 + \gamma \mathbf{G} \cdot \mathbf{r})t} \quad (1.17)$$

where $\rho(\mathbf{r})$ is the spin density of the voxel². In practice, actual signal recording is preceded by a demodulation step, which allows to remove rapid ω_0 oscillation. If signal recording is done rapidly, the T_2 relaxation effect can be ignored. The total MR signal is given by

$$S(t) = \iiint \rho(\mathbf{r}) e^{-i(\gamma \mathbf{G} \cdot \mathbf{r})t} d\mathbf{r}. \quad (1.18)$$

By introducing the concept of the reciprocal \mathbf{k} -space, defined by

$$\mathbf{k} = \gamma \mathbf{G} t, \quad (1.19)$$

the expression for the MR signal can be written as

$$S(\mathbf{k}) = \iiint \rho(\mathbf{r}) e^{-i\mathbf{k} \cdot \mathbf{r}} d\mathbf{r} \quad (1.20)$$

Instead of temporal domain, the measured signal can be expressed in terms of spatial frequencies defined by vectors \mathbf{k} ([rad/m]). Application of time-dependent orthogonal gradients corresponds to a trajectory in the \mathbf{k} -space along which the signal is measured. If during imaging, the whole \mathbf{k} -space

² In fact, ρ represents the effective spin density which includes gain factors from electronic detection system and receive coil geometry factors.

can be covered, the spatial distribution of spins density can be obtained by Fourier transform.

$$\rho(\mathbf{r}) = \iiint S(\mathbf{k}) e^{i\mathbf{k} \cdot \mathbf{r}} d\mathbf{k} \quad (1.21)$$

1.2.1 k-space sampling

In practice, it is difficult to achieve complete 3D coverage of the \mathbf{k} -space in a single MR data readout, because of very short $T_2^{(*)}$ relaxation times (< 100 ms) in most biological tissues. The MR signal (spin echo or gradient echo) from the volume of interest must be created repeatedly and measured using different gradient conditions (amplitudes and duration) allowing coverage of different parts of the \mathbf{k} -space.

The majority of MR imaging methods reduce the 3D problem to a 2D problem by using a technique called selective slice excitation. This is done by applying a finite-bandwidth RF pulse in the presence of a *slice selection* gradient (G_z). The gradient creates a positional dependence of the resonance frequency of the sample in the direction of the gradient (by convention z). When the RF field is applied at $\omega_s = \omega_0 + \gamma G_z z_s$, only the spins in a plane defined by z_s will be excited (fig. 1.7). If the RF field contains a narrow band of frequencies, protons in a thin slice will be excited. The slice thickness is given by

$$\Delta z = \Delta\omega / \gamma G_z \quad (1.22)$$

Using an RF pulse with different central frequency, another slice can be excited, thus allowing 3D imaging from multiple 2D slices. In the physical space, slices can be obtained in any direction by employing a linear combination of three orthogonal gradients.

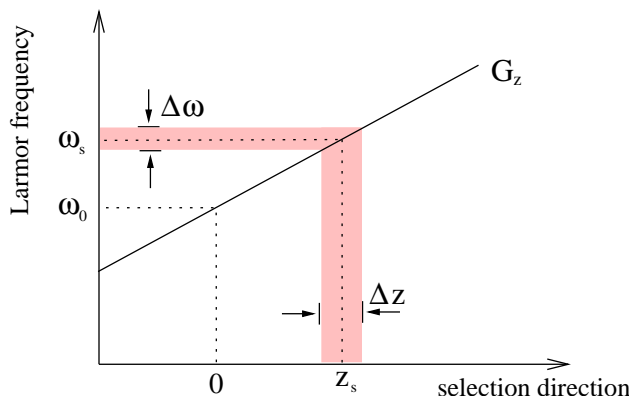


Figure 1.7: Slice selective excitation.

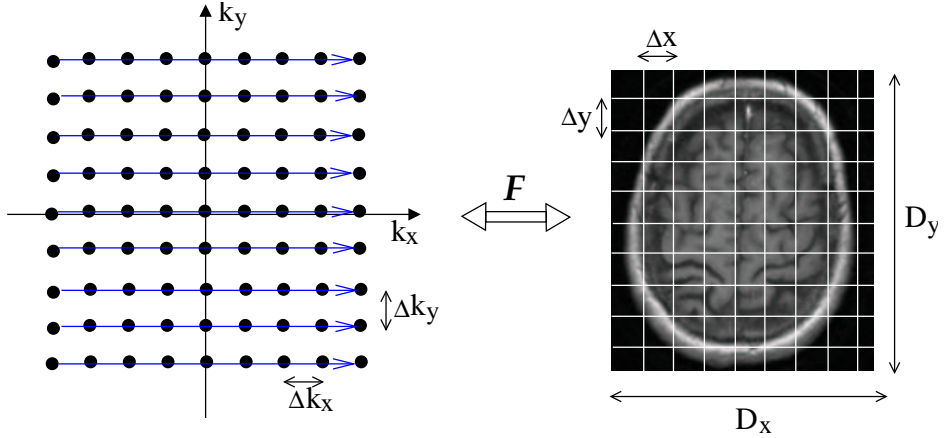


Figure 1.8: 2D k -space and Image space.

The most common way to acquire a 2D MR image is to sample a two dimensional k -space on a regular cartesian grid ($k_x = \gamma G_x t_x, k_y = \gamma G_y t_y$) in a line by line manner (fig. 1.8). This allows an efficient image reconstruction using fast Fourier transform (FFT). Acquisition of each line is done along k_x in the presence of a constant gradient G_x applied in a *frequency encoding* or *readout* x direction. The position of the line along k_y is changed by applying, for a short duration, a gradient of variable amplitude (G_y) in the orthogonal y direction prior to actual data recording. This is called *phase encoding*.

The concept of phase-encoding reflects the fact that while the gradient is turned on, the precessional frequency in the direction of the applied gradient becomes position dependent, and faster precessing spins will gain in phase with respect to slower precessing spins. After the gradient is turned off, the frequency becomes constant again, but the created phase dispersion remains. In fact, because the MR signal is sampled at discrete time points, frequency encoding corresponds also to phase encoding in the readout direction. In other words, k -space is a kind of “spatial phase” domain whose coordinates express the phase advance or retardation per unit length experienced by spins as a result of applying magnetic field gradients.

Figure 1.9a shows the timing diagram of a classical spin echo (SE) MRI sequence. A spin echo signal is created by a 90° slice selective RF pulse followed by a 180° refocusing pulse. It is digitally sampled at N_x time points in the presence of constant readout gradient (G_x), which corresponds to an acquisition of a single line in the k -space. In order to fill the k -space, the spin echo is recreated N_y times at equal time intervals, called repetition time (TR). Between the two RF pulses, a phase-encoding gradient is applied to acquire a different line in the k -space. To obtain sequential top to bottom

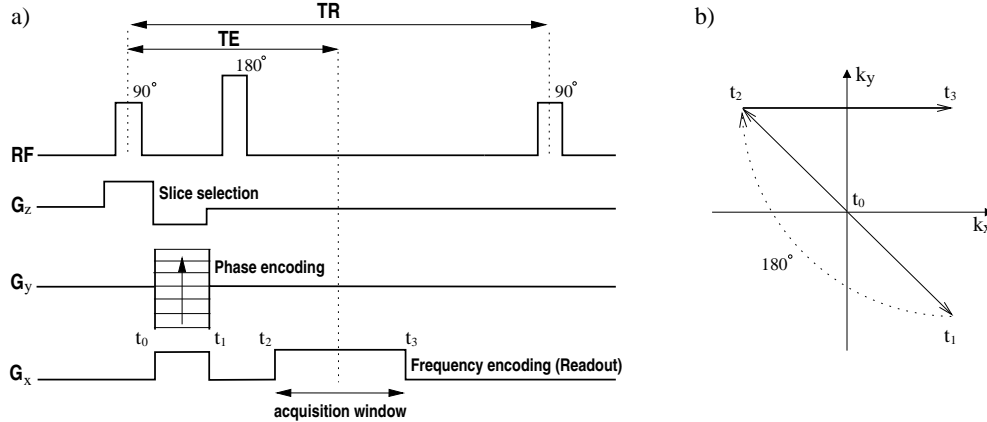


Figure 1.9: a) Spin echo sequence timing diagrams. b) k -space trajectory after first excitation.

filling, phase-encoding starts with a negative G_y^{max} and then incremented by $\Delta G_y = 2G_y^{max}/N_y$ for each phase-encode step. Together with the phase-encoding, a gradient pulse in the readout direction is also applied. It is needed to create spins dephasing which will be canceled by the readout gradient in the middle of the acquisition, allowing true spin echo detection at desired echo time (TE). The phase-encoding and dephasing gradients determine the starting measuring point in the k -space (fig. 1.9b).

The amplitude and duration of the gradients and the sampling frequency (bandwidth) of readout electronics determine the sampling steps of the k -space

$$\Delta k_x = \gamma G_x \Delta t_s, \quad \Delta k_y = \gamma \Delta G_y \tau_{pe} \quad (1.23)$$

where Δt_s is the sampling interval and τ_{pe} is the duration of phase-encoding step. On the other hand, there is a reciprocal relationship between the resolution and extension of k -space and real space

$$\Delta k_x = \frac{2\pi}{D_x} = \frac{2\pi}{N_x \Delta x}, \quad \Delta k_y = \frac{2\pi}{D_y} = \frac{2\pi}{N_y \Delta y}. \quad (1.24)$$

From the above equations, it is possible to compute the gradients requirements needed to obtain an image of desired resolution.

$$\gamma G_x = \frac{1}{D_x \Delta t_s} = \frac{N_x}{D_x T_{read}} = \frac{BW_{read}}{D_x} \quad (1.25a)$$

$$\gamma \Delta G_y = \frac{1}{D_y \tau_{pe}}, \quad \gamma G_y^{max} = \frac{N_y}{2D_y \tau_{pe}} \quad (1.25b)$$

where $\gamma = \gamma/2\pi$.

An important property of the k -space is that its central part corresponds to low spatial frequencies and therefore determines the overall MR image contrast, while the peripheral zones, corresponding to high spatial frequencies, encode image details.

There are many MRI techniques (sequences) that employ different k -space sampling strategies in order to increase the image acquisition speed or to obtain a particular image contrast. Mathematically, the sampling trajectory in the k -space is irrelevant for image reconstruction, provided that the same space is sampled. Nonlinear trajectories are also possible, for example spiraling trajectories can be obtained using sinusoidal gradients. However, these techniques require special image reconstruction algorithms that should take into account non-cartesian sampling.

1.2.2 Image contrast

MRI is a very rich imaging modality in terms of possible contrasts between different body tissues. This is due to the fact that apart from protons density, the MR signal depends also on relaxation parameters T_1 and T_2 (table 1.1). Other contrast generating mechanisms are diffusion, flow and magnetic susceptibility differences because they introduce local magnetic field differences (T_2^* effects).

The basic contrast is the proton density throughout the object being imaged. Regions with low proton content, for example bones, produce very weak MR signal. MRI is more suitable to create images of soft tissues with high water content. However, most tissues have a very similar water content, so the contrast based on proton density is small. A much higher contrast can be obtained from the differences in T_1 and T_2 values of different tissues.

In the spin echo sequence (fig. 1.9), longitudinal magnetization is repeatedly flipped into the transverse plane. The repetition time (TR) determines

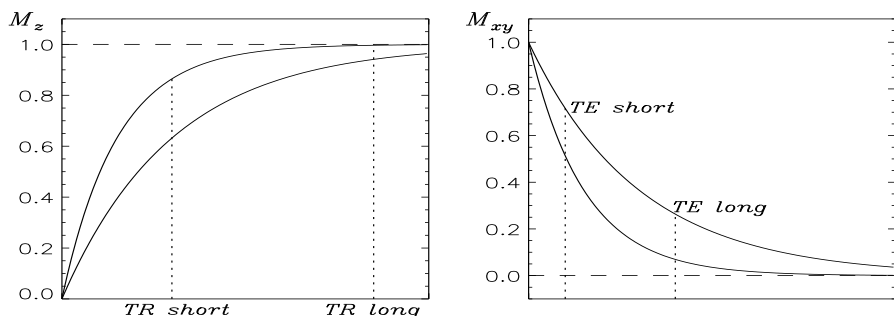


Figure 1.10: Relaxation in tissues with different T_1 and T_2 .

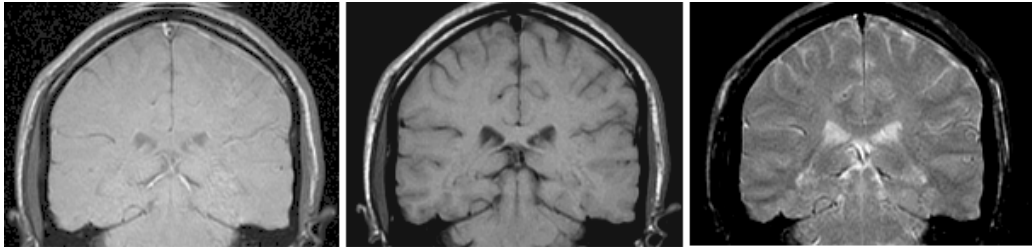


Figure 1.11: Same image with proton-density, T_1 and T_2 weighting

how much longitudinal magnetization is recovered between two successive excitations. Protons in tissues with shorter T_1 will recover quicker, and therefore will produce a stronger MR signal than protons in tissues with longer T_1 . Hence, changing the value of TR allows to introduce T_1 -weighting into the images (fig. 1.11). Since the signal measurement itself is done with a TE delay after excitation, it is affected by T_2 relaxation. Again, because T_2 values vary from tissue to tissue, it is possible to enhance the differences by changing the value of TE. The complete signal intensity for a given tissue A can be written as

$$S_A \sim \rho_A (1 - e^{-\text{TR}/T_{1,A}}) e^{-\text{TE}/T_{2,A}} \quad (1.26)$$

A particular combination of TR and TE parameters of the SE sequence determines the predominant contrast in an images. In clinical practice, images obtained with ($\text{TR} \gg T_1$, $\text{TE} \ll T_2$) are called “proton density weighted”, with ($\text{TR} \sim T_1$, $\text{TE} \ll T_2$) – “ T_1 weighted”, and with ($\text{TR} \gg T_1$, $\text{TE} \sim T_2$) – “ T_2 weighted” (fig. 1.11).

Apart from TR and TE, the contrast depends also on image resolution. In high-resolution imaging, signal intensities are obtained from small volume elements which are more likely to contain tissues of only one type. However, high-resolution images have a low signal-to-noise ratio (SNR) per voxel and contrast differences between neighboring voxels may be difficult to observe. On the other hand, lowering image resolution in order to increase SNR, will decrease image contrast because of partial volume effects.

1.2.3 Echo planar imaging (EPI)

Although MR imaging using conventional spin echo sequence is a useful technique, it requires rather long acquisition time. For example, a single 2D T_1 -weighted image (TR=500 ms, 256 phase encodes) requires 2 minutes of acquisition time, but a T_2 -weighted image (TR = 2000 ms) of the same resolution needs already 8.5 minutes. Without the development of multislice techniques in which images from several slices are gathered simultaneously, MRI would be impractical for clinical applications. Apart from clinical efficiency and patient comfort, the development of faster imaging techniques was motivated by the need to minimize artifacts due to motion (cardiac, respiratory) and by the desire to perform dynamic studies.

In 1977, Mansfield [9] proposed a method, called echo planar imaging (EPI), allowing a 2D image acquisition in about 100 ms, but almost 10 years of technical advances of the MRI technology were necessary before useful EPI images could be produced on the whole-body MRI scanners. At the same time, other fast scanning techniques – gradient echo (GRE) [10], fast spin echo (FSE) [11] and half-Fourier methods [12] – were developed. Because these techniques are less demanding on hardware requirements than EPI and offer acquisitions times in the order of 1 second, they became the standard clinical tools for high-resolution structural imaging. In the end of the 1980s, dynamic imaging using fast GRE sequences combined with the injection of paramagnetic contrast agents [13] showed that MRI could provide functional information about tissues perfusion with blood. This was quickly followed by the demonstration of the possibility to detect brain activation with MRI [14]. However, the use of fast GRE imaging for dynamic studies with high temporal resolution allows very limited spatial coverage with 1 to 3 slices at maximum. For this reason, ultra-fast EPI which allows the acquisition speeds of ten slices per second is now used in practically all dynamic MRI studies.

In fast gradient echo imaging, the increase of the acquisition speed is achieved by using very short TRs (~ 10 ms) in conjunction with reduced flip

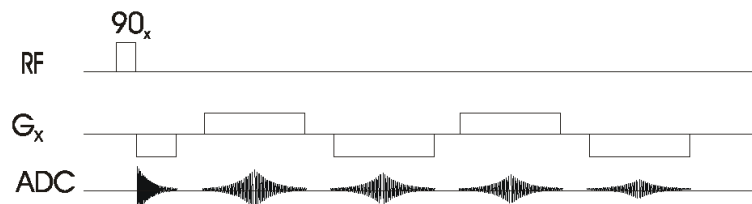


Figure 1.12: Multiple gradient echoes

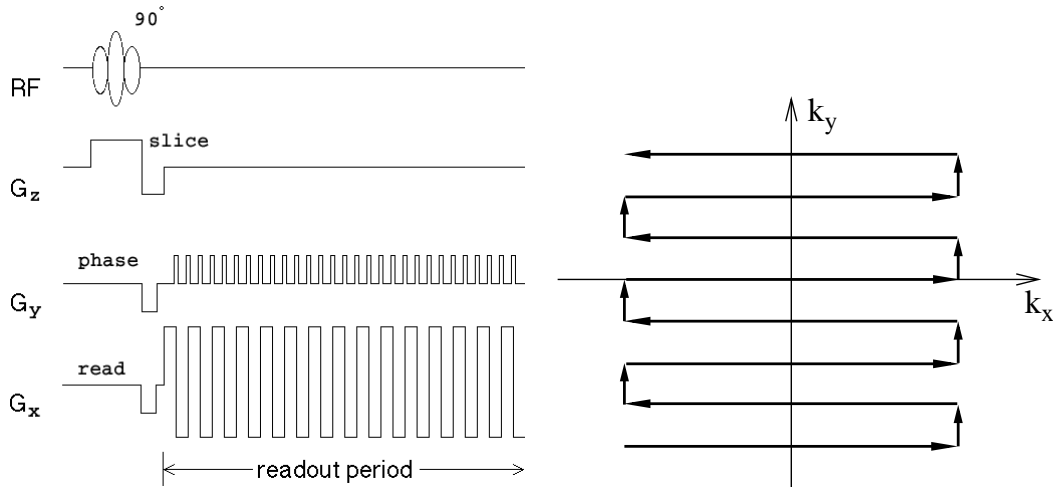


Figure 1.13: Blipped EPI pulse sequence and corresponding trajectory in the k -space.

angles, but the k -space sampling strategy is similar to the conventional spin echo sequence. Echo planar imaging uses another strategy to increase the acquisition speed. Instead of a single line, multiple lines of the k -space are acquired after one RF excitation. This can be obtained by applying an oscillating readout gradient, which creates a train of gradient echoes (fig. 1.12). If each echo can be phase encoded and enough echoes are created before the T_2^* relaxation destroys completely the transverse magnetization, the whole k -space can be sampled after only one RF excitation. This is called *single-shot* gradient echo EPI. Phase encoding can be done in several ways, but the most common way is to use short pulses of the phase-encoding gradient between the reversals the readout gradient. This encoding technique is called blipped EPI.

Figure 1.13 shows the complete timing diagram of this EPI sequence and the corresponding k -space sampling trajectory. After a 90°RF pulse, both readout and phase-encoding gradient are applied for a short time to define the starting acquisition point, then the readout gradient is reversed and the first echo (one line) is collected, a phase-encoding pulse moves the acquisition point one line up, the readout gradient is reversed again, and the second echo is acquired. The process is repeated until all the k -space is covered.

In single-shot gradient echo EPI, the notions of the repetition time and the echo time, which define image contrast, have a slightly different meaning than in conventional imaging. The echo time, more correctly called *effective TE*, is the time interval between the RF pulse and the acquisition of the

k -space center. The central part of the k -space, which corresponds to low spatial frequencies (i.e. large objects), determine the overall image contrast, so changing the effective TE will introduce different T_2^* -weighting into the image. For a single EPI image, the notion of the repetition time has no meaning because the whole image is acquired after one RF excitation. However, EPI is usually used in dynamic studies, and the time between successive image acquisitions determines the amount of the longitudinal magnetization available to create an image, and therefore, influences the T_1 -weighting of the images. Still, because the effective echo time is relatively long, EPI images have generally T_2^* contrast.

Technical issues

At 1.5 T, T_2^* of different tissues in the brain is in the range of 50–100 ms. To make a single-shot EPI with 100 phase encode steps, each line has to be acquired in less than 1 ms, and data collection itself must be done with a sampling rate of 200–400 kHz. Assuming an imaging field of view of 25 cm and using eq. (1.25)a, the requirement for the readout gradient amplitude is about 20–40 mT/m. For comparision, other MRI techniques usually need gradient strengths less than 10 mT/m. In addition to high amplitude, the gradients have to be switched quickly (< 0.3ms) from positive to negative. This requirements necessitated the development of very performant gradient power amplifiers capable of delivering both very high currents (400 [A]) and voltages (600 [V]) into the gradient coils.

The design of single-shot EPI has some important consequences on the resulting image quality. The presence of strong readout gradients require the use of wide receiver bandwidth. Since the noise in any MR image is proportional to the square root of receiver bandwidth, increasing the bandwidth results in descreased SNR of the images. For EPI images, the bandwidth is at least 10 times larger than for any other MR techniques which corresponds to SNR decrease by a factor of 3 or 4. However, this SNR loss is usually compensated by low spatial resolution of the EPI images. A 128×128 EPI image would have essentially the same SNR as a 256×256 spin-echo image of the same object.

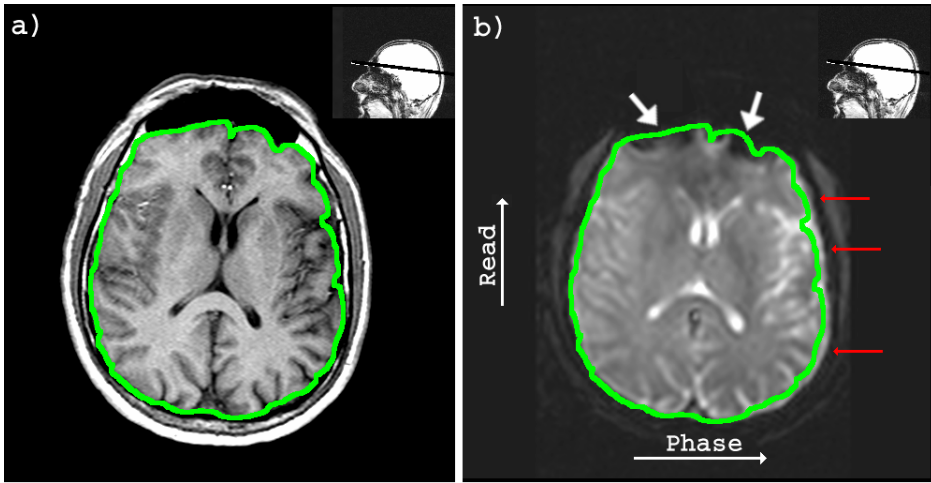


Figure 1.14: Gradient echo image (a) and corresponding EPI image (b) showing susceptibility (white arrows) and distortion (red arrows) artifacts

Image artifacts

Single-shot EPI is very sensitive to any off-resonance effects which can lead to various image artifacts. Off-resonance effects result from local magnetic field inhomogeneities produced by local susceptibility differences, chemical shifts, and imperfect gradient and main B_0 fields. All these effects alter spins precessional frequencies, which translate into incorrect spatial locations in images. In EPI, data acquisition in the readout direction is very fast, so there is little effect in that direction. In the phase-encoding direction, however, the acquisition is much slower, and off-resonance effects create significant phase-shifts by the time the whole k -space is acquired:

$$\Delta\phi = N_y \Delta f_\sigma \Delta t_s \quad (1.27)$$

where Δf_σ is the off-resonance frequency shift and Δt_s is the time between two successive phase encoding steps. Considering a 64×64 image, where each line is acquired in 1 ms, and the chemical shift between fat and water (214 Hz at 1.5 T), the global phase-shift in the phase encoding direction is 13.7 radians. From the Fourier transform shift theorem, this corresponds to 13.7 pixels shift in the image, or about 20% of the imaging field of view. This large misregistration artifact necessitates the use of fat suppression techniques [15] for practically all EPI applications. Field inhomogeneity and susceptibility differences (mostly at air-tissue interfaces) will lead to similar displacement artifacts (fig. 1.14) [16].

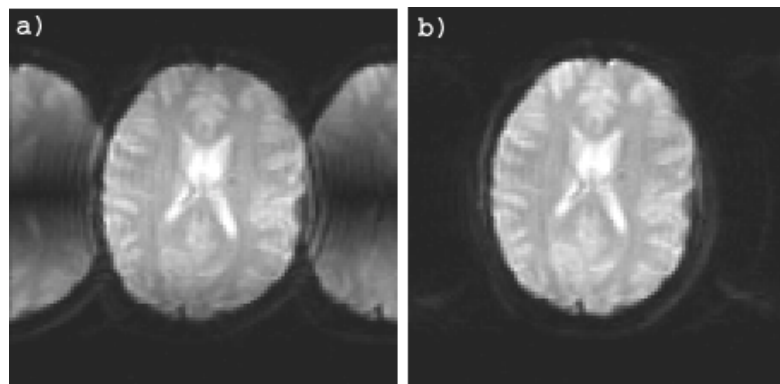


Figure 1.15: Nyquist artifact a) uncorrected b) corrected EPI.

Finally, one type of artefact which is specific to EPI is the Nyquist, or $N/2$ ghost. This arises because odd and even echoes are acquired under opposite read gradients, and the data requires reversal prior to image reconstruction. Inaccurate timing of the sampling relative to the switched gradient, temporal asymmetries in the analogue filter or inhomogeneities in the static field cause a modulation of alternate lines in k-space. This leads to a ghost image shifted by $N/2$ pixels in the phase encode direction (fig. 1.15). This artifact can be reduced using phase correction algorithms [17].

Chapter 2

Functional MRI

“Men ought to know that from nothing else but the brain comes joys, delights, laughter and sports, and sorrows, griefs, despondency, and lamentations. And by this, in an especial manner, we acquire wisdom and knowledge, and see and hear and know what are foul and what are fair, what are bad and what are good, what are sweet, and what are unsavory... And by the same organ we become mad and delirious, and fears and terrors assail us...”

Hippocrates, c. 400 BC [18, p. 29]

The brain is an extraordinarily complex and least understood organ of the human body. Throughout history, its role and functioning was the center of interest of many scientists and philosophers both in relation to brain diseases and aspects of mental activities such as memory, consciousness and thought.

Until the last part of the 19th century, the only existing method for human brain exploration consisted in the autopsies of patients with neurological deficits. These observations, together with animal studies using electrical stimulations and surgically induced lesions, have gradually lead to the acceptance of the idea of localized functional areas within the brain.

Today, it is possible to examine the brain structure and functions directly *in vivo* using modern imaging technologies [19]. Detailed anatomy of the brain can be obtained using computed tomography (CT) and magnetic resonance imaging (MRI) allowing the study of normal and abnormal cerebral development. Functional organization of the human brain can be studied using electro- and magneto-encephalography (EEG and MEG), single photon emission computed tomography (SPECT), positron emission tomography (PET) and functional MRI. The term “functional imaging” usually means localization of specific brain areas involved in the processing of spe-

cific task. EEG and MEG allow direct assessment of the electrical activity of cortical neurons with millisecond temporal resolution, but limited spatial resolution. PET, SPECT and fMRI utilize indirect correlates of the neuronal firing, like increase of glucose consumption or vascular (hemodynamic) changes, to detect activation areas with high spatial resolution, but low temporal resolution. Techniques like magnetic resonance spectroscopy (MRS), diffusion and perfusion MRI, near-infrared spectroscopy (NIRS) could also be included into “functional imaging” category as they provide additional information about the physiology of the brain.

This chapter provides an overview of functional MRI, which, in less than ten years, has become a method of choice for studies of the human brain function both under normal and pathological conditions. This is mainly due to the non-invasiveness of the technique, availability of MRI scanners and relative ease of conducting fMRI studies.

2.1 Human brain

In order to introduce some terminology used in neuroimaging and for a better understanding of this and the following chapters, this section provides a short introduction to the human brain anatomy and its functional organization.

The human nervous system is divided into two parts: central and peripheral. The central nervous system (CNS) includes the brain and the spinal cord, while the peripheral nervous system includes somato-sensory nerves and autonomous nervous system. The basic functional unit of the nervous system is the nerve cell or *neuron*. In the brain, there are approximately 100 billion neurons interconnected into a complex network. The brain contains also an even larger number of *glial* cells that accomplish various supportive, metabolic and phagocytic functions. The neurons are specialized to receive and to transmit information encoded in the form of electrical impulses or *action potentials* between each other. Neurons vary widely in shape and size, but each has four morphologically specialized regions: *cell body*, *dendrites*, *axon* and *axon terminals* (fig. 2.1).

The cell body contains the nucleus and cellular organelles critical for the neuron’s vitality. The dendrites are branching processes, which receive signals from other neurons. Extending from the cell body in one direction is an axon, which conducts the impulses away from the body. The length of an axon can be several centimeters or longer. In order to increase the speed of propagation of action potentials, axon is usually coated in a fatty sheath, called *myelin*. At the end, the axon can split into a few branches terminated

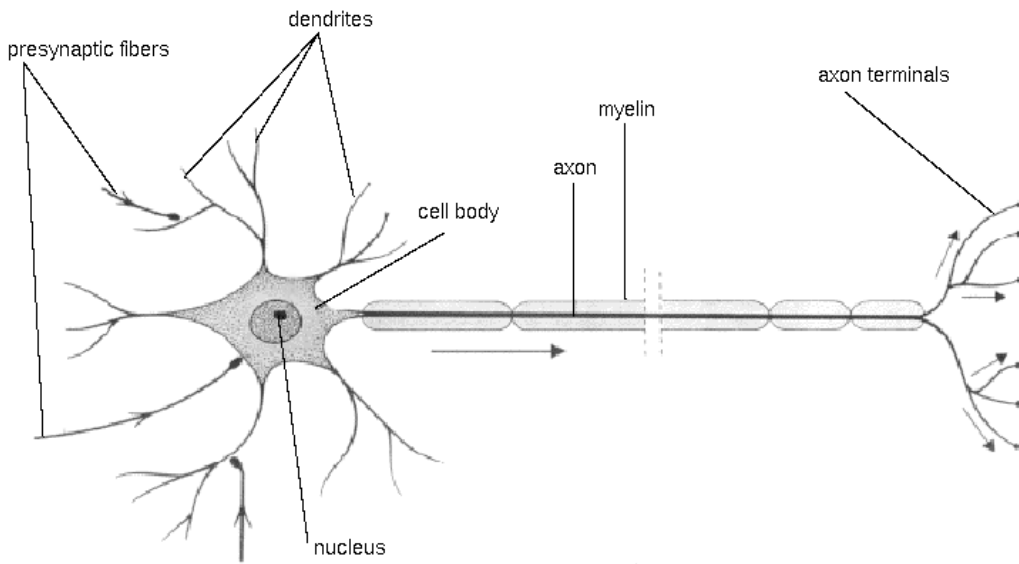


Figure 2.1: Schematic representation of a neuron

by *synaptic knobs*. These knobs make synaptic connections to the dendrites or the cell bodies of other neurons allowing information transfer by means of a *neurotransmitter* molecule.

2.1.1 Anatomy

Seen from the outside, the human brain exhibit some gross anatomical features: the cerebral hemispheres, the cerebellum and the lower part of the brainstem (fig. 2.2). The two hemispheres, connected by a massive bundle of commissural fibers (*corpus callosum*), form the largest part of the brain. Their surface is highly convoluted forming many *gyri* (folds) and *sulci* or *fissures* (grooves). The convoluted surface of the hemispheres comprises a thin (2–5 mm) layer of neurons, referred to as the *cerebral cortex*. Most of the interior of the cerebral hemispheres consists of myelinated axons. The presence of myelin gives these regions a white appearance, and is termed *white matter*. The cortex, which contains the neuronal cell bodies and dendrites, is darker and consequently termed *gray matter*. There are also several large gray matter nuclei, referred to as *basal ganglia*, located in the central regions of the hemispheres. At the rear of the brain is a tightly folded structure called the *cerebellum* which is connected to the rest of CNS via the brainstem. There are also four cavities within the brain filled with *cerebrospinal fluid* (CSF), two lateral ventricles in each hemisphere and two in the brainstem.

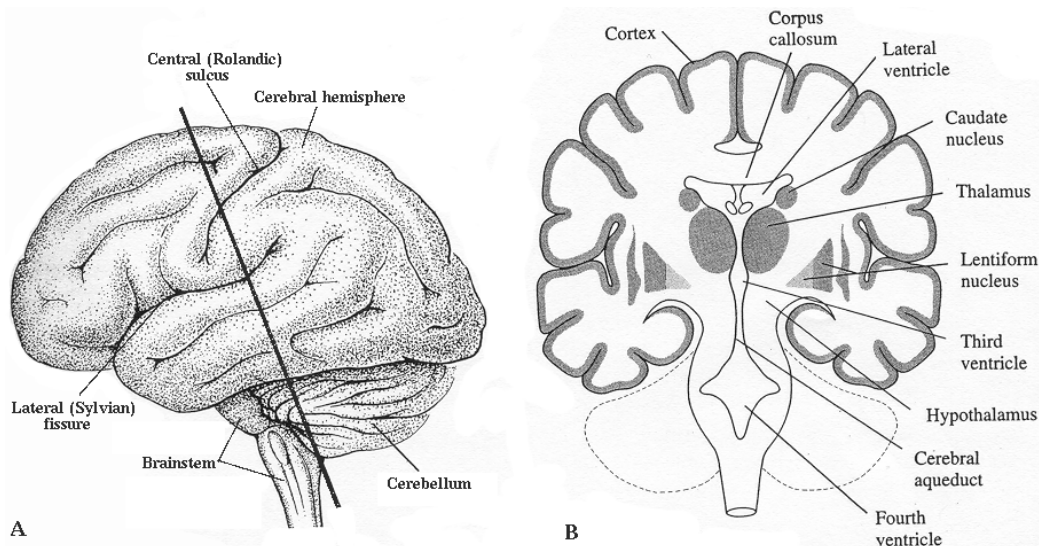


Figure 2.2: **A.** External view of the brain **B.** Cross-section cut through the brain

The internal organization of the brain is depicted in sections through the brain. The sectioning is usually done in one of three common anatomical planes: *sagittal*, *coronal* or *transaxial* (fig. 2.3). In brain imaging, the same planes are considered to describe the slice orientation.

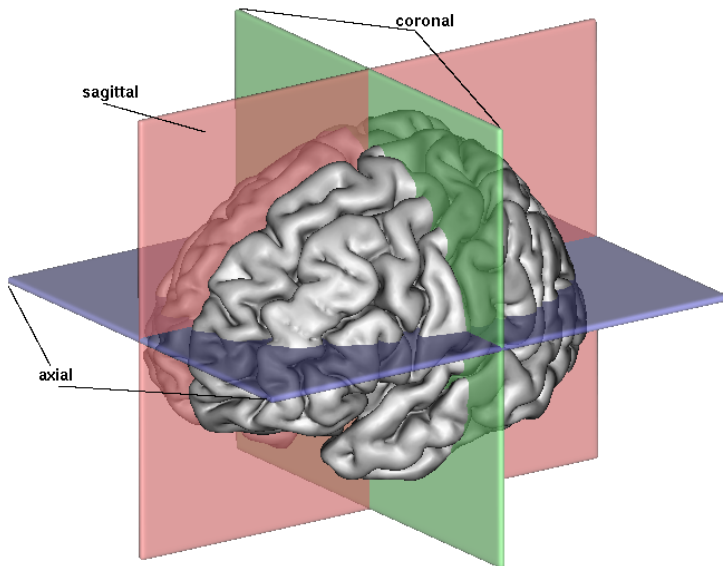


Figure 2.3: Section planes of the brain

2.1.2 Functional organization

The brain functions such as sensory perception and motor control, as well as “higher-order” functions like language and memory are located in the cerebral cortex. The functional organization of the cortex is only poorly understood, except for primary sensory and motor areas. The right and left cerebral hemispheres are very similar anatomically, but have different functional specialization. For example, the right hemisphere controls muscles on the left side of the body and vice-versa. The same applies to the sensory perception (tactile, auditory, visual), i.e. the input from the left or right side goes into contra-lateral hemisphere.

In order to describe the spatial organization of functional areas, some common gyri and sulci can be used as anatomical landmarks. There are two easily identifiable sulci, *central* and *lateral*, that are used to divide each cerebral hemisphere into four lobes: *frontal*, *parietal*, *temporal* and *occipital* (fig. 2.4). The frontal lobe contains primary motor and supplementary motor areas as well as Broca’s language area. The parietal lobe comprises primary and secondary somato-sensory areas. The temporal lobe processes auditory information, and is also involved in memory acquisition. A large part of parietal and temporal lobes contains the so called *association areas* that participate in the integration of multisensory information. Finally, the occipital lobe contains areas specialized in detection and processing of visual information.

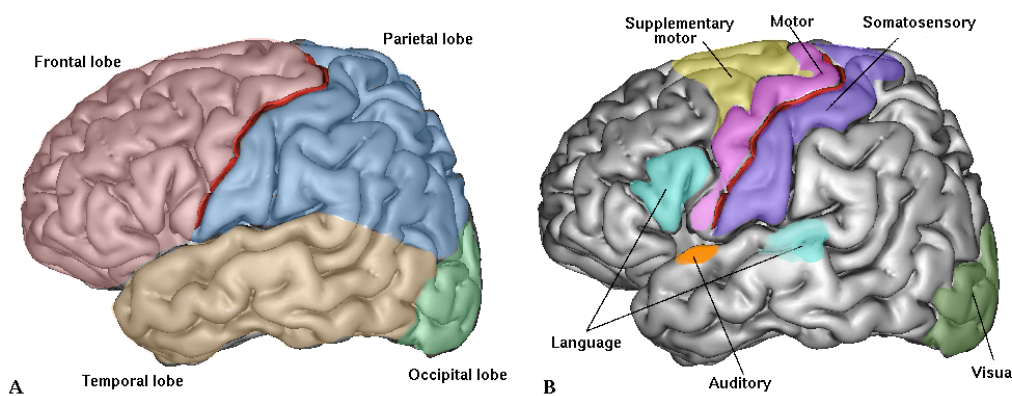


Figure 2.4: **A.** Brain lobes **B.** Primary functional areas

2.2 BOLD effect

Like any other organ of the body, the brain requires energy to perform its work. This energy comes mainly from oxydative metabolism of glucose by neurons and glial cells. Both glucose and oxygen are supplied by the blood. Local increase of neuronal activity requires higher glucose and oxygen metabolic rates (CMRGlc , CMRO_2), the demand which is met by local increases of cerebral blood flow (CBF) and cerebral blood volume (CBV). This close connection between cerebral activity and cerebral blood circulation was already observed over one hundred years ago by Roy and Sherrington [20] and now forms the basis of functional imaging methods like PET and fMRI [21].

In the first demonstration of functional imaging of the human brain by MRI [22], dynamic susceptibility-contrast imaging with intravenously administered paramagnetic contrast agent was used to detect regional blood volume changes under visual stimulation. Almost in parallel, another technique based on the level of blood oxygenation (BOLD) as endogenous functional contrast mechanism was developed [14, 23]. Currently, most brain activation studies are performed using the BOLD technique.

The bulk magnetic susceptibility of blood is mainly determined by the oxygenation state of the hemoglobin (Hb) molecules which contain four iron atoms [24]. Deoxygenated Hb is paramagnetic, while fully oxygenated Hb is diamagnetic. The presence of deoxy-Hb in a blood vessel causes a susceptibility difference between the vessel and its surrounding tissue. Such susceptibility difference cause additional protons' spin dephasing, leading to a reduced T_2^* of the tissue. Since oxy-Hb is diamagnetic and does not produce the same dephasing, changes in blood oxygenation can be observed as the signal changes in T_2^* -weighted images, such as gradient-echo EPI.

It would be expected that upon neuronal activation with associated increase of oxygen consumption, the concentration of deoxyhemoglobin in the blood would also increase, which would translate into a decreased MR signal. However, experiments show an increase of the MR signal implying that the blood becomes more oxygenated in activated areas. This apparent paradox is explained by a mismatch between an increase in oxygen consumption, which is only moderate, and a much larger increase in cerebral blood flow [25] (fig. 2.5). As a result, the blood becomes more oxygenated especially in the venular side of the capillaries. The exact reason for this CBF/ CMRO_2 mismatch remains unknown. One possible explanation is that a surplus of blood oxygenation creates a steeper oxygen concentration gradient between intra- and extravascular space which facilitates oxygen delivery into the brain tissue [26].

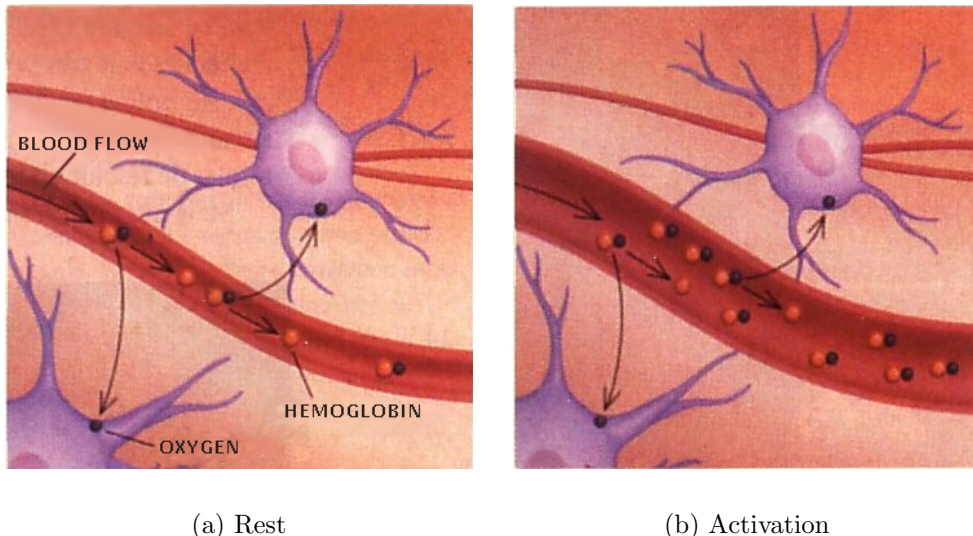


Figure 2.5: Physiological basis of fMRI (adapted from Raichle et al. [19])

2.3 BOLD fMRI

In a typical functional MRI experiment images from the same brain region are obtained repeatedly while the subject is executing some behavioral task. The task comprises a *resting* or *control* condition and one or more *activation* conditions. The images obtained under two different conditions are compared to detect which brain areas change their activity. So, the results of an fMRI experiment depend on three aspects: the scanning protocol, the design of the stimulus paradigm and the way image data is analyzed.

2.3.1 Scanning protocol

The activation-induced BOLD signal change can be measured with T_2^* sensitive gradient-echo sequences, using both conventional (GRE) and echo-planar (EPI) techniques. In most studies, EPI sequence is used because it allows large brain coverage with a temporal resolution of 2–3 s, while with GRE, only 1–3 slices can be obtained at the same time. The amplitude of the BOLD signal change is field dependent (greater susceptibility effect at higher fields). The observed percent signal change in activated primary brain areas at optimal echo-time for functional contrast ($TE \approx 40$ ms $\sim T_2^*$ of gray matter) is in the range of 1–5% at 1.5 T [27] and 5–20% at 4 T [28]. Most clinical scanners operate at 1.5 T and for reliable detection of a relatively small signal, a large number of images needs to be acquired. Typically 80 to

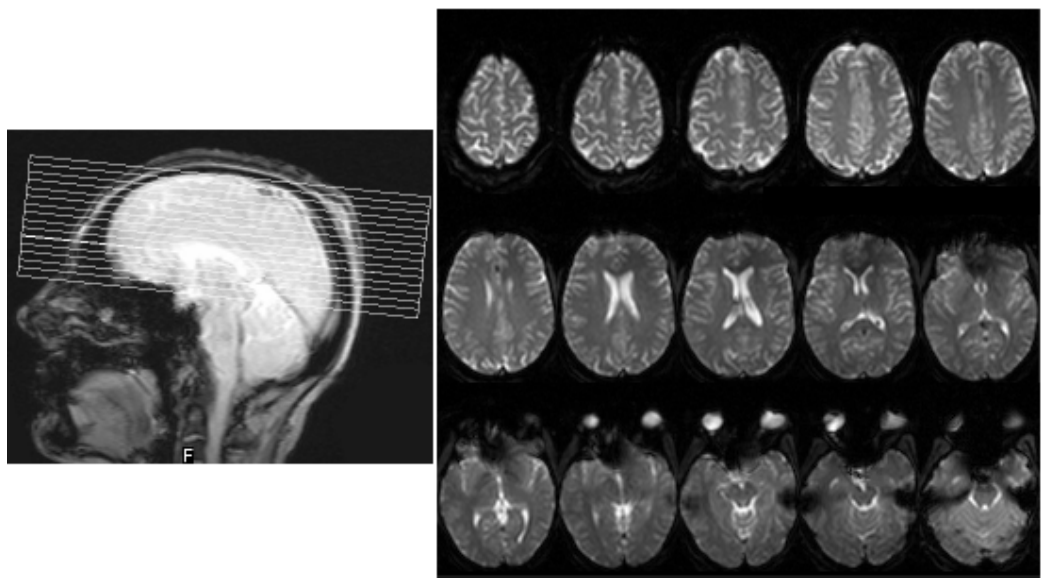


Figure 2.6: Typical EPI volume consisting of fifteen 5 mm slices.

150 brain images are obtained in a functional scan.

Spatial resolution is also an important factor for the BOLD contrast. Small voxels, allowing fine delineation of activation areas, are affected by low signal to noise ratio. On the other hand, larger voxels may have reduced BOLD contrast due to partial volume effects. At 1.5 T, EPI images of the brain (10–20 slices) are usually acquired with a slice thickness of 5–10 mm and an inplane resolution of 2–4 mm (fig. 2.6).

2.3.2 Stimulus paradigm

The stimulus or task paradigm are designed to answer a particular neurological or cognitive question which can be as simple as localization of primary motor or visual cortex or more subtle, like localization of areas involved in memory encoding. The MR scanner environment poses some restrictions on the type of stimuli that can be delivered to the subject. For example, gradient noise during image acquisition, makes it difficult to use auditory stimuli. Electronic devices for stimulation or collection of subject's responses must be tested against potential safety hazards and possible image artifacts.

Paradigm design of the first fMRI experiments was very similar to PET studies, that is two sets of images were acquired under resting and activation conditions in order to detect activation maps through image subtraction. However, since fMRI has a higher temporal resolution than PET, the paradigms have evolved to include temporal aspects of the BOLD signal

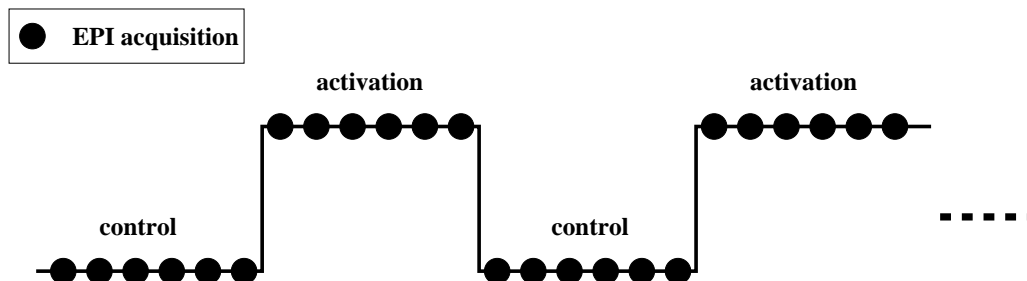


Figure 2.7: Block paradigm

changes upon activation. This allows a better differentiation between the true and spurious activation. The most commonly used stimulation paradigm is the *block* paradigm [29]. It consists of several cycles of alternating “on” and “off” epochs, for example, 4 or 5 cycles of 20 s of control condition followed by 20 s of activation condition (fig. 2.7). During this time, EPI images, such as in fig. 2.6 are acquired repeatedly every 2 to 3 seconds.

One aspect of the block paradigm, which is important for subsequent data analysis, is the duration of the activation and resting conditions. It was noted that the BOLD response takes 5–6 s from the beginning of the stimulation to reach the maximum and about the same time to return to baseline after the end of the stimulation [30]. The duration of the control condition should allow this return to the baseline before the following activation period begins.

The ability to follow dynamic vascular changes with BOLD fMRI raised a lot of interest in neuroscientific community and led to the development of new *event-related* (ER) paradigm designs. Instead of presenting epochs of stimuli lasting 10–20 seconds, it is possible to use brief (< 2 s) stimuli in a way similar to EEG or MEG evoked-potential studies. Even very short stimuli (events) of 10–20 ms produce characteristic BOLD responses that can be detected even at 1.5 T [31, 32], but usually the stimulus duration of about 1 second is used. Event-related paradigms can be designed in two ways, by using either a constant or a variable (randomized) inter-stimulus interval (ISI). Paradigms with constant ISI usually require more image acquisitions than with variable ISI, but the data analysis is easier and requires less assumptions about the BOLD response form [33, 34].

Compared to block paradigms, event-related paradigms provide much more flexibility for the design of complex behavioral tasks and don’t suffer from factors such as habituation or anticipation. On the other hand, fMRI data from event-related experiments is more difficult to analyze and has a lower functional contrast than in block-designed experiments [34].

2.3.3 Data analysis

The goal of an fMRI experiment is to obtain functional activation maps representing brain's response to a given stimulus paradigm. The detection of activation is done by voxel-wise time-series analysis of the images acquired during the experiment.

Prior to the actual statistical analysis, several pre-processing steps are usually performed to remove major sources of artifacts from fMRI data. Probably the most important step is realignment of image volumes to correct for subject's head movements during the experiment. This problem is covered in details in Chapter 3. Similar to image registration, but actually a different problem, is spatial image normalization, where images are brought into the same anatomical space (e.g. Talairach) in order to compare activations from different groups of subjects. Another important pre-processing step is slice-timing correction [35]. Indeed, since volumetric images are obtained using multi-slice EPI, and each slice requires ~ 100 ms of acquisition time, there is an unequal delay between the stimulus onset and the acquisition of particular slice. Other common pre-processing procedures include removal of linear order signal drifts (temporal high-pass filtering) and spatial smoothing of the data to improve the signal to noise ratio [36]. It is worth noting that the amount of storage memory needed for fMRI data processing can be substantial. An fMRI run consisting of 20 slices reconstructed with 128×128 matrix (16 bits/pixel) and repeated 100 times requires 62.5 megabytes. It is not uncommon to save the results of preprocessing operations as new files.

Many statistical procedures have been proposed for analyzing fMRI data. The most frequently used methods are parametric or model driven procedures such as cross-correlation analysis [29], Student's two-sample t statistics and general linear model [37, 38]. The results of these procedures are often referred to as statistical parameter maps (SPM) from which the probability of activation under given hypothesis can be computed. Other methods that do not require prior knowledge about the activation paradigm include principal/independent component analysis (PCA, ICA) [39], and fuzzy clustering techniques [40]. A brief description and comparison of nine different methods of fMRI analysis can be found in [41].

Most of the fMRI results of studies presented in this thesis were obtained using Student's t -test and correlation analysis. The software tools needed for this analysis were implemented in IDL programming environment (Research Systems Inc., Boulder, USA).

The Student's t -test is the standard method to evaluate the differences in means between two groups. It can be easily applied to find significant differences in pixel intensities between activation and rest conditions in block designed fMRI data. The t -score map is calculated for each brain voxel using its time-course \vec{X} by the following formula:

$$t = \frac{\bar{X}_1 - \bar{X}_2}{\sqrt{S_p^2/N_1 + S_p^2/N_2}} \quad (2.1)$$

where S_p is the pooled variance

$$S_p^2 = \frac{\sum(X_1 - \bar{X}_1)^2 + \sum(X_2 - \bar{X}_2)^2}{N_1 + N_2 - 2}$$

The indices 1 and 2 refer to the N_1 and N_2 images acquired during the activation and control periods accordingly. For N_1 and N_2 greater than 30, Student's t -test follows normal gaussian distribution of null mean and variance 1, and t -scores can be referred to as z -scores¹. The activation maps are obtained by selecting pixels having a t -score greater than a cut off value t_c corresponding to the desired probability (p -value) of significant difference.

A very similar activation map can be obtained by correlation analysis between each pixel time-course \vec{X} and a square wave reference function representing activation/control cycles \vec{Y} :

$$cc = \frac{\sum_{i=1}^N (X_i - \bar{X})(Y_i - \bar{Y})}{\left[\sum_{i=1}^N (X_i - \bar{X})^2 \right]^{1/2} \left[\sum_{i=1}^N (Y_i - \bar{Y})^2 \right]^{1/2}} \quad (2.2)$$

where N is the total number of images in the fMRI run. The reference function is usually shifted by 4–6 s to account for the hemodynamic (BOLD) response delay. Again, some threshold condition, for example $cc \geq 0.45$, is used to select activation pixels. The probability that a pixel's time-course is correlated with the reference function can be derived from the equivalent z -score:

$$z = \frac{cc\sqrt{N-2}}{\sqrt{1-cc^2}} \quad (2.3)$$

The advantage of the correlation analysis over the t -test is that the reference function can be chosen to reflect a more realistic expected response. For example, the square stimulus waveform can be convoluted with an estimate

¹ z is a central reduced variable

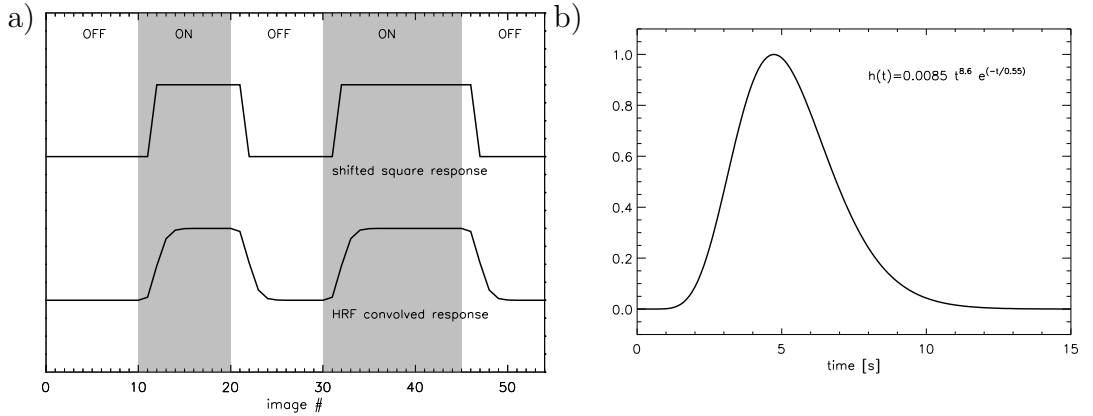


Figure 2.8: a) Example of reference functions for correlation analysis b) Hemodynamic response model

of the hemodynamic impulse response (fig. 2.8 a), which can be obtained from an event-related fMRI study [42]. The hemodynamic response function (HRF) is often modeled as a 3 parameter gamma-variate function (fig. 2.8 b):

$$h(t) = At^b e^{-t/c} \quad (2.4)$$

where A can be adjusted to give the BOLD response amplitude, and the parameters b and c determine the hemodynamic delay (given by the product bc) and the width of the response.

Analysis of the event-related fMRI data depends mostly on the stimulus paradigm. Data from constant inter-stimulus interval experiments can be analyzed by fitting trial averaged time-courses to an HRF model such as eq. (2.4). For randomized inter-stimulus experiments, deconvolution [43] and GLM [44] methods can be applied. Also, it is not uncommon to perform both block and event-related experiments using the same stimulus during the same scanning session, and to analyze the ER-fMRI data only in the regions of interest (ROI) found in block-designed experiment.

2.3.4 Visualization

The results of statistical analysis are usually presented as color-encoded maps superimposed on a high-resolution anatomical images (fig. 2.9). However, one must be aware of possible spatial distortions of the EPI images which may result in small displacements between activation areas and underlying anatomy [16].

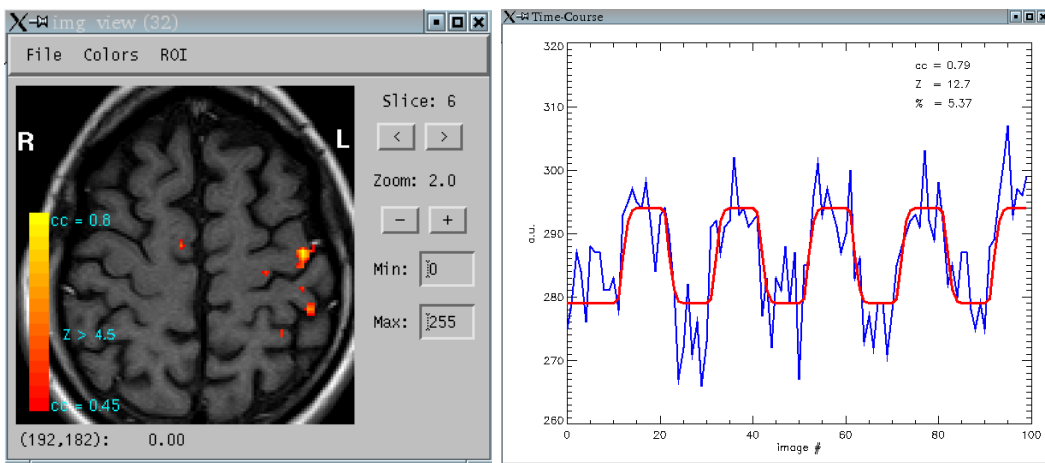


Figure 2.9: Z-score activation map (right-hand finger tapping) and an activation pixel time-course

Instead of showing statistical information, it is possible to display other information extracted from activated pixels time-courses, for example BOLD signal amplitude expressed as percent signal change relative to the rest condition. This can help to discard spurious activated pixels on the basis of larger than expected signal change. The visual quality of “functional” maps can be enhanced by discarding stand-alone or small clusters of activated pixels.

With ER-fMRI data, it is also possible to create activation maps, representing temporal information, for example time to peak of the hemodynamic response.

2.4 fMRI applications in Epilepsy

Functional MRI is quickly becoming a method of choice for non-invasive studies of the human brain function under both normal and pathological conditions. Currently, it is still considered a research tool and a lot of work is being done to gain more insight into the nature of the BOLD signal in relation to brain’s physiology, improvements of experimental designs and data analysis methods. Potential clinical applications are numerous, but before fMRI becomes a diagnostic tool, many large population validation studies have to be performed.

Functional MRI can become a very useful tool in presurgical evaluation of patients with epilepsy. The possibility of precise epileptic focus localization using fMRI is a very promising application. In contrast to common stimulus

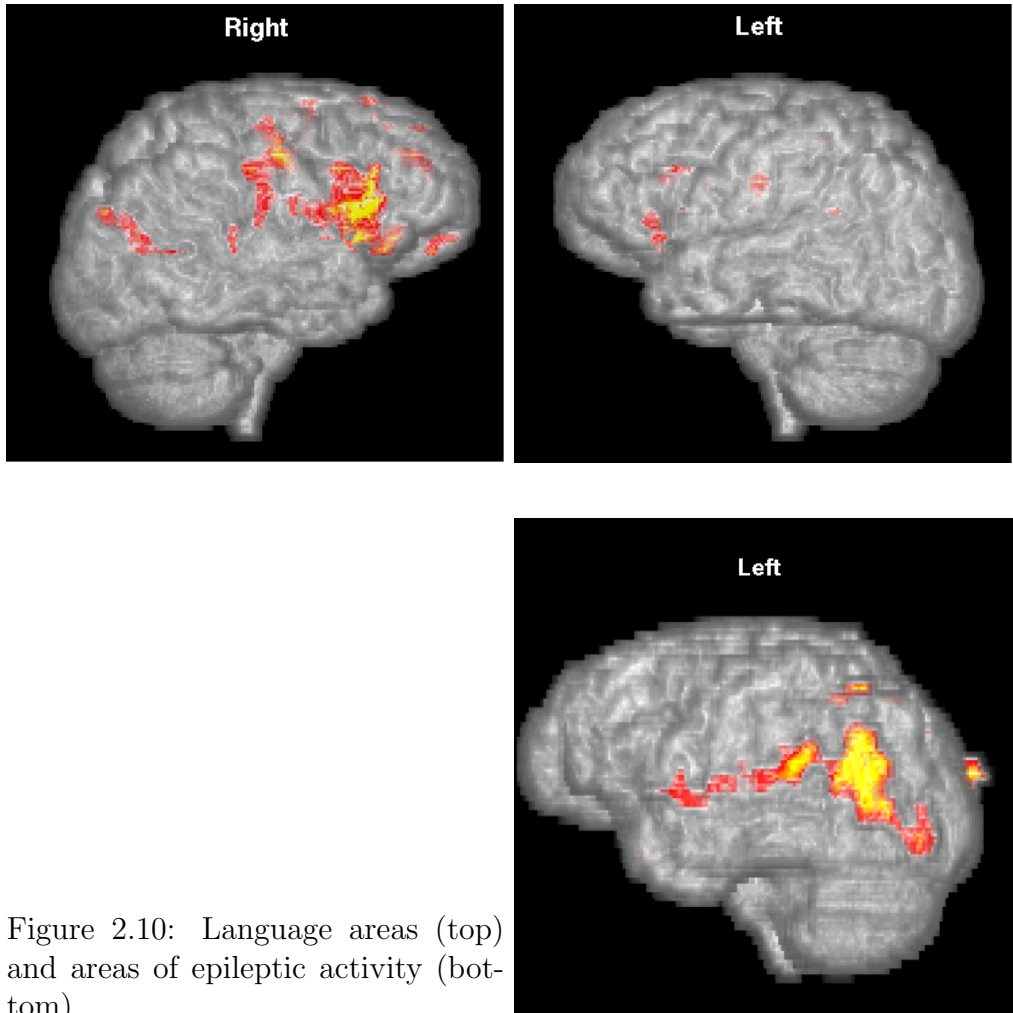


Figure 2.10: Language areas (top) and areas of epileptic activity (bottom)

driven fMRI studies, described in this chapter, focus localization with fMRI is based on EEG recording of epileptic activity in the scanner. The details of “epileptic activation” fMRI studies are given in chapter 5 of this thesis.

Standard fMRI studies can also be very helpful during presurgical evaluation. They can be used to determine functionally viable brain areas (e.g. motor, sensory, language) which is useful for both operation planning and evaluation of postoperative functional deficit [45, 46]. As an example, figure 2.10 shows the results of a language lateralization fMRI study in a patient with an epileptic focus located in the left hemisphere. Localization of language areas in the right hemisphere indicate that the resection of epileptic focus is unlikely to affect language function in this patient.

Chapter 3

Motion Correction in fMRI

Subject motion during an MRI exam is usually a source of artifacts which affects the diagnostic value of images or compromises results of image analysis procedures. Motion occurring during image acquisition results in image blurring and ghosting. This usually happens with high resolution anatomical images that require long acquisition time. Functional imaging, performed with fast scanning techniques such as EPI, is usually not affected by these artifacts. The problem of fMRI is the motion that occurs between successive image acquisitions which invalidates voxel based statistical analysis of image time-series.

There are several approaches to the problem of subject motion. First, head fixation using straps, vacuum cushions or bite bars can be used to reduce motion. However, total immobilization is not possible as it may greatly compromise patient comfort and security. Second approach, described in this chapter, consist in retrospective motion correction using image registration techniques. Finally, there are prospective motion detection and correction techniques consisting of real-time motion tracking and updating of scanner's parameters that control imaging field of view. Motion is detected using either navigator echos [47, 48] or some external detection system [49, 50]. This is probably the best solution for the problem of subject motion, but it is still unavailable on most clinical MR systems.

3.1 Image registration

Image registration is a necessary stage for numerous medical imaging applications. In neuroscience in particular, registration is needed for multi-modality image fusion, detection of brain changes over time, creation of brain atlases and statistical analysis of image time-series. Often, depending on the

application and the type of image data, the registration problem requires a specific solution. For example, an algorithm to align images from the same subject will be very different from the one needed to align images from different subjects. The description of modern image registration methods for neuroscience applications can be found in several recent review articles [51, 52, 53]. Despite the differences, there are many common features in all registration algorithms and the general strategy can be described as follows: choose a reference image, find a spatial transformation that matches a test image to the reference using some kind of similarity measure and apply the transformation to the test image to obtain intensity values at new voxel positions.

3.1.1 Transformations

Registration of images obtained from the same subject, like in fMRI or PET studies, is usually done using rigid-body model. In three dimensions, rigid registration requires six parameters: three translations and three rotations. These transformations are global and linear and can be represented in a matrix form. In this formalism any spatial transformation can be expressed as a single matrix obtained by simple matrix multiplication. In order to combine translations and rotations into a single matrix, 4×4 homogeneous transformation matrices are used to encode a three-dimensional transformation [54].

The mapping of each voxel in the test image $\mathbf{f}(x_1, x_2, x_3)$ into the reference image space $\mathbf{g}(y_1, y_2, y_3)$ can be expressed as:

$$\vec{y} = \mathbf{M}\vec{x} \quad (3.1)$$

or in the matrix form

$$\begin{pmatrix} y_1 \\ y_2 \\ y_3 \\ 1 \end{pmatrix} = \begin{pmatrix} m_{11} & m_{12} & m_{13} & m_{14} \\ m_{21} & m_{22} & m_{23} & m_{24} \\ m_{31} & m_{32} & m_{33} & m_{34} \\ 0 & 0 & 0 & 1 \end{pmatrix} \begin{pmatrix} x_1 \\ x_2 \\ x_3 \\ 1 \end{pmatrix} \quad (3.1')$$

If the voxel sizes of the images \mathbf{f} and \mathbf{g} are both identical and isotropic, then \mathbf{M} can be parametrized in terms of rotations around and translations along the the three coordinate axes. However, in most fMRI studies, images are acquired with anisotropic voxels which need to be considered for performing rigid body registration. Instead of resampling images to obtain cubic voxels, affine transformations that map from voxel coordinates into Euclidean space are included into \mathbf{M} :

$$\mathbf{M} = \mathbf{M}_g^{-1} \mathbf{M}_r \mathbf{M}_f \quad (3.2)$$

where \mathbf{M}_f maps the test image voxels to a Euclidean space with the origin in the center of the image, \mathbf{M}_r is the rigid-body transformation, and \mathbf{M}_g^{-1} maps from the Euclidean space into reference image voxel coordinates. In terms of basic homogeneous transformation matrices, eq. (3.1) becomes:

$$\vec{y} = (\mathbf{S}_g^{-1}\mathbf{T}_g^{-1})(\mathbf{T}\mathbf{R}_x\mathbf{R}_y\mathbf{R}_z)(\mathbf{T}_f\mathbf{S}_f)\vec{x} \quad (3.3)$$

where \mathbf{S} represent scaling,

$$\mathbf{S} = \begin{pmatrix} s_1 & 0 & 0 & 0 \\ 0 & s_2 & 0 & 0 \\ 0 & 0 & s_3 & 0 \\ 0 & 0 & 0 & 1 \end{pmatrix}$$

\mathbf{T} – translations,

$$\mathbf{T} = \begin{pmatrix} 1 & 0 & 0 & d_1 \\ 0 & 1 & 0 & d_2 \\ 0 & 0 & 1 & d_3 \\ 0 & 0 & 0 & 1 \end{pmatrix}$$

and \mathbf{R} – rotations

$$\mathbf{R}_x\mathbf{R}_y\mathbf{R}_z = \begin{pmatrix} 1 & 0 & 0 & 0 \\ 0 & \cos(r_1) & \sin(r_1) & 0 \\ 0 & -\sin(r_1) & \cos(r_1) & 0 \\ 0 & 0 & 0 & 1 \end{pmatrix} \begin{pmatrix} \cos(r_2) & 0 & \sin(r_2) & 0 \\ 0 & 1 & 0 & 0 \\ -\sin(r_2) & 0 & \cos(r_2) & 0 \\ 0 & 0 & 0 & 1 \end{pmatrix} \begin{pmatrix} \cos(r_3) & \sin(r_3) & 0 & 0 \\ -\sin(r_3) & \cos(r_3) & 0 & 0 \\ 0 & 0 & 1 & 0 \\ 0 & 0 & 0 & 1 \end{pmatrix}$$

$\mathbf{S}_{f,g}$ account for voxel anisotropy in the test and reference images and $\mathbf{T}_{f,g}$ translate the origin of the coordinate space to the center of the images.

3.1.2 Image resampling

During the process of registration, successive spatial transforms are applied to the test image until some matching criteria with the reference image is achieved. As with any digital signal, this procedure requires image resampling in order to obtain intensity values at new voxels locations. Image resampling is usually implemented using backward projection technique, where each voxel in the new image space is mapped back into the original image space using the inverse transform (\mathbf{M}^{-1}), and the intensity is determined by interpolation from neighboring pixels (fig. 3.1).

The choice of the interpolation model is always a tradeoff between the quality of the resulting image and the computation cost. For example, the

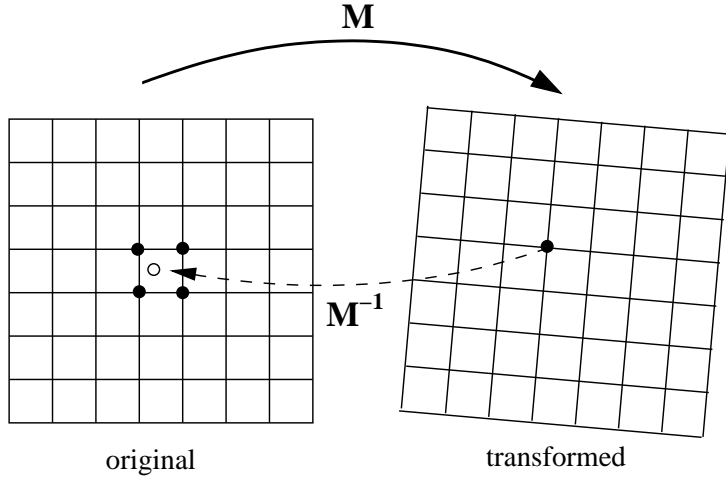


Figure 3.1: Bilinear image interpolation

simplest, so called zero-order approach is to take the value of the nearest neighboring voxel. It is very fast and preserves the original voxel intensities, but the resulting image quality is considerably degraded because several voxels can be assigned the value of the same voxel in the original image. Better results can be achieved using linear interpolation. This is slightly slower than nearest neighbor, because eight points (in 3D) are needed to estimate each new voxel's intensity. However, linear interpolation has the effect of losing some high frequency information from the image (image blurring). The result gets better when more neighbours and higher polynomial function are used for intensity estimation, but at the expense of the computation time.

The optimum method for applying rigid body transformation with minimal interpolation artifact is to do it in Fourier space. In image space, the same result can be achieved using *sinc* interpolation. For exact reconstruction of a band-limited signal, such as an MR image, all the original data should be used to obtain the value of a single point. This is usually not feasible due to computational cost, and in practice, interpolation is done over a limited range of neighboring voxels. Errors due to truncation of the *sinc* function are minimized by using appodizing Hanning window function [55]:

$$\mathbf{f}(X_1, X_2, X_3) = \sum_{x_1} \sum_{x_2} \sum_{x_3} \mathbf{f}(x_1, x_2, x_3) S(x_1, X_1, R_1) S(x_2, X_2, R_2) S(x_3, X_3, R_3) \quad (3.4)$$

with

$$S(x, X, R) = \frac{\sin(\pi|x - X|)}{\pi|x - X|} \cdot \frac{1}{2} \left(1 + \cos\left(\frac{\pi|x - X|}{R}\right) \right)$$

where X_i are noninteger coordinates in the original image space corresponding to integer location in the transformed image, and R_i are interpolation ranges along the three directions. Implementation of *sinc* interpolation can be done more efficiently than eq. (3.4) because the function is separable and interpolation can be performed sequentially one dimension after another, which brings the computation cost from $\mathcal{O}(R^3)$ to $\mathcal{O}(R)$. Another approach, more efficient and probably more accurate than windowed *sinc* is to use cubic B-splines as interpolating functions [56].

3.1.3 Optimization

Image registration requires determination of the spatial transformation that maps a test image to a reference image. This can be done manually using either external markers or anatomical landmarks. Another approach is to determine the transformation parameters using automatic registration techniques [57, 58]. The problem with manual registration is that it is very time consuming, especially when large data sets consisting of tens or hundreds of volumes need to be aligned. Moreover, it is unlikely to be suitable for matching images with subvoxel accuracy.

Any automatic registration method is based on the choice of a criterion that measures the degree of similarity between the two images, also called *cost function*, and an optimization strategy that maximizes the similarity with respect to the transformation parameters. Instead of similarity one can define a *cost function* as a disparity measure and try to minimize it. If \mathbf{g} denotes the reference image and \mathbf{f} is the test image, the problem can be stated as:

$$\mathbf{g}(\vec{x}) = Q_p[\mathbf{f}(\vec{x})] + e(\vec{x}) \quad (3.5)$$

where $Q_p[f]$ is the transformation (including interpolation method) specified by a parameter vector (p_1, \dots, p_6) and $e(\vec{x})$ is the error term estimated through the *cost function*. The task of determining the values of transformation parameters p_i that minimize $e(\vec{x})$ is a classical example of nonlinear least-squares optimization problem. A natural choice for the *cost function* is the sum of squared differences between the two images [55, 58, 59]:

$$\chi_p^2 = \sum_{\text{voxels}} \frac{(\mathbf{g}(\vec{x}) - Q_p[\mathbf{f}(\vec{x})])^2}{N_{\text{voxels}}} \quad (3.6)$$

where N_{voxels} is the number of voxels used in calculations. Other examples of *cost functions* are image ratio [57] and mutual information [60].

Optimization problems are solved by iterative procedures such as Gradient-search or Marquardt-Levenberg and because of large amount of data, they

are very computationally demanding. In order to increase the computational speed, a multiresolution approach have been proposed [59, 61]. The optimization starts with low resolution images to achieve gross registration, and then registration is refined on progressively higher resolution images. This approach also helps to avoid the problem of local minima of the *cost function*.

3.2 Effect on fMRI activation areas

During an fMRI session a series of brain images is acquired. Extracting functional information from these series of images is done by applying statistical time-series analysis, which assumes that the location of a given voxel within the brain does not change over time. However, subject motion during the examination (~ 5 min), which is virtually impossible to avoid, invalidates the assumption that the primary source of time-series signal variation is due to intrinsic brain activity. Therefore, motion correction is a necessary preprocessing step before the actual functional analysis.

Several image registrations algorithms allowing automatic motion detection and correction of functional images have been proposed [58, 62, 63]. Considering small signal changes typically observed in BOLD fMRI, there are two important issues with a registration procedure: accurate detection of small movements and preservation of voxel intensities when applying a transformation. Evaluation of a registration procedure accuracy is usually done using simulated data. It is equally important to asses the accuracy using real fMRI data, but the task is more difficult because there is no gold standard that can be used for comparison.

3.2.1 Methods

The effects of motion correction on fMRI activation areas were studied using Automated Image Registration algorithm (AIR)[64], which was found adequate for motion correction of fMRI data sets [65].

To study the effects of motion and its correction, we performed a simple finger-tapping fMRI study with four normal, right-handed volunteers. Each subject performed the task two times, one while the head was fixed to the scanner head holder with bandages, so that the head motion was reduced, and another with the head free, allowing some gross motion. The images were acquired on a 1.5 T clinical scanner (Eclipse, Marconi Medical Systems, USA) using single-shot gradient-echo EPI (TE=40 ms, flip angle=90°, FOV=27 cm, 128 × 128 matrix). Ten contiguous axial slices (5 mm thickness, no gap) covering the primary motor cortex were acquired repeatedly with a TR of

2 s. The functional protocol consisted of 5 blocks of “resting / activation” conditions with each condition lasting 20 s (10 volumes per condition).

For each subject, three functional activation maps were obtained from head-fixed condition, head-free condition before motion correction and head-free after motion correction. fMRI analysis was done using cross-correlation between brain voxels’ time-courses and a shifted (2 and 3 time points) boxcar function as the reference [29]. Activation areas were determined using a correlation threshold of 0.5 and discarding stand-alone “activated” pixels. Detection of motion parameters was done using *alignlinear* program from the AIR (v. 3.08) package with the following options: 3D rigid body transformation model (-m 6), least-squared cost function (-x 2), convergence threshold (-c) = 10^{-3} , image threshold (-t1, -t2) = 10% of maximum intensity. Images were resampled using *reslice* program with trilinear and 2D sinc (8×8 kernel) interpolation.

3.2.2 Results

The motion parameters found by AIR showed that in the fixed head condition, the maximum rotation angles were usually $\leq 0.2^\circ$ and translations ≤ 0.2 mm, while in the free head condition, the rotation angles were $\leq 3^\circ$ and translations ≤ 1 mm. Figure 3.2 shows the degree of motion of one subject,

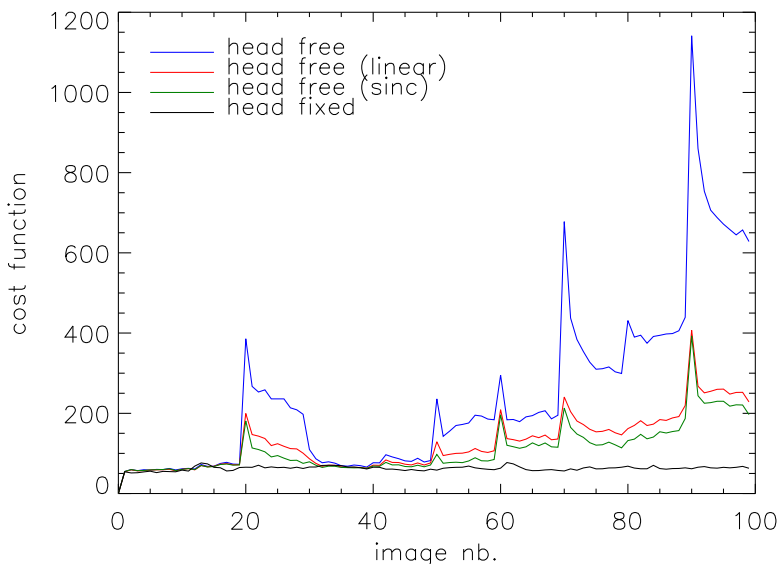


Figure 3.2: Degree of motion in fMRI image series.

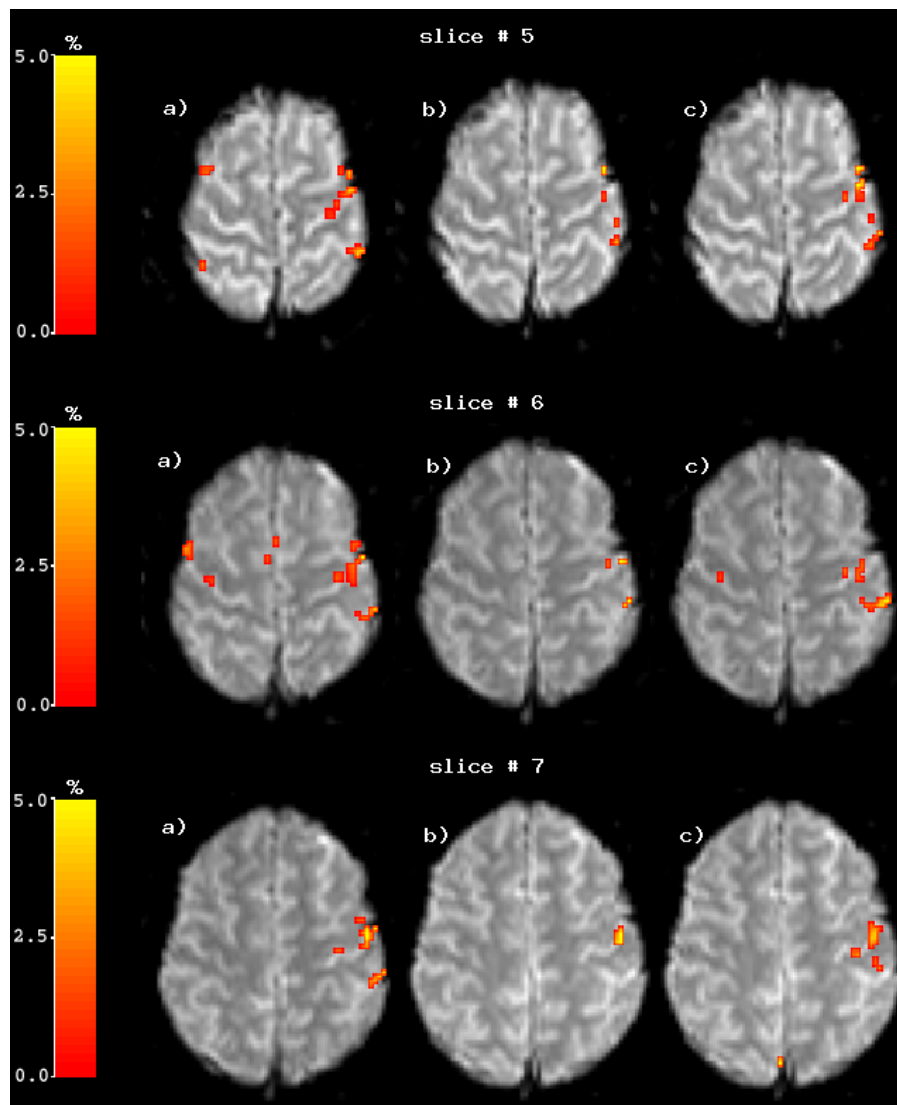


Figure 3.3: Activation maps (a) head-fixed (b) head-free before motion correction (c) head-free after motion correction

estimated through the cost function (χ^2), during the fMRI experiments in the head free and fixed conditions, before and after motion correction. In the fixed head condition, there is a small, but fairly constant missalignment between the first image (reference image) and the rest of the image series, while in the free head condition, image missalignment is greater and more variable. Applying motion correction allows to reduce the degree of motion, however the alignment is not perfect. The use of higher order interpolation leads to slightly better results, but the effects are relatively small.

Figure 3.3 shows the results of the fMRI analysis from the same subject whose motion history is shown in fig. 3.2. Compared to the head fixed condition, subject’s motion during head free condition reduces considerably the size of the activated areas. After motion correction (linear interpolation) of the head-free data, the activation areas look similar to those obtained in the fixed head condition. Considering the size of activation in the fixed head condition as the gold standard, we can compute how much “functional” information is lost due to motion, and how much can be recovered by applying motion correction. Table 3.1 summarizes these results for all the subjects. On average, only 25% of activated pixels are present before the motion correction, and applying the correction allows to recover up to 80% of activation. The activation maps obtained from motion corrected data, resliced with sinc interpolation, were identical to those, obtained with linear interpolation.

Subj #	before MC	after MC
1	43%	78%
2	13%	100%
3	39%	72%
4	27%	81%

Table 3.1: Activated areas before and after motion morrection.

3.2.3 Discussion

Subject’s head motion during an fMRI exam leads to substantial loss of functional information. Post-processing motion correction algorithms, such as AIR, are quite effective at restoring this information, despite the fact that correction is not always perfect. The reason why the use of sinc interpolation didn’t improve the effect of motion correction on fMRI results is due to a particularity of AIR implementation. For computational speed considerations, linear interpolation is used during detection of motion parameters, and if this step fails, the use of higher order interpolation for final image resampling is not useful.

There are several reasons why motion correction algorithms (not only AIR) may fail to detect true motion of some fMRI images. If motion happens during the acquisition of an EPI volume, the slices will not be parallel to each other, and it will be impossible to align this volume to the reference one. Another reason is when motion is relatively large, previously unexcited parts of the brain are moved into the imaging field of view and create large intensity changes, thus introducing additional errors into intensity-based cost

function [66]. Because this mainly affects the first and the last slice of the acquired volume, it may be useful to ignore these slices for computation of the cost function. Finally, because brain activation itself produces small intensity changes, it can lead to incorrect motion detection even in the absence of the real motion [67]. This issue is not so important at 1.5 T, because the BOLD signal change is very small. However, since the BOLD signal is field dependent, this problem can become more important at 3 T and higher fields.

Despite the above issues, motion correction is a necessary preprocessing step for functional data analysis. Although head fixation is useful to minimize movements, it only works well with cooperating healthy subjects, and even in this case, it can not guarantee motion-free data sets.

Chapter 4

Feasibility of simultaneous EEG-fMRI recording

Simultaneous acquisition of electroencephalogram (EEG) and functional MRI has a great potential as a new tool to investigate human brain under normal and pathological conditions. Combination of high temporal resolution of EEG and spatial resolution of MRI may provide new insights into spatio-temporal characteristics of the coupling between brain electrical activity and associated metabolism which is still largely unknown [68]. The two main applications of concurrent EEG/fMRI acquisition are: 1) obtaining fMRI activation maps using EEG signal as a reference in order to localize intrinsic brain activity, for example activity of epileptogenic regions or generators of α -rhythm, and 2) using fMRI maps to gain better understanding of the link between electrical generators and the EEG signal measured on the surface of the head.

Concurrent EEG/MRI recording raises however a number of technical issues. These are patient safety, EEG quality and MR image quality. These issues are covered in detail in this chapter after a short description of our MRI compatible EEG system.

4.1 EEG recording inside an MRI scanner

The MRI environment imposes some restrictions on the presence of electronic devices inside the magnet. In particular, ferro-magnetic materials present a serious safety hazard because of their movement in the magnetic field and potential heating, and also, they affect the magnetic field homogeneity which may decrease the image quality. Active electronic components, such as filters or amplifiers, may generate interfering RF that could also decrease

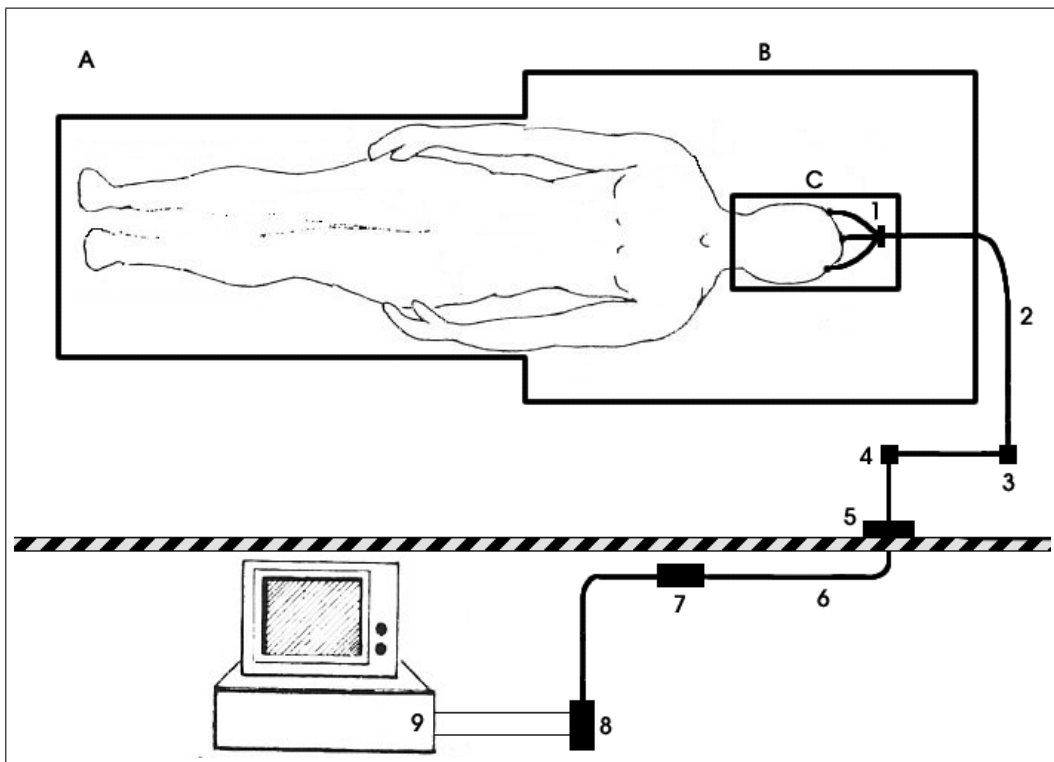


Figure 4.1: Schematic representation of patient EEG recording inside an MR scanner (adapted from Ives et al. [69]).

the diagnostic quality of the images.

The EEG device that we use inside our 1.5 T scanner has been developed by J. R. Ives from Beth Israel Hospital, Boston (USA) [69]. The system components and cable layout are schematically represented in fig. 4.1 showing an MRI unit in a shielded room (A) and a patient positioned for a typical head imaging protocol (head at the isocenter of the magnet (B), head coil (C) for MR signal detection). Patient's EEG is recorded from 18 gold or silver-chloride surface electrodes with 30 mm standard Grass wires (1) connected to a 2 m extention cable (2) that allows to move all electronic components outside of the magnet's bore. This cable is plugged into a 18-channel preamplifier/multiplexor assembly (3) that sends the multiplexed analog signal into a power pack (4) containing data buffers and generating regulated ± 5 V to drive the preamplifiers from ± 12 V supplied from the wall box (5). The wall box contains also an electro-optical transceiver to sent the EEG signal via optical fibers (6) outside the shielded MRI room. This optical link is used to assure that the EEG system doesn't bring any RF noise inside the scanner room. The optical signal is converted back to analog in receiver (7), send

to 18-channel demultiplexor/amplifier (8) and finally digitized, recorded and displayed on a 64-channel EEG machine (Deltamed SA, France) (9).

4.2 Patient safety

Potential health hazards are of great concern with any patient monitoring devices that use electrically conducting materials inside an MRI scanner. In particular, heating of electrodes or cables due to induced currents by various electromagnetic fields may lead to burns. There have been reports of thermal injuries due to electrocardiogram and pulse oxymetry recordings [70, 71]. Another safety aspect, not discussed here, is that monitoring devices may hamper patient handling in case of an emergency [72].

In EEG recording, conducting loops are always present in order to measure potential differences on the head. Under normal conditions, the currents in these loops are limited by high impedance of the EEG amplifiers. However, low-impedance loops may be formed from two or more leads in direct electrical contact, a wire bending on itself or because of a failure of the EEG amplifier circuit. Currents in these loops can be induced by three different mechanisms: movement in the static B_0 field, application of time-varying gradients during imaging and application of the excitation RF field. The electro-motive forces induced in a conducting loop by these three mechanisms can be derived from Faraday induction law:

$$\begin{aligned} V_{B_0} &\sim B_0 \frac{dA}{dt} \\ V_G &\sim S_{max} z A \\ V_{RF} &\sim \omega_0 B_1 A \end{aligned} \tag{4.1}$$

where A is the loop area, S_{max} is the maximum gradient slew rate, z is the distance from the gradient coil isocenter and B_1 is the amplitude of the RF pulse.

In a theoretical article [73], the authors have considered the worst case scenarios for each of the three induction mechanisms, and using eqs. 4.1, found out that the most important risk factor is associated with the RF field. The use of current-limiting resistors of $13\text{ k}\Omega$ attached to the EEG electrodes was suggested to ensure patient's safety. However, the drawback of this approach is that additional resistors will lower the EEG signal and reduce the quality of the EEG recording. In addition, resistors may introduce susceptibility artifacts into MR images.

4.2.1 Temperature measurements

In order to address the question of safety with particular EEG equipment, it is necessary to perform temperature measurements of the electrodes under various MRI conditions. For our setup, we carried out these measurements in five healthy volunteers using four different MRI sequences [74]. The sequences were: echo-planar (EPI), gradient echo (GRE), spin echo (SE) and fast spin echo (FSE). The sequence parameters are listed in table 4.1. Only the first two, EPI and GRE, are usually employed in our fMRI protocol, while SE and FSE were used to measure the effects of higher RF load. Each MRI sequence is characterized by a specific absorption rate (SAR) value, which is an estimation of RF power deposition per unit mass of imaged object. The SAR depends on the subject's body weight, the sequence parameters, the type of RF pulses and the type of RF coil. The SAR value of each sequence was provided by the manufacturer according to the automatic RF calibration procedure. The FSE sequence was set up to use maximum allowable SAR value.

Name	TR [ms]	TE [ms]	Flip	NAV	Time [min]	SAR ^b [W/kg]
EPI	1200	40	90°	140	3.0	0.08 ± 0.01
GRE	167	4.7	90°	4	3.0	0.7 ± 0.02
SE	344	16	90°	2	3.0	1.0 ± 0.05
FSE ^a	6430	90	90°	4	3.0	2.6 ± 0.15

Table 4.1: Sequence parameters (NAV = number of averages, ^aecho train length = 32, ^bmean ± SD across subjects).

Temperature measurements were performed using a type-**K** thermocouple (Ni-Cr/ Ni-Al) which was placed under one frontal electrode. The thermocouple's tip was electrically isolated with a teflon tape. Actual thermometer (TES-1310, Electrical Electronic Corp.) wasn't fully MR compatible and had to be placed outside of the magnet's bore using an extention cable. We were not able to measure the temperature continuously, because of electrical currents induced in extension cable during imaging. Temperature was measured right before and after the MRI acquisitions. With each of the five volunteers temperature measurements were done with and without the EEG system. The measurements without the EEG system served as a control of our setup. An MRI sequence can cause a small skin temperature raise, but it should be below 1°C . An observation of high skin temperature raise would suggest that our measurements are impaired by currents induced in the thermocouple's wire during imaging.

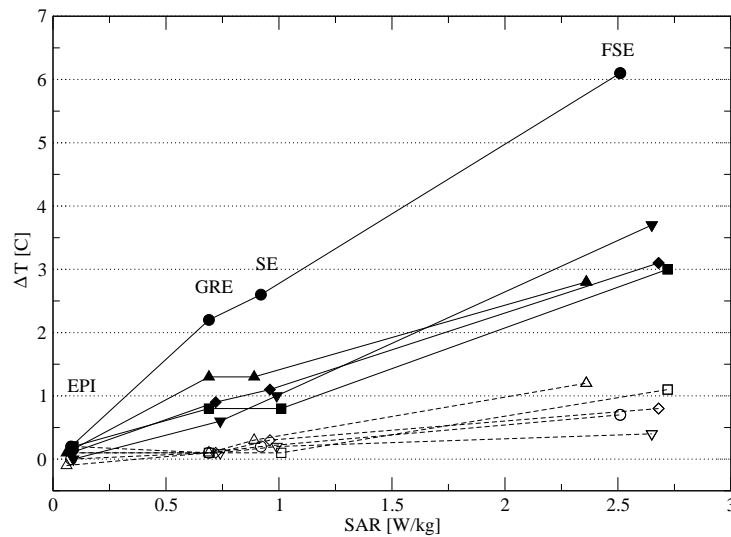


Figure 4.2: Temperature increase vs SAR in five volunteers. The open symbols correspond to measurements without the electrodes attached to the head.

Results

Results of the temperature measurements are presented in figure 4.2 which shows temperature increase vs. SAR value of used MRI sequences for all five subjects. Initial skin temperature was 33 ± 0.12 °C without the EEG system and 32.9 ± 0.3 °C with the EEG leads connected to subjects heads. As expected, with and without the EEG system, the highest skin temperature increase was observed when the FSE sequence was used. Without the EEG system, ΔT_{FSE} was found to be 0.84 ± 0.32 °C , for the SE and GRE sequences ΔT was under 0.5 °C , which can be considered negligible, and for the EPI sequence, no temperature rise was observed. This provided evidence that our temperature measurements were not affected by the MRI.

With the EEG system, ΔT_{FSE} was 3.74 ± 1.36 °C , with a peak value of 6.1 °C in one subject. For the SE and GRE, mean temperature increase was 1.4 ± 0.7 °C and 1.2 ± 0.6 °C respectively, and for the EPI sequence the increase was again negligible (< 0.2 °C). These results show that the heating the EEG electrodes under different MRI conditions do not exceed the safety limits (41 °C), even under the worst SAR conditions.

Up to the present, we have performed about 50 combined EEG/fMRI studies and had no complains about discomfort or feelings of heat. Currently, several groups are performing simultaneous EEG/MRI experiments

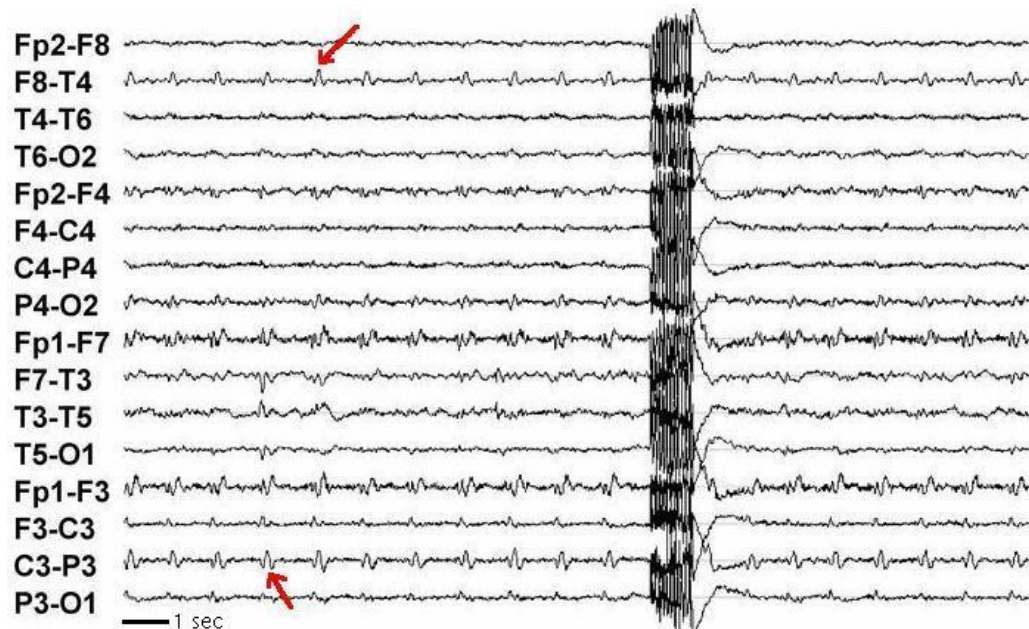


Figure 4.3: Ballistocardiogram (arrows) and an EPI image acquisition artifacts on the EEG recording inside the MR scanner.

and there were no reports of associated patient injuries. Successful EEG/MRI experiments at 3.0 T have also been reported [75, 76]. However, EEG/MRI remains an uncommon procedure and it is crucial to ensure patient safety with the particular EEG equipment introduced into an MRI scanner.

4.3 EEG quality

Successful EEG/fMRI experiment requires good quality EEG recording allowing detection of the EEG events of interest. As mentioned in the previous section, when EEG leads are placed inside an MRI scanner, magnetic gradient fields, radio-frequency pulses and motion of the leads in the static field induce voltages that obscure the EEG signal. Even small motion related to the heart beat yields ballistocardiographic artifact in the EEG that can have the same amplitude as the EEG signals of interest in some channels (fig. 4.3). Several methods have been proposed to deal with the artifacts due to gross and small head motion [77, 78].

The most disturbing artifact is due to magnetic gradient switching used during image acquisition. It affects all the EEG channels making them completely unreadable. In a typical fMRI study (block or event-related design),

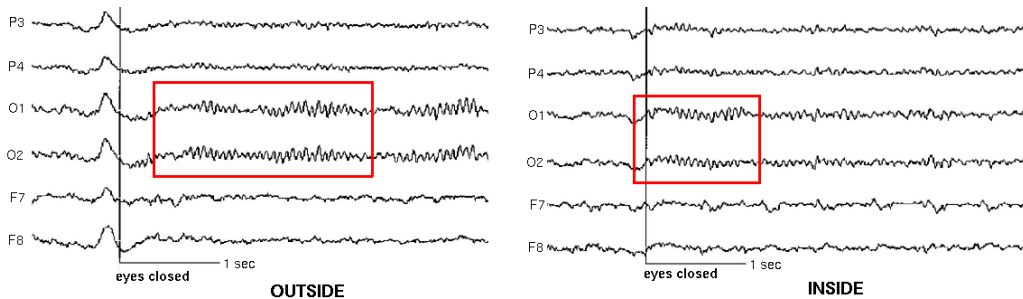


Figure 4.4: EEG recording outside and inside the MR scanner showing the α -rhythm (box).

images are acquired in an almost continuous manner. In order to extract useful information from the EEG record acquired simultaneously, the gradients artifacts have to be removed. Several post-processing methods, based on artifact averaging and subtraction [79] or filtering techniques [80, 81] have been proposed. These techniques are only useful if the EEG preamplifiers have a sufficient dynamic range allowing full digitization of the artifact plus the EEG signal. Another proposed method to reduce the gradient artifacts is to use pair-wise twisted electrodes leads [82]. With this configuration, the induced currents should be self-canceling, but some artifacts remain visible and must be further post-processed.

In contrast to standard fMRI studies, combined EEG/fMRI studies used for epileptic focus localization are based on sparse triggered image acquisitions (see section 5.2). The EEG recording inside the MR scanner is only used to detect epileptic activity in between the image acquisitions. With our system, the quality of the EEG recording was assessed by several trained neurologists by comparing patients EEG (frequency of epileptic events) obtained inside and outside of the scanner. Another qualitative EEG evaluation was done by recording the α -rhythm which is usually smaller in amplitude than typical epileptic events. The topography and frequency of the observed α -rhythm were similar inside and outside the magnet (fig. 4.4). We also noted that proper fixation of the EEG leads and extension cables with weights helps to reduce the ballistographic artifact significantly.

4.4 Image quality

Introduction of EEG equipment into an MRI scanner can disturb the homogeneity of the magnetic field and raise the background noise affecting the quality of resulting MR images. Despite the growing interest of combined

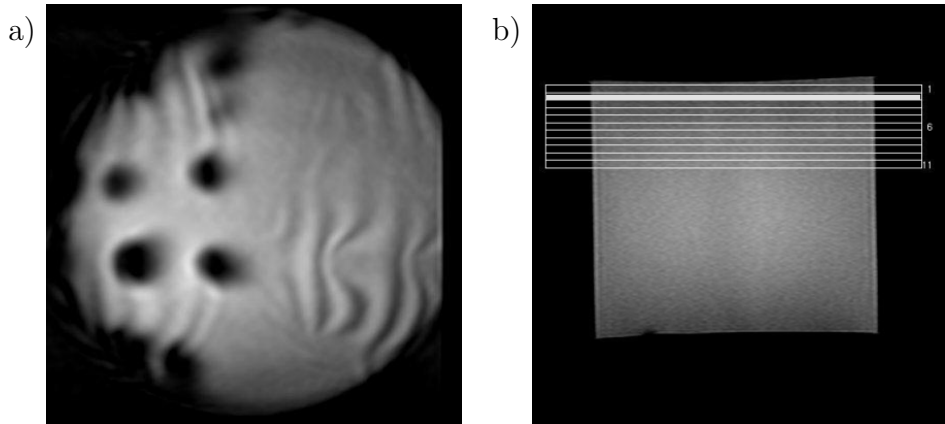


Figure 4.5: a) Susceptibility artifacts due to EEG paste on an EPI image of water phantom b) Slice position of the EPI image on the phantom

EEG/fMRI studies, the question of image quality have been addressed in only a few papers [83, 84].

The effects of EEG system on MR images can be separated into local and global. Local effects are due to susceptibility differences between the skin, the electrodes and the EEG fixation paste or gel. Gradient-echo based images, especially EPI, are very sensitive to these susceptibility differences. The resulting artifacts are local signal drop and possible geometric distortions. It is important that these artifacts do not extend into the brain tissue¹ and compromise the detection of activated areas. The size of the artifacts depends on the type of EEG electrodes, but even more importantly on the type and amount of the EEG paste [83] used to fix the electrodes on the patient's head and to improve electrical contact. Figure 4.5 shows the susceptibility artifacts due to EEG conducting paste (Metraux Electronique, CH) on the EPI image of a water filled phantom. This particular paste produced large artifacts with into-image penetration depth of about 15 mm. The other side of the phantom was covered by the same amount of another EEG paste (EC2 GRASS cream), which didn't produce any visible artifacts on the image.

Another effect due to EEG equipment is the global image signal to noise ratio (SNR) reduction. SNR reduction can be caused by two mechanisms: 1) increased noise due to electromagnetic radiation emitted by the preamplifier/multiplexor and 2) lower signal due to the presence of EEG leads on the head (faraday cage effect). The RF noise generated by EEG can be minimized by bringing all electronically active components outside of the magnet's bore or by applying proper RF shielding and filtering techniques

¹the distance between the skull and the cortex is of the order of 10 mm

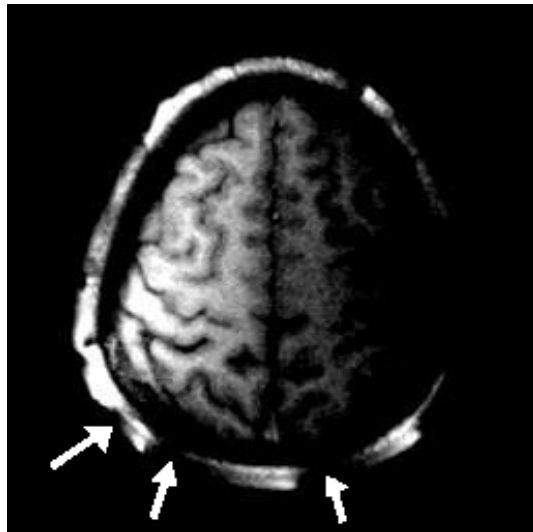


Figure 4.6: Local susceptibility artifacts (arrows) and non-uniform SNR drop on a GRE image

[83]. With our EPI and GRE images, we have observed a SNR decrease of 20 – 30%. It was always due to lower signal in images taken with the EEG system in place compared to images taken without the EEG system. Moreover, non-uniform SNR drop over the image plane, as shown in figure 4.6, was also observed. Such a non-uniform signal drop could be produced by an asymmetric position of the EEG wires over the subject's head.

4.4.1 fMRI feasibility

Images acquired in the presence of the EEG system in the magnet have a lower signal to noise ratio than without the EEG system. It means that the results of statistical image analysis from a concurrent EEG/fMRI study can be compromised. To evaluated the effect of EEG on the fMRI activation areas, we have performed a comparative fMRI versus EEG/fMRI study using a well characterized motor activation paradigm [85].

Five normal right-handed volunteers participated in the study. With each subject, two fMRI scans were performed: 1) regular fMRI without the EEG system and 2) the same fMRI acquisition with the EEG system inside the scanner. The same activation task was performed during both acquisitions. It consisted of four cycles of 20 s of rest followed by 20 s of self paced right-hand fingers tapping. In the second fMRI acquisition, a fully operational

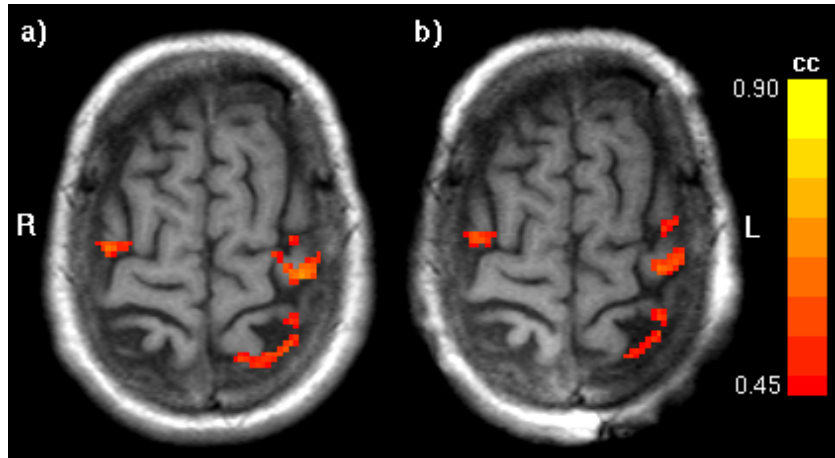


Figure 4.7: Cross-correlation maps a) without b) with EEG

18-channel EEG system with the electrodes placed on the subject's head at the standard 10/20 position was used. The fMRI data was obtained from 13 contiguous 5-mm axial slices using single-shot EPI ($TE = 40$ ms, $FA = 80^\circ$). A total of 85 volumes was acquired with a TR of 2 seconds. In order to minimize motion artifacts, subjects head was fixed with bandages to the head holder. Anatomical reference images were obtained using T_1 -weighted GRE sequence ($TR/TE/FA = 191\text{ms}/4.47\text{ms}/80^\circ$).

Prior to statistical analysis of the fMRI data, motion correction using AIR 3.08 [62] was applied. Functional activation maps were obtained using cross-correlation analysis with a shifted (4 s) boxcar reference function [29]. Correlation threshold of 0.45 was used to select the activation pixels, but discarding the stand-alone pixels. For each subject, activation areas in the motor cortex obtained under two conditions (with/without EEG) were compared in terms of size (number of activated pixels), the mean correlation coefficient and the intensity change between the control and the activation conditions. We also computed relative SNR reduction between the EPI images obtained with and without the EEG recording. The SNR itself was measured as a mean intensity over a large region of interest in the brain divided by mean background noise.

Results

Activation of the contra-lateral motor cortex was found in all subjects without and with the EEG system. The location of activation areas under the two condition was in good agreement, as illustrated in figure 4.7. However, with every subject, we have observed a significant reduction ($>50\%$) of the

number of activated pixels when the EEG was recorded in parallel with fMRI. The results from individual subjects, summarized in table 4.2, show that the relative reduction of the number of activated pixels is proportional to the relative decrease of SNR. The very large reduction of activation observed in the last subject is due to the non-uniform SNR drop over the image (45% over left and 30% over right hemispheres).

The reported average correlation coefficients (mean cc) and the signal intensity variation (mean %) were computed by considering the activation pixels found in each fMRI experiment separately. It is not surprising that mean cc 's are very similar because we used the same correlation threshold. The difference of 1% of signal intensity variation...

Sbj	SNR ¹ / SNR ² / % drop	size ¹ /size ² / % drop	mean cc	mean %
1	53.5 / 42.6 / 20.3%	186 / 87 / 53%	0.58 / 0.58	3.9 / 4.9
2	59.8 / 47.0 / 21.4%	106 / 53 / 50%	0.56 / 0.56	4.5 / 5.8
3	51.7 / 40.4 / 21.9%	59 / 28 / 52%	0.49 / 0.49	3.4 / 4.5
4	57.3 / 41.6 / 27.4%	193 / 83 / 57%	0.58 / 0.57	5.1 / 6.4
5	55.5 / 34.5 / 37.8%	92 / 22 / 76%	0.57 / 0.53	3.3 / 5.0

Table 4.2: Individual subjects results (1 corresponds to the acquisition without EEG and 2 - with EEG).

The results of this study show that concurrent EEG/fMRI is feasible. However, the sensitivity of fMRI is reduced because of overall SNR reduction. Moreover, some activation areas may be missed because of a non-uniform SNR drop across the images due to a particular position and density of the EEG wires over the subject's head. Reduction of fMRI sensitivity can be a limiting factor for the number of EEG channels in simultaneous EEG/fMRI recording.

4.5 Conclusion

In recapitulation, the simultaneous recording of EEG and fMRI is possible. Patient safety can be assured by careful arrangement of the EEG cables and avoiding ferromagnetic materials. It is possible to obtain good quality EEG inside the scanner in periods between image acquisitions, but more work is still needed to obtain real-time EEG during imaging.

EEG affects the MR image quality. It is important to assure that the EEG system does not bring any source of RF interferences into the scanner. Particular care must be taken in the choice of the material of EEG electrodes

and EEG fixating paste in order to minimize the susceptibility artifacts. fMRI images obtained with the EEG system in the scanner have a reduced SNR which results in decreased sensitivity to detect areas of activation. It is very likely that the number of the EEG channels (separate electrodes) has a direct influence on image SNR, and therefore the use of high-resolution EEG (needed for EEG source analysis) in the scanner can be limited.

Chapter 5

Epileptic focus localization using EEG-triggered fMRI

5.1 Epilepsy

Epilepsy (from Greek, *epi-*“upon” and *lepsis-*“seizure”) is one of the oldest medical conditions known to man. The earliest descriptions can be found in ancient medical writings dating back to 4000–2000 BC and which contained accurate description of many seizure types as they are still recognized today. In the earliest writings, epilepsy, known as the “sacred disease”, was thought to result from possession by evil spirits or other supernatural powers. Treatment therefore involved the use of religious, occult and magical methods. This picture of epilepsy was well anchored until the 18–19th centuries, despite the fact that in Hippocrates’ “On the sacred disease” (400 BC) it was described as a brain disorder due to natural causes [18, p. 30]. In fact, fear and stigma of “madness” associated with epilepsy are still present today, especially in developing countries, leading to heavy personal and social consequences for the patients [86].

Epilepsy is a very common neurological disorder affecting 0.5–0.8% of the world’s population and with the incidence rate (the number of new cases) of 30 to 50 per 100'000 per year. Over 60% of patients are children and adolescents under the age of 20, and it is in this group where epilepsy has its most dramatic consequences.

Epilepsy is a brain disorder characterized by recurrent *seizures* which are caused by bursts of abnormal electrical activity of cortical neurons. The localization and extent of the affected nervous tissue determine the wide range of clinical manifestations of epilepsy, which spans from brief loss of awareness to complete loss of consciousness and motor control. The group

of clinically observed signs and symptoms and the type of epileptic seizures that customarily occur together is called an *epileptic syndrome*. Identification of the syndrome helps to choose the appropriate therapy and to make the prognosis. Without a precise clinical context, the term “epilepsy” should be regarded as a general term rather than a diagnosis.

5.1.1 Epileptic seizures

Epileptic seizures are divided into two major classes, generalized and partial. Generalized seizures are associated with discharges that affect the whole or a very large part of the brain. They include *tonic-clonic* (“grand mal”) and *absence* (“petit mal”) seizures during which the consciousness is always altered. A very disabling and dangerous condition, known as generalized *status epilepticus*, is a state in which a person has frequent seizures without recovery of consciousness between each episode. Partial or focal seizures arise from electrical discharges in one or several localized areas of the brain. Partial seizures are further subdivided into *simple* and *complex* depending on whether the consciousness is preserved or not. Some partial seizures can spread to the whole brain causing a secondary generalized seizure.

There are many conditions that may lead to the development of epilepsy. Any type of brain disorder such as a tumor, cerebrovascular disease or head trauma can be the cause of seizures, although not all people with the same disease will have epilepsy. Epilepsies with a known cause are called *symptomatic*. However, in the majority of cases (~70%), seizures occur in structurally normal brains and in the absence of known brain diseases. In some epileptic syndromes, there are known genetic abnormalities that can explain the process of epileptogenesis. These epilepsies are referred to as *idiopathic*. Epilepsies that can not be classified as idiopathic are referred to as *cryptogenic*. An additional difficulty in the research of causes and mechanisms of epilepsy is that seizures themselves may induce both structural and functional changes in the brain increasing the brain susceptibility to recurrent seizures.

Regardless of whether the causes of a particular type of epilepsy are known, it is important to understand the mechanisms of seizure generation and spread. Abnormal electrical activity results from subtle alterations in brain metabolism, biochemistry and neurotransmitters. The current view of epileptogenesis is based on the notion of neuronal hyperexcitability due to alterations in both excitatory and inhibitory neurotransmitter systems. Gamma-aminobutyric acid (GABA) is the primary inhibiting neurotransmitter used in the brain. In animal studies, decrease of GABA receptors’ efficacy leads to an appearance of epileptiform activity in electrophysiolog-

ical recordings [87]. This has been the basis for the development of several new antiepileptic drugs designed to enhance the action of GABA.

Another mechanism which can enhance neuronal hyperexcitability is the synaptic reorganization resulting from cellular loss associated with recurrent seizures [88]. Due to excessive discharges the concentration of some chemicals in the extracellular space may become toxic for neurons and provoke their death. As a result, normal inhibitory circuits may be replaced by excitatory which can further increase the excitability of the neuronal circuit.

5.1.2 Treatment

Since the causes of epilepsy are unknown in the majority of cases, the goal of treating patients with epilepsy is to reduce the number and the severity of epileptic seizures without causing unacceptable side effects. To achieve optimal treatment results, precise diagnosis of epileptic syndrome is required. The diagnosis is usually established on the basis of clinical, electroencephalographic and neuroimaging examinations.

Treatment usually begins with an appropriate anti-epileptic drug (AED) therapy. About 70% of patients can be successfully treated with currently available AEDs [89]. However, in the remaining 30%, seizures can not be controlled adequately with drugs. This condition is called *refractory* or *pharmaco-resistant* epilepsy. Patients from this group are potential candidates for epilepsy surgery.

Epilepsy surgery is a particular type of neurosurgical intervention whose primary objective is to achieve seizure control through resection of the epileptogenic tissue (epileptic focus) or disconnection of brain regions in order to disrupt seizure propagation. The outcome of resective surgery depends mainly on precise localization of epileptic focus, in particular localization of primary focus responsible for seizure onset. When the focus can be identified and when it is not located close to the primary brain functional areas, successful operation rates are very high. For example in temporal lobe epilepsies (TLE), the success rate is close to 80%. On the other hand, in extra-temporal lobe epilepsies where focus localization is generally more difficult, successful operation rates are substantially lower 30-40% [90]. The risks and benefits of a particular surgical intervention for each individual patient must be carefully evaluated during presurgical assessment [91].

5.1.3 Presurgical evaluation

Patients with diagnosed pharmaco-resistant epilepsy must be carefully evaluated by a multi-disciplinary team for possible surgical treatment. A large number of exams are performed aiming at determination of the exact location of seizure activity and evaluation the surrounding areas in the brain for assessment of post-operative functional deficits. The established clinical tools that are used during presurgical evaluation include:

- neurological and neuropsychological testing
- synchronized video-EEG monitoring
- high-resolution MRI
- PET and SPECT

These non-invasive exams constitute what is called phase-I evaluation. Unfortunately, the above exams do not always lead to a conclusion concerning the localization of the focus. This is particularly true for patients with extra-temporal lobe epilepsies. In these cases an invasive phase-II examination has to be carried out. It consists of prolonged recording from surgically implanted intra-cranial electrodes. As an invasive procedure, phase-II evaluation comprises several medical risks associated with the implantation of the electrodes. Another major concern is that intra-cranial recording can be obtained from only a limited number of electrodes, which means that brain regions implicated in seizure generation can be easily missed if they have not been identified during phase-I evaluation. It is therefore highly desirable to improve the existing and develop new non-invasive methods for epileptic focus localization.

5.1.4 New techniques for presurgical evaluation

In addition to well established clinical diagnostic tools, several new non-invasive functional imaging techniques have been shown useful for epileptic foci localization and characterization.

EEG source localization

Multichannel scalp EEG is the most important tool used for epileptic evaluation in general. It provides the confirmation of the presence of abnormal electrical activity and whether this activity is focal or diffuse. In the case

of focal activity, visual inspection of EEG traces can provide an approximate localization of a seizure focus.

With the advent of digital EEG, many methods of data analysis have been proposed. In the context of epileptic focus localization, a particularly useful technique is topographic mapping of the EEG and subsequent 3D localization of electrical activity by solving the so called “inverse problem” (computation of electrical generators from surface potential). First algorithms for EEG source localization were based on the estimation of equivalent current dipoles in a spherical head model. The main drawback of these algorithms is that the number of dipoles (generators) has to be fixed a priory, which can lead to incorrect localization when multiple unknown sources are active simultaneously. Recently, new localization algorithms have been proposed that estimate distributed current density in the brain rather than single dipole sources [92, 93]. Together with the development of high-resolution EEG (128 channels), these new analysis techniques have shown very promising results for epileptic focus localization [94].

MR spectroscopy

Magnetic resonance spectroscopy (MRS) provides a non-invasive means to investigate brain metabolites in normal and diseased brain. Initial MR spectroscopy studies of epileptic patients focused on detecting abnormal energy metabolism using ^{31}P -MRS, but during the last years, ^1H spectroscopy has been found very sensitive to detect abnormalities in epileptogenic tissues [95].

The basic principles underlying MRS are the same as those for magnetic resonance imaging. Different protons within a molecule or from distinct molecules resonate at slightly different frequency due to the electronic cloud configuration and its shielding effect of the electronic density about each nucleus. This effect is called the *chemical shift*. If imaging gets the signal from water molecule, ^1H -MRS detects signals from other molecules, after proper suppression of the water signal. The localization of the spectrum on a specific region of the brain is accomplished by using three mutually orthogonal slices. This technique, called single voxel spectroscopy acquires one spectrum at a time. For more than one region of interest, the acquisition needs to be repeated.

The main resonances of interest in epileptic patients have been those from N-acetylaspartate (NAA), creatine+phosphocreatine (Cr), choline-containing compounds (Cho), and lactate (Lac). A reduction of NAA and the NAA/Cho ratio with a rise in Lactate during acute seizure reflects the neuronal loss and bioenergetic compromise in the excitable cells in the epileptogenic area [96].

In patients with temporal lobe epilepsy, correct lateralization to the side of the seizure onset was found on average in 80–90% of the patients. This was also true for patients with non-lesional epilepsy indicating that ^1H -MRS is a sensitive tool and may depict even discrete histopathological changes [97].

Functional MRI

Despite the fact that functional MRI is a very recent technique, it holds great promise as a diagnostic tool in presurgical evaluation of epileptic patients. Two major issues concerning epilepsy surgery can be addressed with fMRI. First, important functional areas that must be spared during surgery can be mapped in each individual patient. This applies mainly to the delineation of primary motor cortex and language areas. Concerning the language, fMRI has the potential to replace the invasive Wada test, which is currently used to determine language lateralization. The second application is the localization of the epileptic focus itself by detecting changes in blood flow due to epileptic activity.

5.2 EEG-triggered fMRI

Precise identification of epileptic foci using non-invasive methods remains problematic in patients with non-lesional epilepsy. Both PET and SPECT are useful techniques for focus localization [98], but with spatial resolution of about 1 cm and relatively low sensitivity, it is rare that they provide sufficiently precise localization. New techniques, such as EEG source localization and ^1H -MR spectroscopy were shown useful for focus localization, with 1–3 cm spatial resolution. However, they still need clinical evaluation concerning their localizing accuracy.

From numerous PET and SPECT studies of epileptic patients, it is known that there are large increases in regional cerebral blood flow and oxygen consumption during focal seizures. Since functional MRI is also sensitive to these changes, it could be used to determine the focus location with high spatial resolution (< 5 mm). Several case reports have confirmed that this is indeed possible in patients with prolonged focal seizure activity. [99, 100]. However, the number of patients that can undergo such fMRI examination, i.e. frequent seizures and without substantial movements, is very limited.

EEG recording of focal activity often reveals a characteristic pattern of brief abnormal events (spikes, spike-waves) between the seizures. These events are called *interictal* epileptic discharges. Interictal epileptic activity usually does not provoke uncontrollable movements, and thus it is more

appropriate for activation studies using fMRI. By recording the EEG in the magnet [69], fMRI acquisitions can be triggered by these brief discharges in order to visualize brain regions involved in this epileptic activity [101, 102, 103].

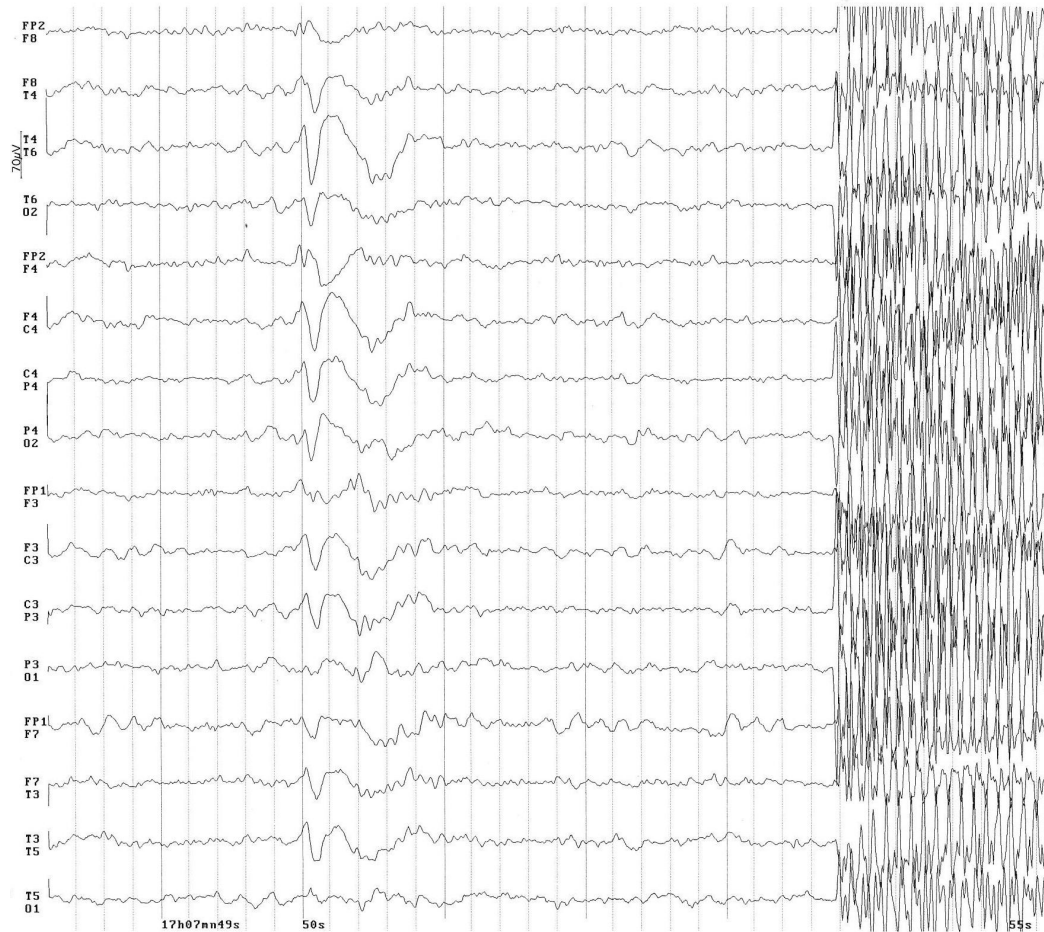


Figure 5.1: Example of spike-wave event used to trigger an EPI acquisition 4 s after detection of the event.

5.2.1 fMRI acquisition protocols

Most EEG-triggered fMRI studies reported so far in the literature were performed on 1.5 T MRI scanners. Like in a regular fMRI study, images are acquired using a single-shot gradient-echo EPI sequence with a typical TE of 40 ms, 64×64 or 128×128 matrix, and a field of view of ~ 25 cm. Volumetric acquisition is obtained from 10–20 slices with a slice thickness of 5–7 mm.

In our setup, EEG monitoring of epileptic activity of the patient in the MR scanner is obtained from 16-channel EEG system with the electrodes placed at the standard 10/20 position.

EEG-triggered fMRI study can be considered as a variant of block-designed fMRI. The main difference with conventional fMRI studies is that the “activation” and “control” conditions are not determined by an external stimulus, but by spontaneous epileptic activity measured by EEG. The “activation” condition is obtained by manually triggering a multi-slice EPI acquisition after the detection of a characteristic epileptiform discharge (spike, spike-wave or burst). As the peak of the BOLD signal occurs ~ 5 seconds after the onset of brain activity, the actual image acquisition is done $\sim 3\text{--}4$ seconds after the observation of the discharge (fig. 5.1). The “control” condition is obtained by acquiring images after prolonged periods (> 15 seconds) of EEG without epileptiform activity.

For reliable detection of epileptic activity, 40–60 images in each condition have to be acquired. Triggered images are obtained non-periodically because of unpredictable appearance of spikes. Unequal delay between successive acquisitions can produce T_1 weighting of the images, which will introduce errors in the statistical analysis. In order to avoid this undesirable T_1 effect, a minimum delay of about 15 seconds must be respected between successive acquisitions (fig. 5.3a). This delay corresponds roughly to $4 \cdot T_1$ of the cerebro-spinal fluid (98% of magnetization regrowth), which has the longest T_1 of brain tissues. Considering this delay and the total number of triggered images to be 100, the minimum examination time (patient in the scanner) would be 25 minutes. In practice, unfortunately, spikes never occur at regular 15 seconds intervals. It is much more likely to observe one discharge every one to five minutes which leads to the total examination time of more than 1 hour.

In our initial EEG-triggered fMRI studies [102, 104], “activation” and “control” images were obtained in two separate blocks. First, 40–60 spike-triggered images, as described above, are acquired. Then the patient receives

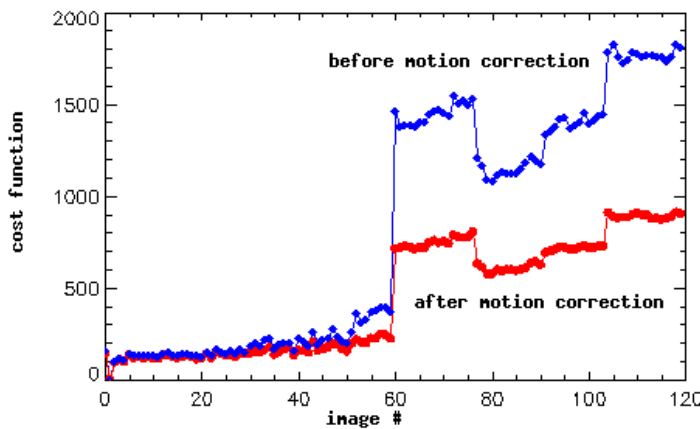


Figure 5.2: Stimulus correlated motion artifact (injection at frame 60).

an intravenous injection of an anti-epileptic drug (1–1.5 mg of Clonazepam), which eliminates the majority of discharges on the EEG, and a second set of 60 “control” images is acquired with a repetition time of 15 seconds. The analysis of activation is done like in a regular block designed fMRI (correlation of t -test) with the only difference that in EEG-triggered fMRI, there is only one “activation/control” cycle.

This approach has been found useful, in particular with patients having frequent discharges. One major limitation of this image acquisition strategy is that it is very sensitive to motion artifacts. If the patient moves during injection, there will be a global displacement between “activation” and “control” image series (fig. 5.2). This is an example of a stimulus-correlated artifact [105] which is very difficult to correct because even with correctly detected motion parameters, the systematic interpolation errors during image resampling will produce signal changes indistinguishable from true activation.

Several improvements of the examination protocol were made in order to overcome the problem of this motion artifacts. The patient’s head fixation was improved by using a vacuum cushion (PAR Scientific A/S, Denmark) and an automatic system was installed to perform the injection of the anti-epileptic drug, so the patient doesn’t know when the injection is done. Despite these measures, the problem of motion at injection was observed in some new patients, so the image acquisition protocol itself was modified. Instead of acquiring images in two separate blocks, only one extended acquisition of 120 or 150 images is used. During the first two thirds of the acquisition block, “activation” and “control” images are acquired in an interleaved fashion. The “control” images are obtained when no epileptic activity is observed

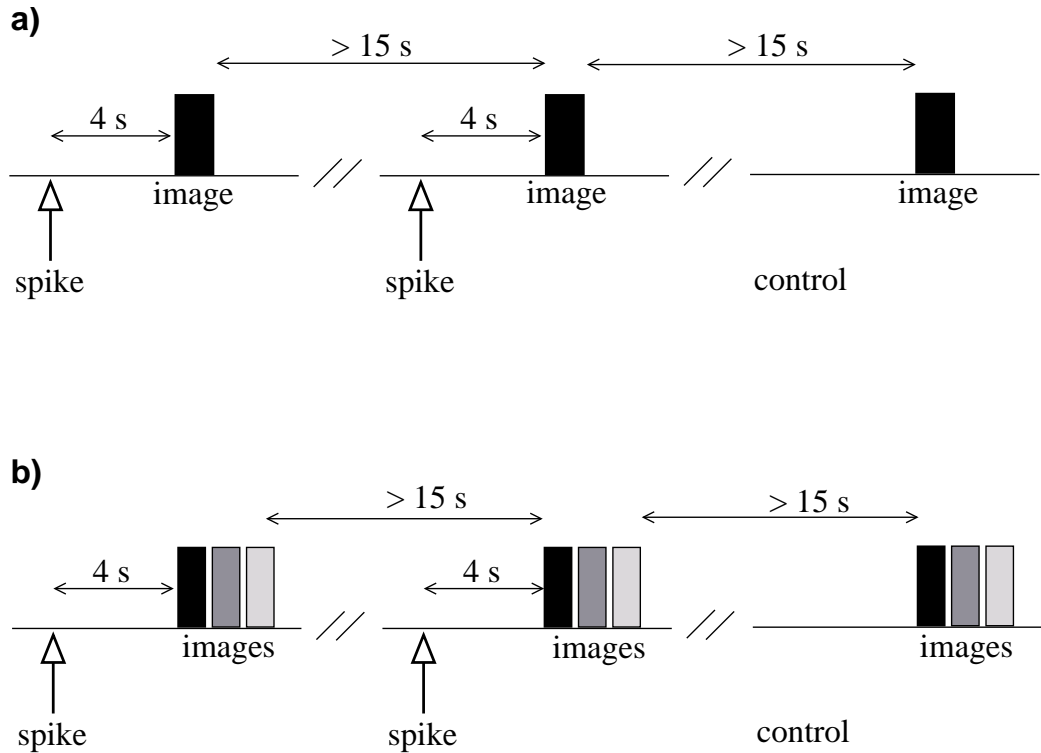


Figure 5.3: Image acquisition protocols a) single volume per spike b) multiple volumes per spike.

on the EEG for at least 15–20 seconds. Then the injection is performed and the remaining images are acquired as another “control” condition. If the patient moves during injection, the analysis can still be done as “activation” vs pre-injection “control” images.

An important issue concerning EEG-triggered fMRI is the delay between the detection of an epileptiform discharge and the actual image acquisition. A delay of 4 seconds is based on the assumption that the “epileptic” BOLD response is similar to the one, observed in a normal cortex under external stimuli, but in fact, very little is known whether the hemodynamics in a pathological brain region such as an epileptic focus are the same as in a normal tissue. In addition, it is known from event-related fMRI studies that the BOLD response (time-to-peak parameter in particular), produced by a particular stimulus, can vary significantly across different subjects [106].

The problem of unknown “epileptic” BOLD response is one of the reasons why several epilepsy research groups are trying alternative image acquisition strategies for epileptic focus localization using combined EEG/fMRI. For ex-

ample, continuous fMRI acquisition with [107, 108] or without [109] removal of MR artifacts from the EEG have been proposed. However, in patients with sparse discharges, EEG-triggered fMRI may still be a more appropriate method. Our approach to this problem was the development of triggered event-related fMRI (see Ch. 6). However, only a simplified version of this method could be applied to the patients because our EEG system doesn't allow to remove MR acquisition artifacts.

Instead of a single volume, multiple volumes (burst) can be acquired after the spike detection (fig. 5.3b). A rapid acquisition of 3 or 4 EPI volumes with a TR of 1–1.5 seconds allows a partial sampling of post-spike BOLD response and increases the likelihood of getting its maximum. Control images should also be acquired in the same way, because short TR produces a heavy T_1 weighting between the first and the subsequent volumes. Otherwise, the acquisition protocol is the same as the single-volume “interleaved” protocol. The analysis of activation can then be done by selecting equally-weighted volumes from the “activation” and “control” bursts.

5.2.2 Patient results

In total, epileptic focus localization using EEG-triggered fMRI has been performed in 35 patients (age 8–50). The majority of patients (25) were studied using the first protocol (single acquisition per spike, baseline after injection), 5 patients were studied with the “interleaved protocol” and the last 5 – with the “burst” protocol. The choice of the imaging protocol depends, to a large degree, on the epileptic activity of a given patient. For example, in case of frequent discharges, it is difficult to use the “interleaved” protocol, because pre-injection “control” images can not be obtained.

The results of the first 11 patients who underwent extensive presurgical evaluation, including PET and SPECT, have been reported in [104]. Overall, in 8 out of 11 patients, EEG-fMRI findings confirmed the clinical diagnosis, either by the presence ($n=7$) or absence ($n=1$, genetic disorder) of distinct areas of BOLD signal enhancement. The results are summarized in table 5.1. In 6 patients, intracranial recordings were carried out, and in 5 cases, epileptogenic activity was found in the areas corresponding to fMRI activation areas. In the remaining 3 cases, the focus localization was impossible due to motion artifacts (patient # 9), quasi total absence of interictal activity (patient # 7) and a basal focus localization too close to air cavities (patient # 6).

Nr	Age	Presurgical evaluation	EEG-fMRI
1	18	Left frontal	Left frontal
2	36	Left occipito-temporal	Left occipital
3	41	Right occipito-temporal	Right occipital and temporal
4	14	Multifocal with predominance of the right posterior temporal region	Multifocal with predominant right posterior
5	28	Right parieto-temporal	Right posterior temporal
6	23	Left temporal and frontal	No focal enhancement
7	28	Left posterior temporal	No focal enhancement
8	41	Left posterior temporal	Left posterior temporal
9	16	Right frontal	No focal enhancement
10	13	Diffuse (genetic disorder)	No focal enhancement
11	33	Left temporal	Left anterior and mid temporal

Table 5.1: Epileptic focus localization from presurgical evaluation (phase-I) and EEG-fMRI findings

Global analysis of the remaining 24 patients has not yet been performed, as many patient are still under clinical evaluation. Out of 24 patients, 14 EEG-fMRI examinations were successful in the sense that the analysis of fMRI data revealed distinct areas of activation. An example of focal activation in left parieto-temporal cortex is shown in fig. 5.4. In the remaining 10 patients, 5 did not show any focal activation, and in the other 5 cases, fMRI data analysis could not be performed because of important motion artifacts. In the successful group, the localization of the focus by EEG-fMRI was concordant with other presurgical examinations in 11 patients (intracranial EEG in 5 cases, pre-operative electrocorticography in 1 case,

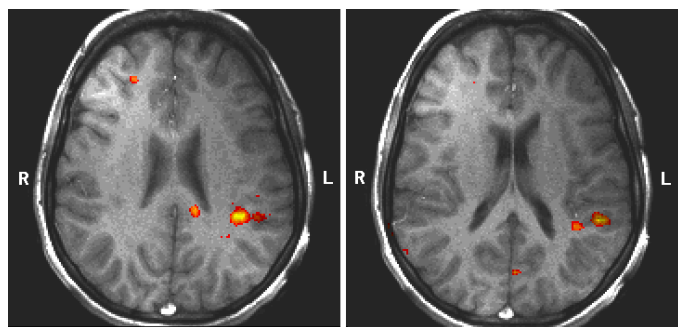


Figure 5.4: Focal activation by EEG-triggered fMRI.

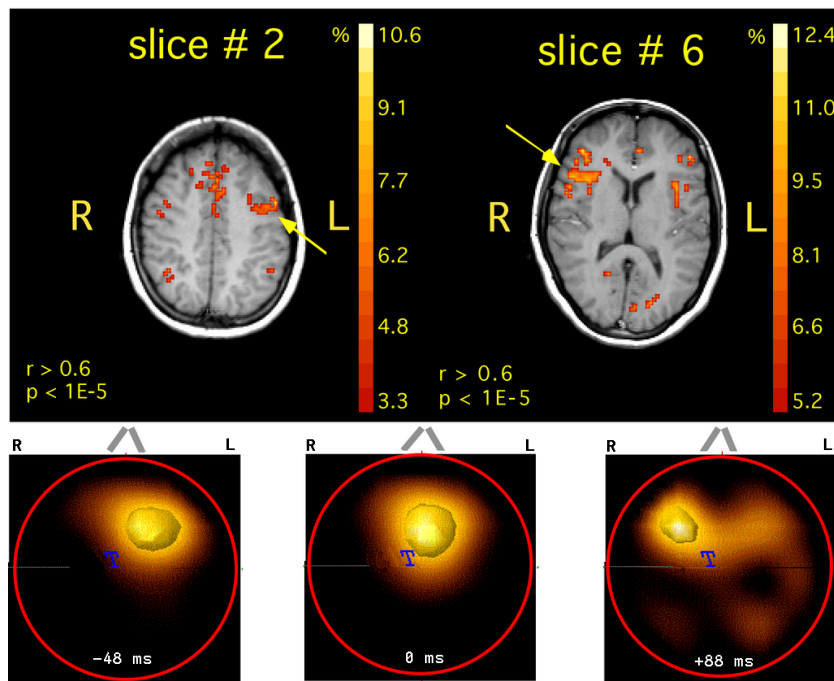


Figure 5.5: Multi-focal activation found by EEG-fMRI (top) and 3D-localization using linear inverse solution showing propagation of electrical activity from the left to the right hemisphere (bottom).

3D EEG source localization in 3 cases, ^1H -MR spectroscopy in 3 cases), and for the remaining 3 patients, the localization was discordant with PET findings in 1 case and localization in 2 others have not yet been confirmed by any other technique.

EEG-fMRI combined with EEG source localization

In several patients, EEG-triggered fMRI revealed multiple areas of activation. In these cases, it is important to determine, whether these areas represent multi-focal epileptic activity or a very rapid propagation of activity from primary to secondary epileptic areas. Using only EEG-triggered fMRI results, it is impossible to answer this question, because fMRI can not capture rapid electrical events that happen on a millisecond scale. This temporal information can be derived from EEG source localization analysis. By combining EEG-triggered fMRI and 3D EEG source localization, epileptic activity can be tracked with both high spatial and temporal resolution [102].

Figure 5.5 shows an example of such combination. EEG-triggered fMRI shows three distinct activation areas in the frontal interhemispheric, frontal left and frontal right parts of the brain. The 3D current density estimation obtained from 29-channel EEG (recorded outside the MRI in a separate session) shows the activity in the similar brain areas, but the estimations are done at three time points with 120 ms separation between the first and last one. The activity starts in the left frontal area and propagates over the the interhemispheric region to the right frontal lobe. These findings were confirmed subsequently by intracranial EEG recording, and ultimately, by partial resection of the frontal left area, corresponding to EEG-fMRI activation, which resulted in marked reduction of seizure frequency.

Now, this type of combined analysis is done using a 128-channel EEG recording, which allows a more precise source localization [110].

EEG-fMRI combined with ^1H -MR spectroscopy

Combining EEG-triggered fMRI with ^1H -MR spectroscopy may become another useful method to improve the localization and characterization of epileptic foci in patients with non-lesional extratemporal lobe epilepsies. ^1H -MRS is very sensitive at detecting abnormal brain metabolism related to focal epileptic activity, but only if the measurement voxels are placed correctly over the suspected brain areas. Until now, it was mainly used in patients with mesio-temporal epilepsy, where voxel position can be guided by anatomical landmarks (e.g. hippocampus). In extratemporal lobe epilepsy, however, ^1H -MRS seems less valuable due to the difficulty to place the voxels of interest correctly without any anatomical indication.

Such an indication can now be provided by EEG-triggered fMRI. The voxels of interest can be placed over the EEG-fMRI activated areas. In return, ^1H -MRS will provide a measure of brain metabolite disturbance in these areas, and therefore it will confirm the EEG-fMRI findings, and might be helpful with the interpretation of the results in case of multiple activation areas [111].

An example of ^1H -MRS combined with EEG-fMRI is shown in figure 5.6. In this patient, suffering from right frontal epilepsy, EEG-fMRI revealed 3 distinct areas of activation. Single voxel PRESS sequence ($\text{TE}=288$ ms, $\text{TR}=1600$ ms, $\text{NAV}=256$) was used to obtain spectra from 6 voxels, 3 over the activation ares and 3 corresponding references. A clear reduction of the NAA/Cho ratio in two superior areas, relative to the normal tissue, was observed, while in the lower area, there was practically no difference in NAA/Cho. The ratios and the asymmetry index ($\text{AI} = [\text{right-left}] / [\text{right+left}]$) are presented in the table 5.2.

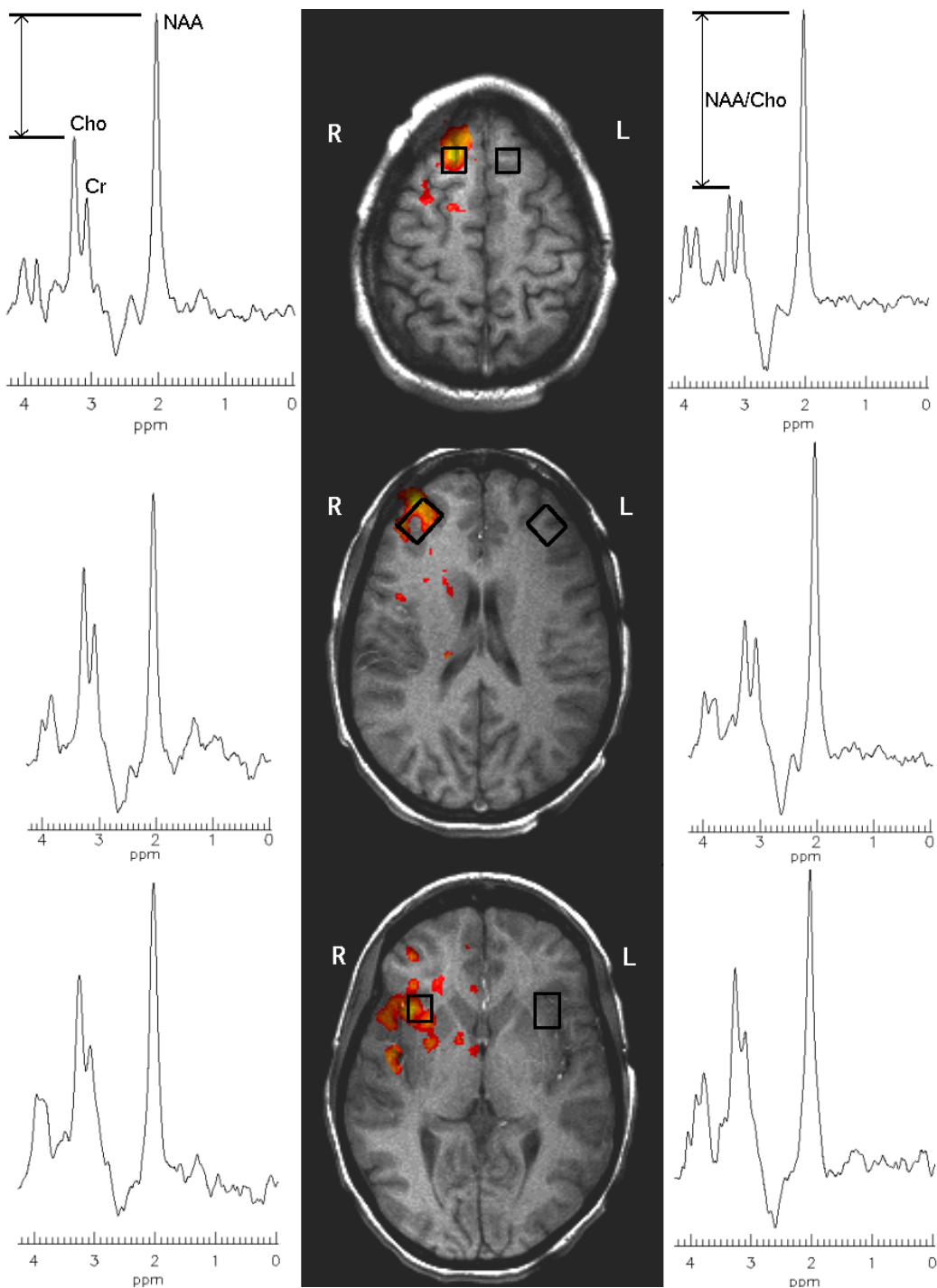


Figure 5.6: ^1H spectroscopy based on EEG-fMRI findings.

	NAA/Cho (R)	NAA/Cho (L)	AI
Frontal superior	1.78	2.88	-23.5%
Frontal median	1.51	2.55	-25.6%
Insular	1.63	1.66	-1%

Table 5.2: Ipsi (R) and contra-lateral (L) NAA/Cho ratios and the asymmetry index.

Similar reductions of NAA/Cho ratio have been observed in patients with known temporal lobe epilepsy. In our case, spectroscopy reveals abnormal metabolism in the two superior areas, thus validating EEG-fMRI findings, and suggests that the third area, located in a vessel rich insular region, is likely to be a draining vascular artifact.

5.2.3 Discussion

Global analysis of patients results suggests that EEG-triggered fMRI is a useful technique for non-invasive epileptic focus localization, in particular for patients with extratemporal lobe epilepsy. In 20 (2 pending) out of 35 patients, the regions of BOLD signal increase associated with interictal discharges were confirmed as epileptogenic zones by various other (both invasive and non-invasive) localizing techniques. When fMRI data is not corrupted by patient's motion, the absence of activation (6 cases) may indicate a diffuse disorder, which is also useful clinical information. Combining the spatial accuracy of EEG-triggered fMRI with the temporal accuracy of EEG-based electromagnetic tomography allows very precise localization of the epileptic focus, and further combination with ^1H -MR spectroscopy may allow better functional characterization of the epileptogenic regions.

There are, however, several limitations of EEG-triggered fMRI that must be considered for patients selection. If the focus is supposedly located close to the air cavities, it can be missed because of the susceptibility artifacts in the EPI images. There are other MR sequences, less sensitive to susceptibility artifacts, for example, PRESTO sequence [112] or a recently developed SENSE imaging technique [113], that can be used for functional imaging. Their use for EEG-triggered fMRI need to be evaluated in future studies. The major limitation, however, is due to motion artifacts which can be expected from non-cooperating and young patients. Patients with sparse epileptic activity (< 1 discharge every 5 minutes) are also likely to move more, because the total examination time becomes excessively long. The type of the discharges observed on EEG can also be an issue. For example, a small and

brief (< 10 ms) event originating from a small brain region would produce only a minute change in hemodynamics which is difficult to detect at 1.5 T. At higher fields, we can expect to detect small hemodynamic changes more reliably.

Apart from technical difficulties, there are some methodological issues concerning EEG-triggered fMRI. It is quite likely that the hemodynamic regulation, which is the basis of BOLD fMRI, in an epileptogenic region is different from normal brain tissue because of neuronal loss and abnormal metabolism. For this reason, triggered image acquisition using the “burst” method, which allows at least partial sampling of the BOLD response, is probably the best imaging protocol for EEG-triggered fMRI. Another issue with the imaging protocols is the use of an anti-epileptic drug to obtain the baseline condition. Due to their sedative effects, AEDs may affect the blood regulation and the oxygen consumption in the brain with possible repercussions on the fMRI activation areas. A few studies attempted to determine the effects of neuro-depressant drugs on cerebral hemodynamics, but the results are somewhat controversial. The use of a relatively large dose (10 mg) of diazepam in [114] didn’t produce any measurable effects compared to an injection of a placebo. On the other hand, the use of another drug (carbamazepine, 2.4–11 mg) resulted in decreased fMRI activation areas in a memory task at high doses. In our case, the use of anti-epileptic drugs was motivated by the fact that this is the only way to control the epileptic activity, and because EEG-triggered fMRI findings were confirmed in many patients by other focus localization techniques, the effects due to AEDs are rather small.

Despite the above issues, we believe that EEG-triggered fMRI will become a very valuable tool in presurgical evaluation of epileptic patients, in particular with non-lesional extratemporal epilepsy. Ultimately, the clinical utility of EEG-triggered fMRI in presurgical evaluation of epileptic patients will be determined from the surgical outcome in a large patient group.

Chapter 6

Triggered Event-Related fMRI

6.1 Introduction

EEG-triggered fMRI is a useful technique for epileptic focus localization. However, the image acquisition protocols described in the previous chapter, suffer from two important drawbacks. First, to collect 40 images following an epileptic event from a patient with sparse discharges requires very long examination time (up to 2 hours), which is impractical for clinical applications and often leads to severe motion artifacts. The second problem is the unknown form of the BOLD response following a particular epileptic event. If the delay between spike detection and image acquisition is wrong, then the true activation is likely to be missed.

The above issues can be addressed by extending the image acquisition strategy into triggered event-related (ER) fMRI approach. Instead of obtaining a single image after spike detection, short image series can be acquired rapidly during a time window of about 20 seconds, thus effectively sampling the BOLD response following an epileptic event. In order to estimate the BOLD response and find the activation areas, 10–15 triggered series would be sufficient because of the available temporal information. Since this requires a smaller number of epileptic discharges, the total examination time can be reduced considerably.

There is, however, one difficulty with this triggered approach. In regular ER-fMRI studies, where image acquisition is done continuously, it is common practice to obtain 3 to 5 dummy images before the stimulation protocol begins. This is done to ensure that the longitudinal magnetization is in the steady-state condition. With EEG-triggered image series, it is impossible to perform such dummy scans, and therefore, the signal in each image series will be heavily weighted by the longitudinal magnetization decay to the steady-

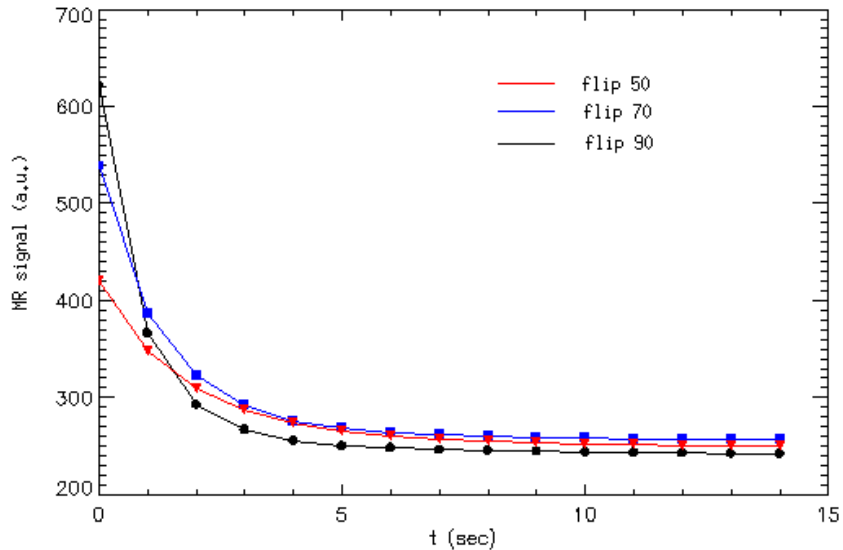


Figure 6.1: Longitudinal magnetization decay to the steady-state condition (TR=1s, flip angle = 50,70,90°)

state condition. The time to reach the steady state depends on the flip angle, TR and T_1 of the tissue. In the brain, it is in the range of 5 to 6 seconds when imaging with a TR of 1 second and using a flip angle of 50-90°(fig. 6.1). Since about the same time is needed for the BOLD response to reach its maximum, the estimation of the BOLD signal will be impossible without any correction method.

Our first approach to the problem of T_1 -weighting was to drive the magnetization into the steady state by using continuous RF excitation, but without doing any image acquisition after each RF pulse. Only when needed (ex. detection of a spike), a trigger can be sent to the scan control computer to activate the imaging module for a specified number of the following RF pulses, thus allowing the acquisition of an image series. In principle, this sequence should allow good quality EEG recording apart from periods of data collection when EEG is obscured by rapidly switching gradients. Unfortunately, when the sequence was implemented and tested, the RF pulses created brief but disturbing artifacts on the EEG. This approach was abandoned and another method was developed.

The idea of the second approach is to use a simple subtraction between two types of triggered image series (“task” and “control”) [115]. A “task” series corresponds to an acquisition following a brief stimulus, such as spike, and a “control” series corresponds to an identical image acquisition but without

any stimulus. Both series would have an identical longitudinal magnetization weighting, but different functional contrast, so the subtraction between the two should allow to recover the BOLD signal.

6.1.1 EPI sequence modification

In order to carry out triggered ER-fMRI experiments, the EPI sequences, available on our MR scanner (1.5 T, Eclipse, Marconi Medical Systems), had to be modified. First, the manual trigger function was simplified in order to reduce the trigger delay (time between user action and actual data acquisition) to the minimum (< 500 ms). The second modification was in the EPI loop control procedure, to allow the acquisition of triggered image series of desired length. In the original implementation, manual triggering applied to every EPI volume (multi-slice) acquisition. An additional loop was inserted to allow multiple acquisitions. Below is the pseudocode of the modified loop control procedure:

```
loop series (1..N)
    interrupt new_manual_start()
    loop group (1..M) #----- multiple acquisitions
        loop slice (1..K)
            acquisition_block()
        end slice
    end group
end series
```

6.2 Validation study

A validation study was performed in order to evaluate triggered event-related fMRI combined with the subtraction method as an approach to detect and characterize brain activation produced by non-periodic stimuli. Non-periodic stimulation has been simulated using a well-characterized motor activation paradigm, and the results obtained with triggered ER-fMRI were compared with the results obtained with conventional (continuous acquisition) ER-fMRI. The objective was to compare the activation maps and the BOLD responses from the two experiments.

6.2.1 Methods

Subjects

Five healthy right-handed volunteers (age 24–42) participated in the study. Each volunteer had two fMRI acquisitions: (1) continuous ER-fMRI and (2) triggered ER-fMRI. The subjects were asked to perform brief right hand finger-tapping initiated by a visual cue (task duration 1 s). A vacuum cushion (PAR Scientific A/S, Denmark) was used to minimize head movement during imaging.

Imaging procedure

In the first (continuous) experiment, functional images were acquired using single-shot gradient-echo EPI ($TE = 40$ ms, flip angle = 90°). Each image had 5-mm thickness, 128×128 matrix and 25 cm field of view. A total of 205 volumes consisting of seven contiguous axial slices covering sensory-motor cortex were collected with a TR of 1 s. Ten trials (visual cue) starting at volume 6 (in order to ensure magnetization steady state) and repeated every 20 s were applied.

Modified EPI sequence was used for the triggered experiment. Using the same MR parameters and image location as in the first experiment, 20 triggered image series were collected. Each series consisted of 20 volumes acquired with a TR of 1 s. Between the end and the beginning of successive series, a delay of 15 s was used to allow full recovery of the longitudinal magnetization. Ten series were obtained with a stimulus preceding the image acquisition (“task” series) and another ten were obtained without any stimulus (“control” series). Task and control series were mixed pseudo randomly (fig. 6.2).

Anatomical reference images were obtained using T_1 weighted multi-slice gradient echo sequence with the following parameters: TR = 162 ms, TE = 4.47 ms, flip angle = 80° .

Data Analysis

Subject’s motion was assessed using SPM99 [58]. In two subjects, translations ≥ 1 mm and rotations $\geq 1^\circ$ were detected, and motion correction procedure was applied.

Functional analysis was performed using in-house developed programs written in IDL (Research Systems, Inc, Boulder, CO). In order to increase signal to noise ratio, EPI images were spatially smoothed with a gaussian kernel ($4 \times 4\text{-mm}^2$ FWHM). Data from the first experiment was averaged

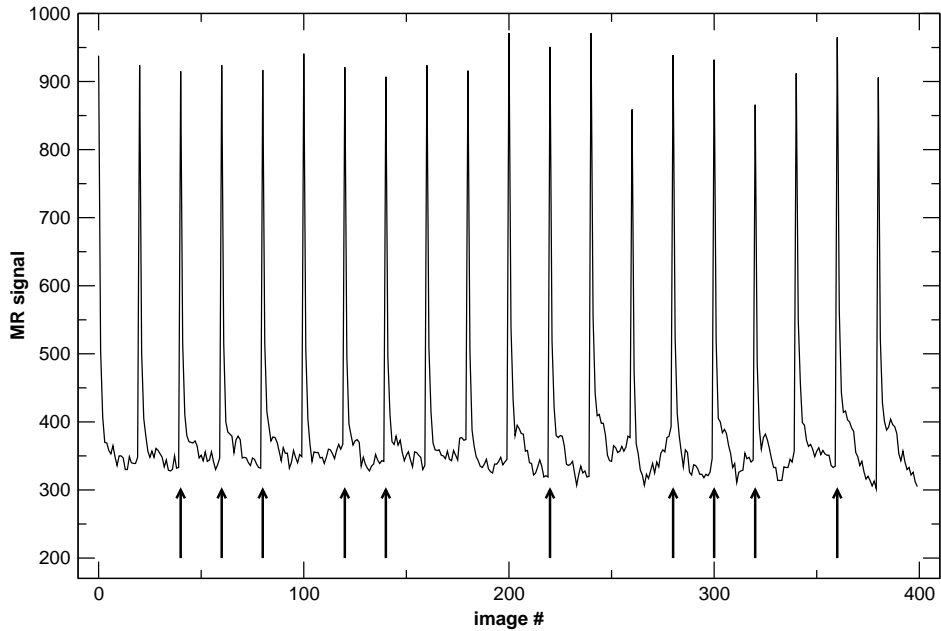


Figure 6.2: Raw MR signal from a single pixel from triggered ER-fMRI experiment showing signal saturation effects at the beginning of each image series (arrows indicate task series).

across 10 trials resulting in 20 s mean “activation” series. For the second experiment, “task” series and “control” series were averaged separately to produce 20 s mean “task” series and 20 s mean “control” series. The difference between mean “task” and mean “control” series produced another 20 s mean “activation” series. Regions of neuronal activation were determined by correlation analysis of each pixel time-course from “activation” series with a three-parameter gamma variate function [42, 116]:

$$S(t) = At^b e^{-t/c} \quad (6.1)$$

where b and c were varied to account for inter-subject variability of BOLD responses [106].

Clusters of at least 4 pixels with correlation coefficient of 0.7 and above were selected, converted to equivalent t -values [117] and superimposed on the anatomic images following radiological convention. Activation maps from the two experiments were compared qualitatively in terms of size and location of activated areas. For quantitative analysis, activation of left primary motor cortex (contralateral M1) in one slice was compared in terms of size and overlap between the two experiments. BOLD responses from pixels in overlapping activated areas were fitted to eq. 1 to obtain BOLD signal amplitude

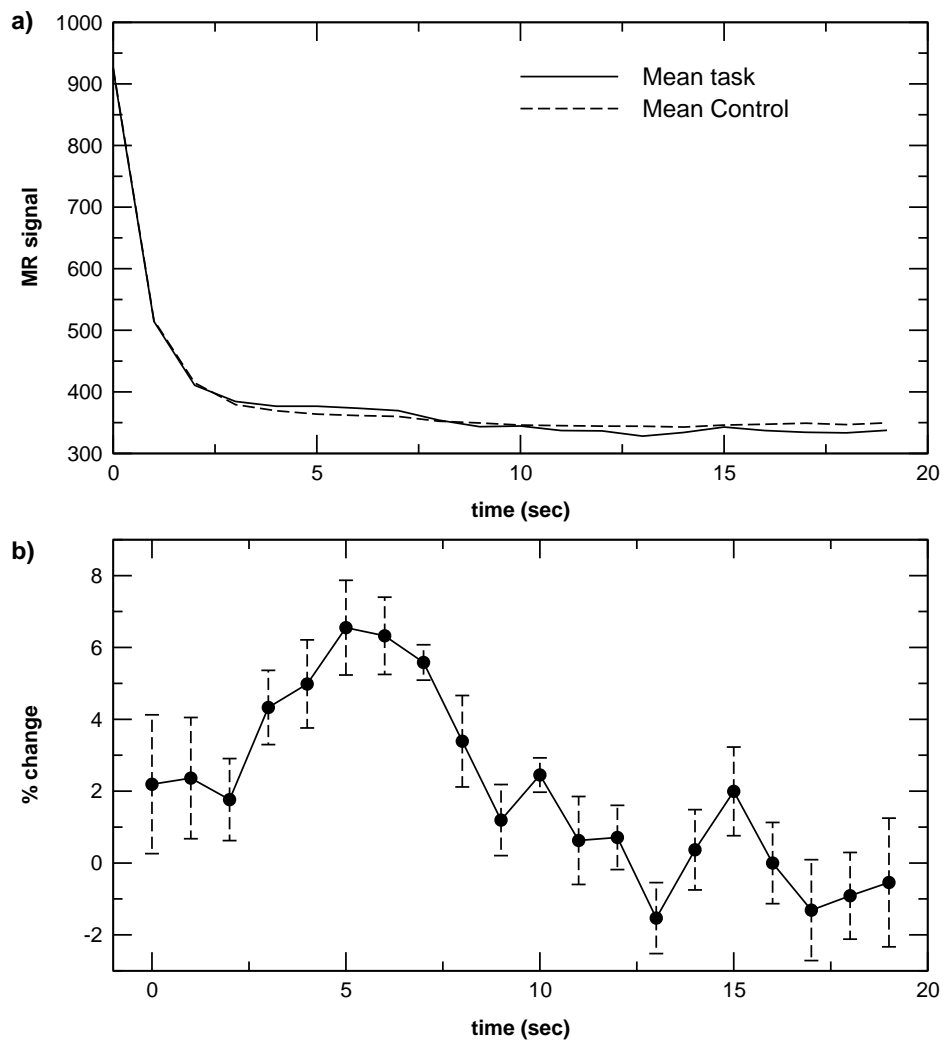


Figure 6.3: Mean task and control series (a) obtained from signal in fig. 6.2 and their difference (b).

and time-to-peak parameter ($b \cdot c$). The differences in these parameters between the two experiments were assessed using the standard t -test at the significance level $P < 0.05$.

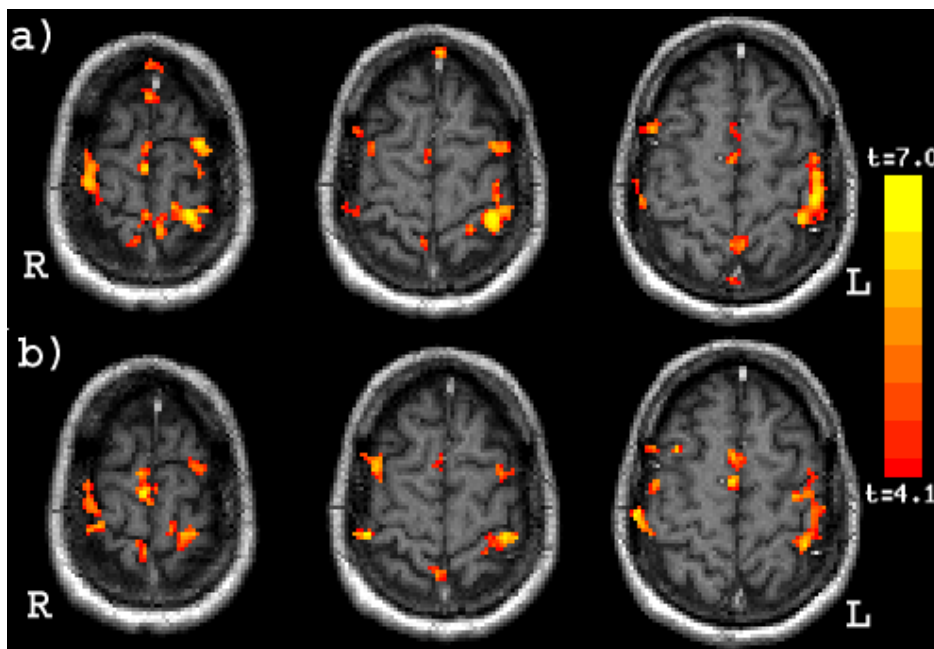


Figure 6.4: Activation maps showing 3 consecutive slices of one subject obtained from (a) continuous and (b) triggered experiments.

6.2.2 Results

Raw signal from a single pixel in the motor area (M1) from the triggered experiment is shown in figure 6.2 (“task” series marked with arrows). Peaks indicate the beginning of each series and show typical signal decay due to magnetization saturation effect. The averages of ten “task” series and ten “control” series are shown in figure 6.3a. Both “task” and “control” series are affected by longitudinal magnetization decay in the same way. Magnetization reaches the steady-state after about 4 s. The difference between mean “task” and mean “control” series, expressed as signal percent change, is shown in figure 6.3b, and reveals the expected BOLD response waveform.

All subjects showed activation in primary sensory-motor and supplementary motor areas. In three subjects, bilateral activation was observed and two other subjects showed a more lateralized activation in the left hemisphere. Figure 6.4 shows three consecutive slices with activation areas of one subject obtained from continuous (a) and triggered (b) ER-fMRI experiments. Activation maps from both experiments exhibit good spatial correspondence. However, the size of activation areas in the triggered experiment is reduced on the average by 30% (10%–50%) at the same statistical threshold.

Results of the quantitative analysis, performed on contralateral M1, are presented in table 6.1. Between 67% and 100% of activated pixels found in the triggered experiment were also found in the continuous experiment, demonstrating good spatial colocalization. BOLD response parameters, amplitude and time-to-peak, found in both experiments were very similar. No significant differences, except for time to peak of one subject, were found. Figure 6.5a shows fitted BOLD response to the spatially averaged time-course from contralateral M1 of one subject from the continuous experiment, and figure 6.5b shows a very similar BOLD response from the same area found in the triggered experiment.

Subj	Exp	Nb pix	Overlap	Ampl.[%]	peak [s]	b	c
1	C	39	16	2.41(1.00)	5.77(0.38)	6.34	0.91
	T	24		2.75(1.10)	5.23(0.74)	5.08	1.06
2	C	21	18	2.77(1.01)	*8.63(0.36)	9.10	0.94
	T	23		3.25(1.12)	7.81(0.39)	7.92	0.99
3	C	36	12	2.84(0.58)	6.17(0.61)	6.72	0.91
	T	15		2.51(0.67)	6.21(0.53)	7.93	0.79
4	C	25	19	3.12(1.08)	6.32(0.46)	7.15	0.88
	T	22		3.02(1.12)	6.18(0.35)	6.72	0.92
5	C	29	11	2.27(0.75)	5.69(0.30)	6.48	0.88
	T	11		2.98(0.82)	5.90(0.52)	10.71	0.55

Table 6.1: Analysis of activation in contralateral M1 from continuous (C) and triggered (T) experiments and BOLD response parameters estimated from the same area (*significant difference $P < 10^{-4}$).

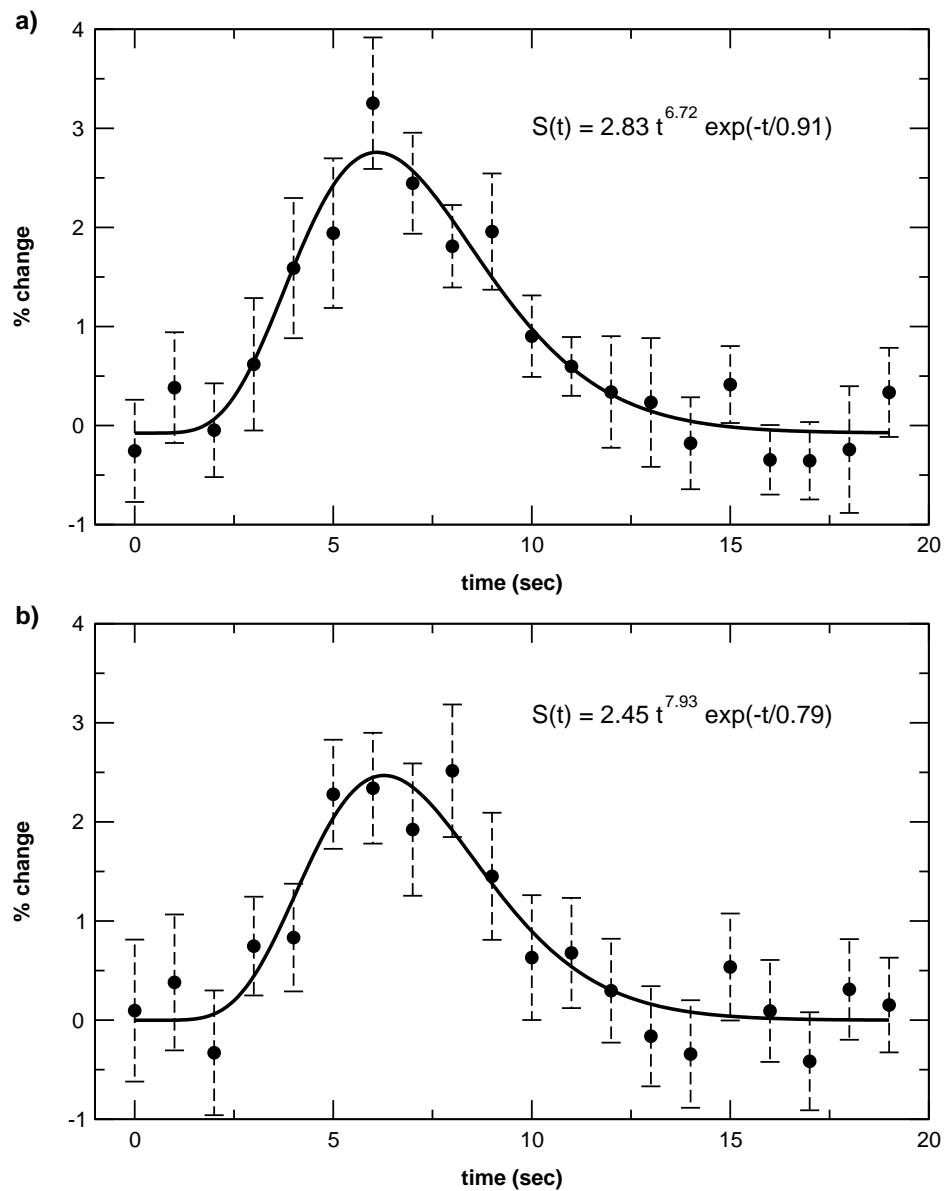


Figure 6.5: Spatially averaged time-course from left motor cortex of one subject with fitted gamma function from continuous (a) and triggered (b) experiments. Data corresponds to subject 3 in table 6.1.

6.2.3 Discussion

The main purpose of this validation study was to test the feasibility of triggered ER-fMRI based on a subtraction method to eliminate longitudinal magnetization saturation effects. The results, both in terms of spatial localization of activation and temporal aspects of the BOLD responses, were concordant with the conventional ER-fMRI. The BOLD response parameters (amplitude and time to peak) were also in good agreement with previous ER-fMRI studies of the motor cortex [118]. Reduction of overall activation areas in the triggered method can be explained by the SNR reduction by a factor of $\sqrt{2}$, due to subtraction of “task” and “control” image series [119]. It would be possible to compensate for SNR loss by lowering image spatial resolution or by acquiring more triggered image series.

Triggered ER-fMRI was developed as an alternative image acquisition strategy for epileptic activation studies, especially for patients with sparse interictal events. In comparison to previously used EEG-triggered fMRI, as described in Chapter 5.2 , this method will allow considerable reduction of total examination time because it requires a smaller number of epileptic events for reliable activation detection. In addition, BOLD responses produced by interictal events can be estimated directly. Epileptic related BOLD response estimation has been reported recently using continuous fMRI acquisition [107]. The authors showed promising results in a case report of a patient with unilateral left-hemispheric dysfunction (Rasmussen’s encephalitis), exhibiting frequent spikes (1 every 50 s on average). Under these conditions, 24000 images were acquires over a period of 30 min for BOLD response estimation. Triggered ER-fMRI doesn’t require acquisition of such large data volumes and may be better suited for patients with less frequent interictal events.

There is, however, one difficulty of direct application of triggered ER-fMRI for epileptic activation studies. During image acquisition, MR gradients create very strong artifacts on the EEG making it unreadable. Triggered image series, both “task” and “control”, require approximately 20 s of acquisition time and additional epileptic discharges may happen during this time. It is therefore necessary to remove the artifacts from EEG (preferably online) [79, 80] in order to make correct assumptions about the form of the BOLD responses in each triggered image series. Because our current EEG system doesn’t allow to remove this artifacts (saturation of EEG amplifiers), triggered ER-fMRI has not yet been applied to epileptic patients.

Although triggered ER-fMRI was developed in the context of epilepsy, it can be also applied to other fMRI studies, where brain activation can not be easily predicted, for example in studies of sleep [120] or drug action on the human brain [121]. In addition, triggered ER-fMRI may provide additional time flexibility, compared to continuous ER-fMRI, needed for the experimental design of studies where subject performance is an important issue, for example in behavioral studies.

Conclusion

The main goal of this thesis was the development of EEG-triggered fMRI as a new method for non-invasive epileptic focus localization. We have addressed several important technical questions concerning the overall feasibility of this technique, and then applied it to 35 patients suffering from pharmacoresistant epilepsy. In parallel, new image acquisition strategies were developed in order to overcome some limitations of the original EEG-triggered fMRI.

The feasibility studies showed that simultaneous acquisition of EEG and fMRI is possible. Our temperature measurements showed that the heating of the EEG electrodes by MR sequences used in a typical fMRI exam are well below the safety limits. Patient safety can be assured by avoiding conducting loops when placing the EEG electrodes on the subject's head. A careful choice of the EEG fixation paste allows to minimize the susceptibility artifacts in the MR images, and despite reduced SNR, a reliable detection of functional activation is possible in the presence of the EEG system. Although the quality of EEG recording in the scanner is reduced, it is sufficient to correctly monitor the epileptic activity and trigger fMRI acquisitions by characteristic discharges.

EEG-triggered fMRI technique can be easily performed in patients in a safe manner. It can also be used with pediatric patients. In Geneva, 35 patients have been studied with EEG-triggered fMRI and no complaints about any sort of discomfort during the examination were reported. EEG-triggered fMRI revealed discrete areas of activation in many patients with extratemporal epilepsy that converged with the epileptogenic focus as determined by several other non-invasive and (if indicated) invasive focus localization techniques. The temporal characteristics of BOLD fMRI are unlikely to discriminate between the primary focus and the areas of propagation. Combining the fMRI results with new 3D EEG source localization techniques allows very precise spatio-temporal focus localization. ^1H -MR spectroscopy, based on the EEG-triggered fMRI findings may also provide important functional characterization of epileptogenic regions.

Several limitations of EEG-triggered fMRI were encountered. It is well known that long echo time EPI is sensitive to susceptibility artifacts. The MR signal in regions lying close to the air-tissue interfaces is greatly reduced. Patients with the epileptic activity supposedly located in the inferior frontal lobes and the anterior and basal temporal lobes are less likely to benefit from EEG-triggered fMRI. Another limitation of the technique is its sensitivity to motion artifacts. In our experience, it is with patients having very sparse epileptic activity that EEG-fMRI exam failed because of excessive motion. The problem of motion was our main motivation to develop alternative image acquisition strategies. The “interleaved” protocol, which in fact does not require an injection of an anti-epileptic drug, is less sensitive to motion, but its utility must be evaluated on a larger group of patients. The last limitation of EEG-triggered fMRI is related to unknown “epileptic” BOLD response and the difficulty to choose an optimal delay between the epileptic event and image acquisition. To overcome this difficulty, we have developed and validated the triggered event-related fMRI. Application of this method to epileptic patients requires an EEG recording free from MR acquisition artifacts, which needs further development. Nonetheless, a simplified version of this method – “burst” acquisition – allowing at least some partial sampling of the BOLD response has been used in five patients and promising preliminary results were obtained.

It is well known that patients with extratemporal lobe epilepsy have lower chances of becoming seizure free post-operatively. Despite the difficulties, our results demonstrate that EEG-triggering fMRI represents a promising tool to help the localization of the epileptic focus in this particular patient group. After completion of the presurgical evaluation of our 35 patients, we will have a better understanding of the real clinical utility of EEG-triggered fMRI.

As a concluding note, the development of simultaneous EEG/fMRI acquisition techniques and multi-modal combinations, like fMRI/EEG source localization, may find very useful applications in fields other than epilepsy. In particular, in basic neuroscience research, these techniques may allow to get a better understanding of the link between the brain’s electrical activity and the hemodynamic/metabolic responses, which in turn will allow a better understanding of what we measure with the techniques like PET, fMRI, EEG and MEG.

Bibliography

- [1] F. Bloch, W. W. Hansen, M. Packard. Nuclear Induction. *Rhys Rev*, **69**:127 (1946).
- [2] E. M. Purcell, H. C. Torrey, R. V. Pound. Resonance absorption by nuclear magnetic moments in a solid. *Phys Rev*, **69**:37 (1946).
- [3] R. Damadian. Tumor Detection by Nuclear Magnetic Resonance. *Science*, **171**:1151–1153 (1971).
- [4] P. C. Lauterbur. Image Formation by Induced Local Interactions: Examples Employing Nuclear Magnetic Resonance. *Nature*, **242**:190–191 (1973).
- [5] P. T. Callaghan. *Principles of Nuclear Magnetic Resonance Microscopy*. Oxford University Press (1993).
- [6] E. M. Haacke, R. W. Brown, M. R. Thompson, R. Venkatesan. *Magnetic Resonance Imaging: Physical Principles and Sequence Design*. Wiley-Liss (1999).
- [7] R. R. Ernst, G. Bodenhausen, A. Wokaun. *Principles of Nuclear Magnetic Resonance in One and Two Dimensions*. Oxford University Press (1991).
- [8] E. L. Hahn. Spin echoes. *Phys. Rev.*, **80**:580–594 (1950).
- [9] P. Mansfield. Multi-Planar Image Formation using NMR Spin-Echoes. *J Phys C*, **10**:55–58 (1977).
- [10] J. Frahm, A. Haase, D. Matthaei. Rapid NMR imaging of dynamic processes using the FLASH technique. *Magn Reson Med*, **3**:321–327 (1986).
- [11] J. Hennig, A. Naureth, H. Friedburg. RARE imaging: a fast imaging methods for clinical MR. *Magn Reson Med*, **3**:823–833 (1986).

- [12] P. Margosian, F. Schmitt, D. Purdy. Faster MR imaging: imaging with half the data. *Health Care Instrum*, **1**:195–197 (1986).
- [13] A. Villringer, B. R. Rosen, J. W. Belliveau, J. L. Ackerman, R. B. Lauffer, R. B. Buxton, Y. S. Chao, V. J. Wedeen, T. J. Brady. Dynamic imaging with lanthanide chelates in normal brain: contrast due to magnetic susceptibility effects. *Magn Reson Med*, **6**:164–174 (1988).
- [14] S. Ogawa, T. M. Lee, A. R. Kay, D. W. Tank. Brain magnetic resonance imaging with contrast dependent on blood oxygenation. *Proc Natl Acad Sci USA*, **87**:9868–9872 (1990).
- [15] C. H. Meyer, J. M. Pauly, A. Macovski, D. G. Nishimura. Simultaneous spatial and spectral selective excitation. *Magn Reson Med*, **15**:170–175 (1990).
- [16] P. Jezzard, S. Clare. Sources of Distortion in Functional MRI Data. *Human Brain Map*, **8**:80–85 (1999).
- [17] M. H. Buonocore, L. Gao. Ghost artifact reduction for echo planar imaging using image phase correction. *Magn Reson Med*, **38**:89–100 (1997).
- [18] S. Finger. *Minds Behind the Brain*. Oxford University Press (2000).
- [19] M. E. Raichle. Visualizing the mind. *Scientific American*, **270**:58 – 64 (1994).
- [20] C. S. Roy, C. S. Sherrington. On the regulation of the blood-supply of the brain. *J Physiol*, **11**:85–108 (1890).
- [21] P. T. Fox, M. A. Mintun, M. E. Raichle, P. Herscovitch. A Noninvasive Approach to Quantitative Functional Brain Mapping with $H_2^{15}O$ and Positron Emission Tomography. *J Cereb Blood Flow Metab*, **4**:329–333 (1984).
- [22] J. W. Belliveau, D. N. Kennedy, R. C. McKinstry, B. R. Buchbinder, R. M. Weisskoff, M. S. Cohen, J. M. Vevea, T. J. Brady, B. R. Rosen. Functional Mapping of the Human Visual Cortex by Magnetic Resonance Imaging. *Science*, **254**:716–719 (1991).
- [23] S. Ogawa, D. W. Tank, R. Menon, J. M. Ellermann, S.-G. Kim, H. Merkle, K. Ugurbil. Intrinsic signal changes accompanying sensory stimulation: Functional brain mapping with magnetic resonance imaging. *Proc Natl Acad Sci USA*, **89**:5951–5955 (1992).

- [24] K. R. Thulborn, J. C. Waterton, P. M. Matthews, G. K. Radda. Oxygenation dependence of the transverse relaxation time of water protons in whole blood at high field. *Biochim Biophys Acta*, **714**(2):265–270 (1982).
- [25] P. T. Fox, M. E. Raichle. Focal physiological uncoupling of cerebral blood flow and oxydative metabolism during somatosensory stimulation in human subjects. *Proc Natl Acad Sci USA*, **83**:1140–1144 (1986).
- [26] R. B. Buxton, E. C. Wong, L. R. Frank. Dynamics of Blood Flow and Oxygenation Changes During Brain Activation: The Balloon Model. *Magn Reson Med*, **39**:855–864 (1998).
- [27] P. A. Bandettini, E. C. Wong, R. S. Hinks, R. S. Tikofsky, J. S. Hyde. Time Course EPI of Human Brain Function during Task Activation. *Magn Reson Med*, **25**:390–397 (1992).
- [28] R. Turner, P. Jezzard, H. Wen, K. K. Kwong, D. Le Bihan, T. Zeffiro, R. S. Balaban. Functional mapping of the human visual cortex at 4 and 1.5 Tesla using deoxygenation contrast. *Magn Reson Med*, **29**:277–279 (1993).
- [29] P. A. Bandettini, A. Jesmanowicz, E. C. Wong, J. S. Hyde. Processing Strategies for Time-Course Data Sets in Functional MRI of the Human Brain. *Magn Reson Med*, **30**:161–173 (1993).
- [30] A. M. Blamire, S. Ogawa, K. Ugurbil, D. Rothman, G. McCarthy, J. Ellermann, F. Hyder, Z. Rattner, R. G. Shulman. Echo-Planar imaging of the activated Human visual cortex shows a time delay between stimulus and activation. In *Proc. 11th SMRM, Berlin*, p. 1823 (1992).
- [31] R. L. Savoy, P. A. Bandettini, K. M. O’Craven, K. K. Kwong, T. L. Davis, J. R. Baker, R. M. Weisskoff, B. R. Rosen. Pushing the temporal resolution of fMRI: Studies of very brief visual stimuli, onset variability and asynchrony and stimulus-correlated changes in noise. In *Proc. 3d ISMRM, Nice*, p. 450 (1995).
- [32] R. L. Buckner, P. A. Bandettini, K. M. O’Craven, R. L. Savoy, S. E. Petersen, M. E. Raichle, B. R. Rosen. Detection of cortical activation during averaged single trials of a cognitive task using functional magnetic resonance imaging. *PNAS*, **93**:14878–83 (1996).

- [33] A. M. Dale. Optimal Experimental Design for Event-Related fMRI. *Human Brain Map*, **8**:109–114 (1999).
- [34] P. A. Bandettini, R. W. Cox. Event-Related fMRI Contrast When Using Constant Interstimulus Interval: Theory and Experiment. *Magn Reson Med*, **43**:540–548 (2000).
- [35] A. M. Howseman, S. Grootoont, D. A. Porter, J. Ramdeen, A. P. Holmes, R. Turner. The effect of slice order and thickness on fMRI activation data using multislice echo-planar imaging. *Neuroimage*, **9**(4):363–76 (1999).
- [36] K. J. Friston, O. Josephs, E. Zarahn, A. P. Holmes, S. Rouquette, J.-B. Poline. To Smooth or Not to Smooth? Bias and Efficiency in fMRI Time-Series Analysis. *Neuroimage*, **12**(2):196–208 (2000).
- [37] K. J. Friston, A. P. Holmes, J. B. Poline, P. J. Grasby, S. C. R. Williams, R. S. J. Frackowiak, R. Turner. Analysis of fMRI Time Series Revisited . *Neuroimage*, **2**:45–53 (1995).
- [38] K. J. Friston, A. P. Holmes, K. J. Worsley, C. D. Frith, R. S. J. Frackowiak. Statistical Parametric Maps in Functional Imaging: A General Linear Approach. *Human Brain Map*, **2**:189–210 (1995).
- [39] M. J. McKeown, S. Makeig, G. G. Brown, T.-P. Jung, S. S. Kindermann, T. J. Sejnowski. Analysis of fMRI by Blind Separation into Independent Spatial Components. *Human Brain Map*, **6**(3):160–188 (1998).
- [40] X. Golay, S. Kollias, G. Stoll, D. Meier, A. Valavanis, P. Boesiger. A New Correlation-Based Fuzzy Logic Clustering Algorithm for fMRI. *Magn Reson Med*, **40**:249–260 (1998).
- [41] N. Lange, S. C. Strother, J. R. Anderson, F. A. Nielsen, A. P. Holmes, T. Kolenda, R. Savoy, L. K. Hansen. Plurality and Resemblance in fMRI Data Analysis. *Neuroimage*, **10**:282–303 (1999).
- [42] M. S. Cohen. Parametric Analysis of fMRI Data Using Linear Systems Methods. *Neuroimage*, **6**:93–103 (1997).
- [43] G. H. Glover. Deconvolution of Impulse Response in Event-Related BOLD fMRI. *Neuroimage*, **9**:416–429 (1999).
- [44] O. Josephs, R. Turner, K. Friston. Event-related fMRI. *Human Brain Map*, **5**:243–248 (1997).

- [45] S. Y. Bookheimer. Functional MRI in Clinical Epilepsy. *NeuroImage*, **4**(3):S139–S146 (1996).
- [46] J. A. Detre, L. Maccotta, D. King, D. C. Alsop, G. Glosser, M. D’Esposito, E. Zarahn, G. K. Aguirre, J. A. French. Functional MRI lateralization of memory in temporal lobe epilepsy. *Neurology*, **50**(4):926–932 (1998).
- [47] C. C. Lee, R. C. Grimm, A. Manduca, J. P. Felmlee, R. L. Ehman, S. J. Riederer, C. R. Jack, Jr. A Prospective Approach to Correct for Inter-Image Head Rotation in FMRI. *Magn Reson Med*, **39**:234–243 (1998).
- [48] E. B. Welch, A. Manduca, R. C. Grimm, H. A. Ward, J. Clifford R. Jack. Spherical Navigator Echoes for Full 3D Rigid Body Motion Measurement in MRI. *Magn Reson Med*, **47**:32–41 (2002).
- [49] J. A. Derbshire, G. A. Wright, R. M. Henkelman, R. S. Hinks. Dynamic scan-plane tracking using MR position monitoring. *J Magn Reson Imaging*, **8**(4):924–932 (1996).
- [50] S.-C. Hwang, J.-H. Chen. 3D MR Motion Artifact Correction with Head Tracking System . *Proc. Human Brain Mapping*, p. 10045 (2002).
- [51] J. B. A. Maintz, M. A. Viergever. A Survey of Medical Image Registration. *Medical Image Analysis*, **2**(1):1–37 (1998).
- [52] D. L. G. Hill, P. G. Batchelor, M. Holden, D. J. Hawkes. Medical image registration. *Phys Med Biol*, **46**:1–45 (2001).
- [53] A. W. Toga, P. M. Thompson. The Role of Image Registration in Brain Mapping. *Image and Vision Computing*, **19**(1-2):3–24 (2001).
- [54] A. Rossenfeld, A. C. Kak. *Digital Picture Processing*. Academic Press, second edition (1982).
- [55] J. V. Hajnal, N. Saeed, E. J. Soar, A. Oatridge, I. R. Young, G. M. Bydder. A Registration and Interpolation Procedure for Subvoxel Matching of Serially Acquired MR Images. *J Comput Assist Tomogr*, **19**(2):289–296 (1995).
- [56] P. Thévenaz, T. Blu, M. Unser. Interpolation Revisited. *IEEE Trans Med Imag*, **19**(7):739–758 (2000).

- [57] R. P. Woods, S. R. Cherry, J. C. Mazziotta. Rapid Automated Algorithm for Aligning and Reslicing PET Images. *J Comput Assist Tomogr*, **16**(4):620–633 (1992).
- [58] K. J. Friston, J. Ashburner, C. D. Frith, J.-B. Poline, J. D. Heather, R. S. J. Frackowiak. Spatial Registration and Normalization of Images. *Human Brain Map*, **2**:165–189 (1995).
- [59] P. Thévenaz, U. E. Rutimann, M. Unser. A Pyramid Approach to Subpixel Registration Based on Intensity. *IEEE Trans Imag Proc*, **7**(1):1–15 (1998).
- [60] P. Thévenaz, , M. Unser. Optimization of Mutual Information for Multiresolution Image Registration. *IEEE Trans Imag Proc*, **9**(12):2083–2099 (2000).
- [61] O. Nestares, D. J. Heeger. Robust Multiresolution Alignement of MRI Brain Volumes. *Magn Reson Med*, **43**(5):705–715 (2000).
- [62] R. P. Woods, S. T. Grafton, C. J. Holmes, S. R. Cherry, J. C. Mazziotta. Automated Image Registration: I. General Methods and Intrasubject, Intramodality Validation. *J Comput Assist Tomogr*, **22**(1):139–152 (1998).
- [63] R. P. Woods, S. T. Grafton, J. D. G. Watson, N. L. Sicotte, J. C. Mazziotta. Automated Image Resistration: II. Intersubject Validation of Linear and Nonlinear Models. *J Comput Assist Tomogr*, **22**(1):153–165 (1998).
- [64] R. R. Woods. Automated Image Registration. <http://bishopw.loni.ucla.edu/AIR3/index.html>.
- [65] A. Jiang, D. N. Kennedy, J. R. Baker, R. M. Weisskoff, R. B. H. Tootell, R. P. Woods, R. R. Benson, K. K. Kwong, T. J. Brady, B. R. Rosen, J. W. Belliveau. Motion Detection and Correction in Functional MRI Imaging. *Human Brain Map*, **3**:224–235 (1995).
- [66] D. H. Wu, J. S. Lewin, J. L. Duerk. Inadequacy of Motion Correction Algorithms in Functional MRI: Role of Susceptibility-Induced Artifacts. *J Magn Reson Imaging*, **7**(2):365–370 (1997).
- [67] L. Freire, J.-F. Mangin. Motion Correction Algorithms May Create Spurious Brain Activations in the Absence of Subject Motion. *Neuroimage*, **14**:709–722 (2001).

- [68] P. L. Nunez, R. B. Silberstein. On the Relationship of Synaptic Activity to Macroscopic Measurements: Does Co-Registration of EEG with fMRI Make Sense? . *Brain Topography*, **13**(2):79–96 (2000).
- [69] J. R. Ives, S. Warach, F. Schmitt, R. R. Edelman, D. L. Schomer. Monitoring the patient's EEG during echo planar MRI. *Electroencephalogr Clin Neurophysiol*, **87**(6):417–420 (1993).
- [70] E. Kanal, F. G. Shellock. Burns associated with clinical MR examinations. *Radiology*, **175**:585 (1990).
- [71] G. Bashein, G. Syrový. Burns associated with pulse oxymetry during magnetic resonance imaging. *Anesthesiology*, **75**:382–382 (1991).
- [72] F. G. Shellock, E. Kanal. *Magnetic Resonance: Bioeffects, Safety and Patient Management*. Lippincott-Raven, 2 edition (1996).
- [73] L. Lemieux, P. J. Allen, F. Franconi, M. R. Symms, D. R. Fish. Recording of EEG during fMRI experiments: patient safety. *Magn Reson Med*, **38**(6):943–952 (1997).
- [74] F. Lazeyras, I. Zimine, O. Blanke, S. Perrig, M. Seeck. Functional MRI with simultaneous EEG recording: Feasibility and application to motor and visual activation. *J Magn Reson Imaging*, **13**(6):943–948 (2001).
- [75] G. Bonmassar, K. Anami, J. R. Ives, J. W. Belliveau. Visual evoked potential (VEP) measured by simultaneous 64-channel EEG and 3T fMRI. *Neuroreport*, **10**(9):1893–1897 (1999).
- [76] F. Kruggel, C. J. Wiggins, C. S. Herrmann, D. Y. von Cramon. Recording of the Event-Related Potentials During Functional MRI at 3.0 Tesla Field Strength. *Magn Reson Med*, **44**(2):277–282 (2000).
- [77] R. A. Hill, K. H. Chiappa, F. Huang-Hellinger, B. G. Jenkins. EEG during MR imaging: differentiation of movement artifact from paroxysmal cortical activity. *Neurology*, **45**(10):1942–1943 (1995).
- [78] P. J. Allen, G. Polizzi, K. Krakow, D. R. Fish, L. Lemieux. Identification of EEG events in the MR scanner: the problem of pulse artifact and a method for its subtraction. *NeuroImage*, **8**(3):229–239 (1998).
- [79] P. J. Allen, O. Josephs, R. Turner. A Method for Removing Imaging Artifact from Continuous EEG Recorded during Functional MRI. *NeuroImage*, **12**:230–239 (2000).

- [80] A. Hoffmann, L. Jager, K. J. Werhahn, M. Jaschke, S. Noachtar, M. Reiser. Electroencephalography during functional echo-planar imaging: detection of epileptic spikes using post-processing methods. *Magn Reson Med*, **44**(5):791–798 (2000). Lowest interference was observed with common reference montage. main artifact is from slice loop.
- [81] J. Sijbers, J. Van Audekerke, M. Verhoye, A. Van der Linden, D. Van Dyck. Reduction of ECG and gradient related artifacts in simultaneously recorded human EEG/MRI data. *Magn Reson Imaging*, **18**(7):881–886 (2000).
- [82] R. I. Goldman, J. M. Stern, J. Engel, Jr., M. S. Cohen. Acquiring simultaneous EEG and functional MRI. *Clinical Neurophysiology*, **111**:1974–1980 (2000).
- [83] K. Krakow, P. J. Allen, M. R. Symms, L. Lemieux, O. Josephs, D. R. Fish. EEG Recording During fMRI Experiments: Image Quality. *Human Brain Map*, **10**(1):10–15 (2000).
- [84] G. Bonmassar, N. Hadjikhani, J. R. Ives, H. D., J. W. Belliveau. Influence of EEG Electrodes on the BOLD fMRI Signal. *Human Brain Map*, **14**:108–115 (2001).
- [85] I. Zimine, F. Lazeyras, S. Perrig, P. Descouts. FMRI feasibility with simultaneous EEG recording. In *Proc. 8th ISMRM, Denver*, p. 819 (2000).
- [86] WHO. Epilepsy: Social consequences and economic aspects (2001). Fact sheet 166, <http://www.who.int/inf-fs/en/fact166.html>.
- [87] J. E. Franck, D. D. Kunkel, D. G. Baskin, P. A. Schwartzkroin. Inhibition in kainate-lesioned epileptogenic hippocampi: physiologic, autoradiographic and immunocytochemical observations. *J Neurosci*, **8**:1991–2002 (1988).
- [88] T. Sutula, G. Cascino, J. Cavazos, I. Parada, L. Ramirex. Mossy fiber synaptic reorganization in epileptic human temporal lobe. *Ann Neurol*, **26**:321–330 (1989).
- [89] D. Schmidt. The clinical impact of new antiepileptic drugs after a decade of use in epilepsy. *Epilepsy Research*, **50**(1):21–32 (2002).
- [90] J. Engel, Jr. Surgery for seizures. *N Engl J Med*, **334**:647–652 (1996).

- [91] European Federation of Neurological Societies Task Force. Pre-surgical evaluation for epilepsy surgery - European Standards. *European Journal of Neurology*, **7**(1):119–122 (2000).
- [92] R. D. Pasqual-Marqui, C. M. Michel, D. Lehmann. Low resolution electromagnetic tomography. *Int J Psychophysiol*, **18**:49–65 (1994).
- [93] C. M. Michel, M. Seeck, T. Landis. Spatiotemporal dynamics of human cognition. *News Physiol Sci*, **14**:206–214 (1999).
- [94] G. Lantz, C. M. Michel, R. D. Pascual-Marqui, L. Spinelli, M. Seeck, S. Seri, T. Landis, I. Rosen. Extracranial localization of intracranial interictal epileptiform activity using loreta. *Electroenceph Clin Neurophysiol*, **102**:414–422 (1997).
- [95] R. I. Kuzniecky, G. D. Jackson. *Magnetic Resonance in Epilepsy*. Raven Press (1995).
- [96] J. W. Hugg, K. D. Laxer, G. B. Matson, A. A. Maudsley, M. W. Weiner. Neuron loss localizes human temporal lobe epilepsy by in vivo proton magnetic resonance spectroscopic imaging. *Ann Neurol*, **34**:788–794 (1993).
- [97] A. Connelly, P. W. Van, D. Porter, C. Johnson, J. Duncan, D. Gadian. Proton magnetic resonance spectroscopy in mri-negative temporal lobe epilepsy. *Neurology*, **51**:61–66 (1998).
- [98] T. R. Henry, P. B. Pennell. Neuropharmacological imaging in epilepsy with pet and spect. *Q J Nucl Med*, **42**:199–210 (1998).
- [99] G. D. Jackson, A. Connelly, J. H. Cross, I. Gordon, D. G. Gadian. Functional magnetic resonance imaging of focal seizures. *Neurology*, **44**:850–856 (1994).
- [100] J. A. Detre, J. I. Sirven, D. C. Alsop, M. J. O'Connor, J. A. French. Localization of subclinical ictal activity by functional magnetic resonance imaging: correlation with invasive monitoring. *Ann Neurol*, **38**:618–624 (1995).
- [101] S. Warach, J. R. Ives, G. Schlaug, M. R. Patel, D. G. Darby, V. Thangaraj, R. R. Edelman, D. L. Schomer. EEG-triggered echo-planar functional MRI in epilepsy. *Neurology*, **47**(1):89–93 (1996).

- [102] M. Seeck, F. Lazeyras, C. M. Michel, O. Blanke, C. A. Gericke, J. Ives, J. Delavelle, X. Golay, C. A. Haenggeli, N. de Tribolet, T. Landis. Non invasive epileptic focus localization using EEG-triggered functional MRI and electromagnetic tomography. *EEG Clin Neurophysiol*, **106**:508–512 (1998).
- [103] K. Krakow, F. G. Woermann, M. R. Symms, J. P. Allen, L. Lemieux, G. J. Barker, D. K. S., D. R. Fish. EEG -triggered functional MRI of interictal epileptiform activity in patients with partial seizures. *Brain*, **122**:1679–1688 (1999).
- [104] F. Lazeyras, O. Blanke, S. Perrig, I. Zimine, X. Golay, J. Delavelle, C. M. Michel, N. de Tribolet, J.-G. Villemure, M. Seeck. EEG-Triggered Functional MRI in Patients With Pharmacoresistant Epilepsy. *J Magn Reson Imaging*, **12**(1):177–185 (2000).
- [105] J. V. Hajnal, R. Myers, A. Oatridge, J. E. Schwieso, I. R. Young, G. M. Bydder. Artifacts Due to Stimulus Correlated Motion in Functional Imaging of the Brain. *Magn Reson Med*, **31**:283–291 (1994).
- [106] G. K. Aguirre, E. Zarahn, M. D’Esposito. The variability of human, BOLD hemodynamic responses. *Neuroimage*, **8**(4):360–369 (1998).
- [107] L. Lemieux, A. Salek-Haddadi, O. Josephs, P. Allen, N. Toms, C. Scott, K. Krakow, R. Turner, D. R. Fish. Event-Related fMRI with Simultaneous and Continuous EEG: Description of the Method and Initial Case Report. *NeuroImage*, **14**:780–787 (2001).
- [108] C.-G. Bénar, D. W. Gross, Y. Wang, V. Petre, B. Pike, F. Debeau, J. Gotman. The BOLD Response to Interictal Epileptiform Discharges. *NeuroImage*, **17**(3):1182–1192 (2002).
- [109] J. Baudewig, H. J. Bitternamm, W. Paulus, J. Frahm. Simultaneous EEG and functional MRI of epileptic activity: a case report. *Clin Neurophysiol*, **18**:479–484 (2000).
- [110] G. Lantz, L. Spinelli, R. G. de Peralta Menedez, M. Seeck, C. M. Michel. Localization de sources distribuées et comparaison avec l’IRM fonctionnelle. *Epileptic Disord*, **3**:45–57 (2001). (Special issue 1).
- [111] I. Zimine, F. Lazeyras, M. L. Seghier, G. Lantz, M. Seeck. Combined triggered EEG-fMRI and ^1H spectroscopy in the localization of extra-temporal epileptic activity. In *Proc. 11th ISMRM, Toronto* (2003).

- [112] G. Liu, G. Sobering, J. Duyn, C. T. Moonen. A fuctional MRI technique combining principles of echo-shifting with a train of observations (PRESTO). *Magn Reson Med*, **30**:764–768 (1993).
- [113] K. P. Pruessmann, M. Weiger, M. B. Scheidegger, P. Boesiger. SENSE: Sensitivity encoding for fast MRI. *Magn Reson Med*, **42**:952–962 (1999).
- [114] A. Kleinschmidt, H. Bruhn, G. Kruger, K. D. Merboldt, G. Stoppe, J. Frahm. Effects of sedation, stimulation, and placebo on cerebral blood oxygenation: a magnetic resonance neuroimaging study of psychotropic drug action. *NMR Biomed*, **12**(5):286–292 (1999).
- [115] P. A. Bandettini, A. Jesmanowicz, J. van Kylen, R. M. Birn, J. S. Hyde. Functional MRI of Brain Activation Induced by Scanner Acoustic Noise. *Magn Reson Med*, **39**:410–416 (1998).
- [116] R. M. Birn, P. A. Bandettini, R. W. Cox, R. Shaker. Event - related fMRI of tasks involving brief motion. *Human Brain Map*, **7**:106–114 (1999).
- [117] W. H. Press, S. A. Teukolsky, W. T. Vetterling, B. P. Flannery. *Numerical Recipes in C - The Art of Scientific Computing*. Cambridge Univ Press (1992).
- [118] F. M. Miezin, L. Maccotta, J. M. Ollinger, S. E. Petersen, R. L. Buckner. Characterizing the hemodynamic response: effects of presentation rate, sampling procedure, and the possibility of ordering brain activity based on relative timing. *Neuroimage*, **11**(6):735–759 (2000).
- [119] T. B. Parrish, D. R. Gitelman, K. S. LaBar, M.-M. Mesulam. Impact of Signal-to-Noise on Functional MRI. *Magn Reson Med*, **44**:925–932 (2000).
- [120] C. M. Portas, K. Krakow, P. Allen, O. Josephs, J. L. Armony, C. D. Frith. Auditory Processing across the Sleep-Wake Cycle: Simultaneous EEG and fMRI Monitoring in Humans. *Neuron*, **28**:991–999 (2000).
- [121] E. A. Stein. fMRI: A New Tool for the In Vivo Localization of Drug Actions in the Brain. *J Anal Toxicol.*, **24**:419–424 (2001).

Publications

Journal papers

1. I. Zimine, M. L. Seghier, M. Seeck and F. Lazeyras. *Brain Activation using triggered event-related fMRI*. NeuroImage, **18**:410–415 (2003).
2. M. K. Ivancevic, I. Zimine, F. Lazeyras, D. Foxall and J.-P. Vallee. *FAST sequences optimization for contrast media pharmacokinetic quantification in tissue*. J. Magn. Reson. Imaging, **14**:771-778 (2001).
3. N. Valenza, R. Ptak, I. Zimine, M. Badan, F. Lazeyras and A. Schnider. *Dissociated active and passive tactile shape recognition: a case study of pure tactile apraxia*, Brain, **124**:2287–2298 (2001)
4. F. Lazeyras, I. Zimine, O. Blanke, S. Perrig and M. Seeck, *Functional MRI with simultaneous EEG recording: Feasibility and application to motor and visual activation*, J. Magn. Reson. Imaging, **13**:943–948 (2001).
5. F. Lazeyras, O. Blanke, S. Perrig, I. Zimine, X. Golay, J. Delavelle, C.M. Michel, N. de Tribolet, J.G. Villemure and M. Seeck, *EEG-triggered functional MRI in patients with pharmacoresistant epilepsy*, J. Magn. Reson. Imaging, **12**:177–185 (2000).
6. F. Lazeyras, O. Blanke, I. Zimine, J. Delavelle, S. Perrig and M. Seeck, *MRI, ¹H-MRS and functional MRI in a patient during and after prolonged nonconvulsive seizure activity*, Neurology, **55**:1677–1682 (2000).

Conferences

1. I. Zimine, F. Lazeyras, M. L. Seghier, G. Lantz and M. Seeck. *Combined triggered EEG-fMRI and 1H spectroscopy in the localization of extratemporal epileptic activity*, 11th ISMRM, Toronto, 2003.
2. I. Zimine, M. L. Seghier, M. Seeck, F. Lazeyras. *Feasibility of triggered event-related fMRI*, 19th ESMRMB, Cannes, 2002, Nr. 350.
3. I. Zimine, F. Lazeyras, S. Perrig and P. Descouts, *FMRI feasibility with simultaneous EEG recording*, in Proc. 8th ISMRM, Denver, 2000, p. 819.
4. I. Zimine, F. Lazeyras, J.-P. Vallée, D.A. Rüfenacht and P. Descouts *Effect of Motion Correction on the FMRI Activated Areas*, in Proc. 7th ISMRM, Philadelphia, 1999, p. 1678.